TAMPEREEN TEKNILLINEN YLIOPISTO
TAMPERE UNIVERSITY OF TECHNOLOGY
Julkaisu 708 • Publication 708

Dmytro Paliy

Local Approximations in Demosaicing and Deblurring of Digital Sensor Data

Tampere 2007

Tampereen teknillinen yliopisto. Julkaisu 708
Tampere University of Technology. Publication 708

Dmytro Paliy

Local Approximations in Demosaicing and Deblurring of Digital Sensor Data

Thesis for the degree of Doctor of Technology to be presented with due permission for public examination and criticism in Tietotalo Building, Auditorium TB219, at Tampere University of Technology, on the 3rd of December 2007, at 12 noon.

Tampereen teknillinen yliopisto - Tampere University of Technology
Tampere 2007

ISBN 978-952-15-1893-5 (printed)
ISBN 978-952-15-1956-7 (PDF)
ISSN 1459-2045

Abstract

This thesis is dedicated to demosaicing and deblurring problems in digital image processing and their solution exploiting signal adaptive filtering. In particular, we use filtering based on the local polynomial approximation (LPA) and the paradigm of the intersection of confidence intervals (ICI) for the adaptive selection of the scales of LPA. This filtering is nonlinear and spatially-adaptive with respect to the smoothness and irregularities of the image.

In the first part of the thesis, demosaicing is studied. It refers to the problem of interpolation of complete red, green, and blue values for each pixel, to make a color RGB image, from downsampled gray-scale mosaic-like raw data recorded by a single-chip digital camera. We propose a novel technique for demosaicing that shows results that, to the best of our knowledge, are a significant improvement over the state of the art.

Traditionally, in demosaicing the input signal is assumed to be noise-free. However, the raw data is always noisy and thus prefiltering has commonly been used prior to demosaicing. We show that the demosaicing and denoising designed as a single procedure can be significantly more efficient than analogous independent procedures. In this thesis, we do not restrict ourselves to the conventional stationary Gaussian noise model. In the developed technique, we also take into account the signal-dependant Poisson noise which is much more relevant for digital imaging sensors. As a result, we achieve higher quality of image restoration as demonstrated by extensive experiments for both artificial and real data taken directly from the sensor of a camera phone.

The second part of the thesis is dedicated to image deblurring. We develop several techniques as an evolution from conventional deconvolution with a known blur to blind deconvolution with an unknown blur. We propose techniques for digital optical sectioning, multi-channel and single-channel blind deconvolution, and techniques for automatic selection of the regularization parameter.

Acknowledgments

This work has been carried out at the Institute of Signal Processing in Tampere University of Technology, Finland. I am deeply thankful to my supervisor Prof. Karen Egiazarian for guiding me through the doctoral thesis and my studies in Tampere.

I would like to express my special thanks to Prof. Vladimir Katkovnik for his supervision, help, and endless patience. Also, I am very honored and proud by work in one team with Dr. Alessandro Foi. Discussions with him were always extremely practical and fruitful.

I am indebted to the reviewers of my thesis Prof. Patrizio Campisi and Dr. Keigo Hirakawa for their helpful and constructive comments.

I gratefully thank Prof. Igor Aizenberg who started guiding me many years ago in Ukraine. Fruitful collaboration with him became traditional. Also, I would like to thank to Prof. Naum Aizenberg with whom I have started my trip to the world of science.

I would like to sincerely thank the professors of the Institute of Signal Processing for creating such an open and friendly research environment, especially Prof. Jaakko Astola and Prof. Moncef Gabbouj.

I thank our colleagues and friends Dr. Radu Bilcu, Dr. Sakari Alenius, Dr. Mejdi Trimeche, Lic.Tech. Marku Vehviläinen, and Dr. Marius Tico from Nokia Research Center in Tampere, for their collaboration and active position in research on challenging and interesting research problems in industrial applications.

I gratefully thank our colleagues Prof. Alexander Totsky, Prof. Vladimir Lukin, and Dr. Mykola Ponomarenko from Kharkov National Aerospace University, Ukraine. I highly appreciate comments and suggestions of Prof. Vladimir Lukin that helped me to improve significantly this thesis.

I deeply thankful to my friends and colleagues in our Transforms and Spectral Techniques group, to all the personnel of the Institute of Signal Processing in Tampere University of Technology that created warm and friendly environment.

Also, I am very proud of my friendship with Dmytro Rusanovskyy, Andriy Bazhyna, Dr. Ekaterina Pogossova, Dr. Peyman Arian, Kostadin Dabov, Ossi Pirinen, Andrey Norkin, Susanna Minasyan, Evgeny Krestyannikov, and many other my friends in Tampere and around the world.

I would like to express my gratitude to my parents, mother Liudmila and father Victor, and to my brother Alexander for their constant support. Finally, my warmest thanks are to my dear Hanna.

Contents

Abstract iii

Acknowledgments v

Contents vii

List of Publications ix

Abbreviations xiii

1 Introduction 1
- 1.1 Image Reconstruction Chain . . . 1
- 1.2 Image Acquisition Models . . . 2
  - 1.2.1 Additive Noise Models . . . 2
  - 1.2.2 Color Filter Array Interpolation for Bayer Pattern . . . 5
  - 1.2.3 Color Filter Array Interpolation of Noisy Bayer Data . . . 6
  - 1.2.4 Deconvolution and Blind Deconvolution . . . 6
- 1.3 Thesis Structure . . . 8

2 Spatially Adaptive Filtering 9
- 2.1 Design of Directional Linear Filters and Interpolators in Polynomial Basis 10
- 2.2 Adaptive Window-Size Selection . . . 12
  - 2.2.1 Motivation . . . 12
  - 2.2.2 Multiple Hypothesis Testing based on Confidence Intervals . . . 14
- 2.3 Aggregation of Directional Estimates . . . 16

3 Demosaicing of Data Acquired by CCD/CMOS Sensor of Digital Camera 17
- 3.1 Problem Formulation . . . 17
  - 3.1.1 Correlation Models in Demosaicing . . . 18
  - 3.1.2 Demosaicing Methods . . . 18
  - 3.1.3 Demosaicing of Noisy Sensor Data . . . 19
- 3.2 Proposed Demosaicing Based on the Adaptive LPA-ICI . . . 20
- 3.3 Adaptation of Color Filter Array Interpolation to Noisy Data . . . 23
- 3.4 Experiments with Artificial and Real Sensor Data . . . 26

4 Deconvolution Methods **31**
4.1 Deconvolution for Optical Sectioning 32
4.1.1 Regularized Inverse 35
4.1.2 Regularized Wiener Inverse 36
4.1.3 Experiments 37
4.2 Deconvolution for Mobile Devices 39
4.2.1 Overview 39
4.2.2 Proposed Approach 40
4.3 Multi-Channel Blind Deconvolution 43
4.3.1 Gradient-Projection Algorithm 45
4.3.2 Experiments 49
4.4 Single-Channel Blind Deconvolution 50
4.4.1 Multilayer Neural Network Based on Multi-Valued Neurons as a Classifier 51
4.4.2 Training and Testing Patterns 55
4.4.3 Blur Models 57
4.4.4 Neural Network Structure 57
4.4.5 Performance Evaluation 57
4.5 Techniques to Select the Varying Regularization Parameter 60

Conclusions **65**

Bibliography **67**

Publications **79**

List of Publications

This thesis is based on the following publications. In the text these publications are referred as Publication I, Publication II, etc.

I. Paliy, D., V. Katkovnik, R. Bilcu, S. Alenius, K. Egiazarian, "Spatially Adaptive Color Filter Array Interpolation for Noiseless and Noisy Data", *International Journal of Imaging Systems and Technology, Special Issue on Applied Color Image Processing*, vol. 17, iss. 3, pp. 105-122, October 2007 (Paliy, 2007c).

II. Paliy, D., R. Bilcu, V. Katkovnik, M. Vehvilainen, "Color Filter Array Interpolation Based on Spatial Adaptivity", Proc. SPIE-IS&T Electronic Imaging 2007, Computational Imaging IV, vol. 6497, San Jose, CA, January 2007 (Paliy, 2007a).

III. Paliy, D., M. Trimeche, V. Katkovnik, S. Alenius, "Demosaicing of Noisy Data: Spatially Adaptive Approach", Proc. SPIE-IS&T Electronic Imaging 2007, Computational Imaging IV, vol. 6497, San Jose, CA, January 2007 (Paliy, 2007b).

IV. Paliy, D., V. Katkovnik, and K. Egiazarian, "Spatially Adaptive 3D Inverse for Optical Sectioning", Proc. of SPIE-IS&T Electronic Imaging 2006, San Jose, CA, vol. 6065, pp. 61-72, January 2006 (Paliy, 2006a).

V. Katkovnik, V., Paliy D., Egiazarian K., Astola J., "Frequency domain blind deconvolution in multiframe imaging using anisotropic spatially-adaptive denoising", EUSIPCO 2006, September 2006 (Katkovnik, 2006a).

VI. Aizenberg, I.N., D.V. Paliy, J.M. Zurada, J.T. Astola, "Blur Identification by Multilayer Neural Network based on Multi-Valued Neurons", *IEEE Trans. on Neural Networks*, (Accepted for publication) (Aizenberg, 2007a).

VII. Paliy, D., V. Katkovnik, S. Alenius, K. Egiazarian, "Selection of Varying Spatially Adaptive Regularization Parameter for Image Deconvolution", International Workshop on Spectral Methods & Multirate Signal Processing, SMMSP 2007, num. 37, pp. 23-28, September 2007 (Paliy, 2007d).

It is worth to stress that all the papers were published as a result of a team work and tense cooperation between all the co-authors and also other people involved in the related research areas.

The author's contribution to the publications listed above is as follows. As the first author of Publications I, II, III, D. Paliy has proposed, developed, and implemented the techniques and written the manuscripts for most part.

Publications IV, V, VII where developed under supervision and in tense collaboration with prof. V. Katkovnik (Tampere University of Technology, Finland). This includes techniques' design, implementation, and writing a manuscript.

D. Paliy has developed Publications VI in tense cooperation with prof. I. Aizenberg (Texas A&M University-Texarkana, USA) and under his supervision. This includes techniques' design, implementation, and writing a manuscript.

D. Paliy is also an author or co-author of the following related publications:

1. Paliy, D., V. Katkovnik, and K. Egiazarian, "Scale-Adaptive Inverse in 3D Imaging", Proc. Int. TICSP Workshop Spectral Meth. Multirate Signal Process., SMMSP 2005, Riga, 2005 (Paliy, 2005).

2. Paliy, D., V. Katkovnik, S. Alenius, and M. Vehviäinen, "Adaptive Neighborhood Interpolation of Noisy Images on Quincunx Grid", International Workshop on Spectral Methods & Multirate Signal Processing, SMMSP 2006, Florence, pp. 155-162, September 2006 (Paliy, 2006b).

3. Trimeche, M., D. Paliy, Vehvilainen M., Katkovnik V., "Multi-Channel Image Deblurring of Raw Color Components", Proceedings of SPIE, vol. 5674, Computational Imaging III, pp. 169-178, March 2005 (Trimeche, 2005).

4. Aizenberg, I., D. Paliy, and Astola J. "Multilayer Neural Network based on Multi-Valued Neurons and the Blur Identification Problem", 2006 IEEE World Congress on Computational Intelligence. Proceedings of the 2006 IEEE Joint Conference on Neural Networks, ISBN: 0-7803-9490-9, Vancouver, Canada, pp. 1200-1207, July 2006 (Aizenberg, 2006a).

5. Aizenberg, I., D. Paliy, C. Moraga, and J. Astola, "Blur Identification Using Neural Network for Image Restoration ", Proc. of Fuzzy Days 2006, Dortmund, pp. 441-455, September 2006 (Aizenberg, 2006b).

6. Aizenberg, I., Butakoff C., and Paliy D., "Impulsive Noise Removal using Threshold Boolean Filtering based on the Impulse Detecting Functions", *IEEE Signal Processing Letters*, vol. 12, iss. 1, pp. 63-66, Jan. 2005 (Aizenberg, 2005a).

7. Aizenberg, I., C. Moraga and D. Paliy, "A Feedforward Neural Network Based on Multi-valued Neurons", Advances in Soft Computing: Computational Intelligence, Theory and Applications, Springer Berlin/Heidelberg, New York, pp. 599-612, 2006 (Aizenberg, 2006c).

8. Aizenberg, I., Astola J., Bregin T., Butakoff C., Egiazarian K. and Paliy D. "Detectors of the impulsive noise and new effective filters for impulsive noise reduction", Proceedings of SPIE Electronic Imaging, Image Processing: Algorithms and Systems II, Santa Clara, California, USA, vol. 5014, pp. 419-428, Jan. 2003 (Aizenberg, 2003a).

9. Aizenberg, I., Astola J., Butakoff C., Egiazarian K. and Paliy D. "Effective Detection and Elimination of Impulsive Noise with a Minimal Image Smoothing", International Conference on Image Processing, ICIP 2003: vol. 3, pp. III- 357-360, 14-17 Sept. 2003 (Aizenberg, 2003b).

10. Aizenberg, I., Bregin T. and Paliy D. "Method for Impulsive Noise Detection and Its Applications to the Improvement of Impulsive Noise-Filtering Algorithms", SPIE Proceedings on Image Processing: Algorithms and Systems, vol. 4667, pp. 204-214, 2002 (Aizenberg, 2002a).

11. Totsky A., Fevralev D., Lukin V., Katkovnik V., Paliy D., Egiazarian K., Pogrebnyak O., Astola J., "Performance Study of Adaptive Filtering in Bispectrum Signal Reconstruction", *Circuits, Systems, and Signal Processing*, Birkhäuser Boston, vol. 25, no. 3, pp. 315-342, 2006 (Totsky, 2006).

Abbreviations

1D, 2D, 3D	-	One-, Two-, Three-Dimensional
AWB	-	Automatic White Balance
AWGN	-	Additive White Gaussian Noise
BSNR	-	Blurred Signal-to-Noise Ratio
CCD	-	Charge-Coupled Device
CFA	-	Color Filter Array
CFAI	-	Color Filter Array Interpolation
CMOS	-	Complementary-Symmetry/Metal-Oxide Semiconductor
CMY	-	Cyan, Magenta, Yellow color space
DFT	-	Discrete Fourier Transform
ICI	-	Intersection of Confidence Intervals
IDFT	-	Inverse Discrete Fourier Transform
LPA	-	Local Polynomial Approximation
ML	-	Maximum Likelihood
MLF	-	Multi-Layered Feedforward neural network
MLMVN	-	Multi-Layer neural network based on Multi-Valued Neurons
MVN	-	Multi-Valued Neuron
MSE	-	Mean Square Error
PDF	-	Probability Density Function
PSF	-	Point Spread Function
RGB	-	Red, Green, Blue color space
RI	-	Regularized Inverse
RWI	-	Regularized Wiener Inverse
SAR	-	Synthetic Aperture Radar
SIMO	-	Single-Input Multiple-Output
SNR	-	Signal-to-Noise Ratio
SVM	-	Support Vector Machine

Chapter 1

Introduction

The recent decade was outlined with drastic growth of high-tech consumer and industrial electronics. As a part of this process, imaging made an overwhelming step from analogue to digital photography and video. A number of different cutting-edge digital imaging technologies found their places in real-life appliances, among which charge-coupled device (CCD), complementary-symmetry/metal-oxide semiconductor (CMOS), synthetic aperture radar (SAR), sensors for thermal, multispectral imaging, etc. The size of devices and prices are continuously becoming smaller while the possibilities that they provide are impressively increasing. Nowadays, nobody can be surprised by a mobile camera phone that takes a high-resolution color image and sends it to an another mobile phone, desktop computer, or printer. Digital imaging equipment became not only usual for us but also often a necessary one.

This growth was impressively fast and gave us plenty of new opportunities. Nevertheless, the digital imaging still is extremely challenging problem targeted and designed even for such devices and applications as digital photo and video cameras, fluorescence and confocal microscopes, space telescopes, etc. This results in developing advanced optical systems, imaging sensors, specific image-processing processors, technologies that reduce power consumption. On the other hand, many aspects are unrealistic for mobile camera phones due to the hardware limitations that makes problems related to the digital imaging sometimes even more difficult. Often computational imaging restoration techniques implemented in software are very attractive to replace effectively their hardware counterparts.

1.1 Image Reconstruction Chain

In a typical digital camera, the image restoration chain can contain the following usually cascaded operations:

- Noise reduction,
- Color filter array interpolation (CFAI),
- Deblurring of color component,

- Automatic white balance (AWB),
- Color gamut conversion,
- Geometrical correction and vignetting elimination.

It is evident that the final image quality depends on the effective and optimized use of all these operations in the reconstruction chain. Typically, the most effective implementations of these algorithms are non-linear (Trimeche, 2005).

In this dissertation, the following stages from the image restoration chain were studied: noise reduction, color filter array interpolation, and deblurring. In particular, we cover mainly three problems of digital image processing formulated as signal-adaptive denoising, noise-resistant interpolation, and deconvolution related applications. The crucial part of the developed approach to these problems is the filtering adaptive to signal. The main intention is done on the spatial (temporal) adaptivity based on the LPA-ICI technique that proved its efficiency in a variety of applications.

Let us start from the mathematical image formation models used in this work.

1.2 Image Acquisition Models

1.2.1 Additive Noise Models

It is the well-known fact that any image recorded by a digital camera sensor is noisy. The most wide-spread and well-studied modeling is perhaps the model with additive noise:

$$z(x) = y(x) + n(x), \tag{1.1}$$

where $z(x)$ is the observed signal, $y(x)$ is the true signal to be estimated, $n(x)$ is the noise at every point x, $x \in X = \{x = (x_1, x_2) : \ x_1 = 1, ..., 2N, \ \ x_2 = 1, ..., 2M\}$ are the spatial coordinates.

It is convenient to represent the noise in (1.1) in the form

$$n(x) = \sigma(x)\eta(x), \tag{1.2}$$

where $\eta(x)$ is an independent zero-mean noise with variance equal to one at every point x and thus $\sigma(x)$ is the standard deviation of $z(x)$. It is not necessarily invariant with respect to the spatial variable x.

The following noise models are considered in this work:

a) The additive stationary white Gaussian noise with the invariant standard deviation

$$\sigma(x) = const \tag{1.3}$$

for all $x \in X$ (exploited in Publications I-VII), and the term $\eta(x) \sim \mathcal{N}(0, 1)$ is the white Gaussian noise with the variance equal to one. An example of Blocks 1D signal with this type of noise with $\sigma = 0.5$ is illustrated in Fig.1.1b.

However, dependence of the noise from the signal is more realistic in practice, for instance, in photon-counting applications. An important property of such a noise is the dependence of its variance from the signal (Hirakawa, 2005b; Foi, 2007a; Foi, 2006b).

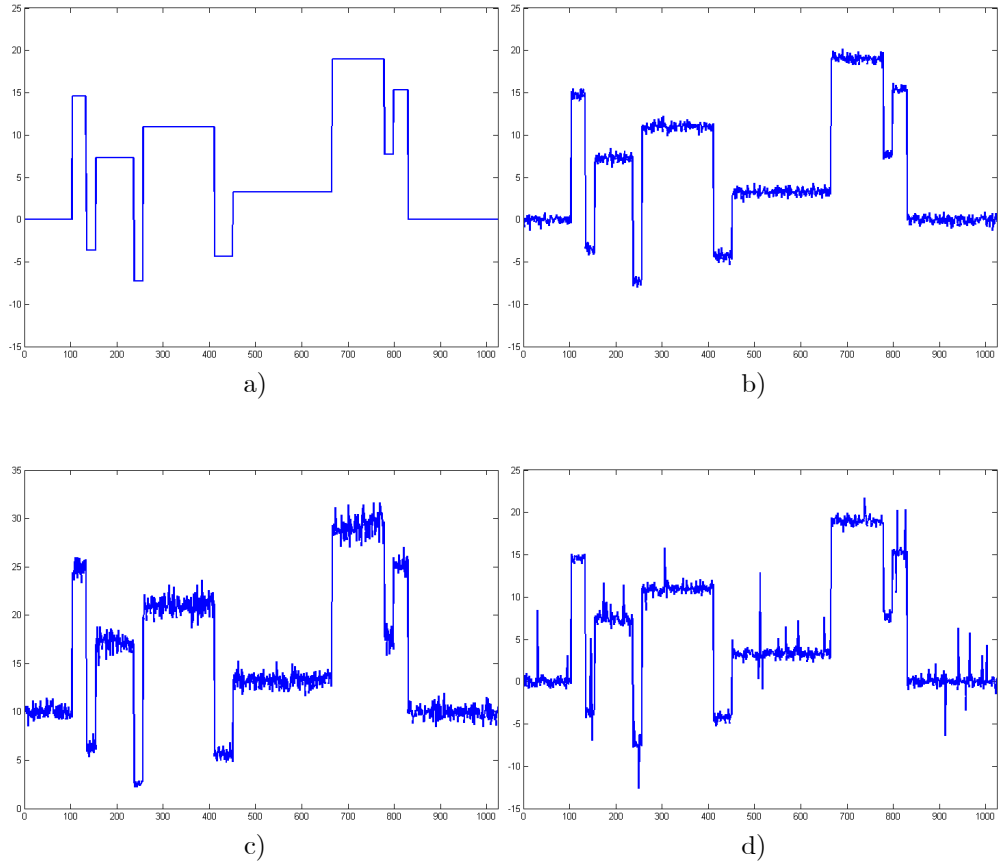

Figure 1.1: Illustration of different noise models: a) true signal; b) additive Gaussian noise; c) Poissonian noise; d) mixture of Gaussian noises.

The most widely encountered models for this dependence are film-grain, multiplicative, speckle noise, and, in particular, Poissonian noise. In probability theory and statistics, the Poisson distribution is a discrete probability distribution that expresses well stochastic counting processes (Ross, 1997; Khuri, 2003). This distribution is associated with the random number of events that take place over a fixed period of time and provided that probability of an arrival occurring during this time interval does not depend on what happened prior to it. Such modeling is common for CCD and CMOS digital image sensors. Photons that strike digital imaging sensor during the opening shutter of a camera is an example of such a process. Sometimes it is called as photon-counting noise (Bovik, 2000).

b) The signal-dependent Poissonian model of the form $\chi z(x) \sim \mathcal{P}(\chi y(x))$ is considered in this work. This noise can be written explicitly in the additive form (1.1) where

the standard deviation depends on the image intensity as

$$\sigma(x) = std\{z(x)\} = \sqrt{y(x)/\chi}. \tag{1.4}$$

Here χ is the parameter that controls the noisiness of the observed data $z(x)$. It is shown in (Foi, 2007a; Foi, 2006b) that such a model can be used for generic CCD/CMOS digital imaging sensors (exploited in Publications I, III). An example of Blocks 1D signal with this type of noise is illustrated in Fig.1.1c. The shown signal was modified in such a way that all his values are larger than 0, particularly, $\chi z(x) \sim \mathcal{P}(\chi(y(x) + 10))$ with $\chi = 20$.

c) The nonstationary Gaussian noise with the signal-dependant standard deviation (Hirakawa, 2005b; Hirakawa, 2005c)

$$\sigma(x) = k_0 + k_1 y(x) \tag{1.5}$$

exploited in Publication I, where, k_0 and k_1 are the parameters that control the noisiness of the observed data $z(x)$. This noise model can be used as an efficient approximation for CCD/CMOS digital imaging sensors

A more advanced noise modeling for CMOS/CCD sensor data, as a mixture of Poissonian and Gaussian noises where effects of over- and undersaturation are taken into account, is proposed in (Foi, 2007b). The authors also propose a technique to determine the noise model parameters from any single observation.

The modeling for the impulsive noise may be used in some applications. It can be caused by malfunctioning pixels in camera sensors, faulty memory locations in hardware, transmission in noisy channel (Chan, 2005; Bovik, 2000). The salt-and-pepper noise is widely used as a particular case of the impulsive noise, as in (Chan, 2005). More general than the salt-and-pepper model was studied in (Aizenberg, 2005b; Aizenberg, 2002a; Aizenberg, 2003a), where a corrupted pixel is a random value with the uniform distribution.

d) A mixture of Gaussian noises was used in (Huber, 1981; Katkovnik, 2006b) as another model for the impulsive noise:

$$n(x) \sim f,\ f = (1-\alpha)f_0 + \alpha f_1, \tag{1.6}$$

where $f_0 = \mathcal{N}(0, \sigma_0^2)$, $f_1 = \mathcal{N}(0, \sigma_1^2)$, $\sigma_1 \gg \sigma_0$, and $0 \leq \alpha \leq 1$. The parameter α defines the proportion of the high-variance random impulses/outliers in the observed signal (Fig.1.1f). It is equal in our example to 5%, i.e. $\alpha = 0.05$, $\sigma_0 = 0.5$, and $\sigma_1 = 5$.

Usually, the parameters in (1.3)-(1.6) are determined from a camera calibration procedure.

It is worth to mention that in general noise models used in practice are not restricted to the given in (1.1)-(1.6) ones.

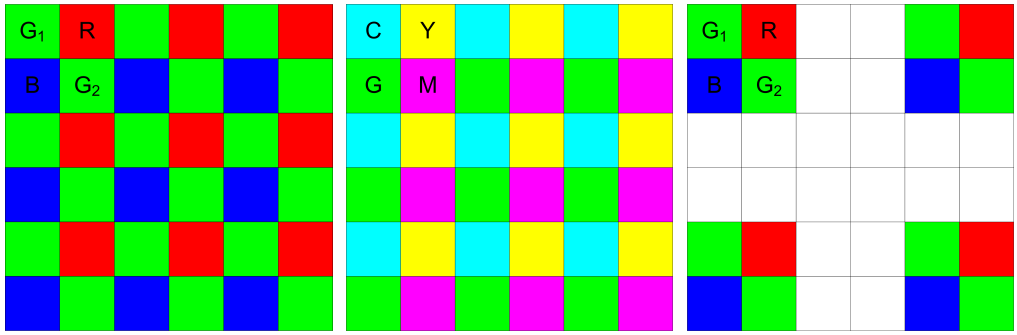

a) b) c)

Figure 1.2: Examples of CFAs: a) Bayer pattern; b) CMY+G; c) pattern with transparent cites.

1.2.2 Color Filter Array Interpolation for Bayer Pattern

The common approach in single-chip digital cameras is to use a color filter array (CFA) to sample different spectral components like red, green, and blue. The sensor records one value per pixel location. The resulting image is a gray-scale mosaic-like one. Demosaicing algorithm interpolates sets of complete red, green, and blue values for each pixel, to make an RGB image.

The CFA is a crucial element in design of single-sensor digital cameras. Perhaps the most widespread nowadays CFA is the Bayer CFA (Bayer, 1976) (Fig.1.2a) that samples red (R), green (G), and blue (B) colors. Study on a variety of R, G, and B sampling patterns may be found in (Lukac, 2004e). Different characteristics in design of CFA affect both performance and computational efficiency of the demosaicing solution (Lukac, 2004e; Adams, 1998a). Alternatively, the complementary mosaic pattern may be used that contains cyan, yellow, magenta, and green photocites (Parulski, 2002) (Fig.1.2b). Recently, CFA with transparent elements was proposed in order to improve signal-to-noise ratio (SNR) (Luo, 2007) (Fig.1.2c). The fundamentals about digital color image acquisition with single-sensor can be found in (Lukac, 2006b; Parulski, 2002).

Considering the fact that the Bayer CFA (Fig.1.2a) is one of the most often exploited today, we developed techniques for this particular CFA. We follow the general Bayer mask image formation model (Fig.1.2a):

$$z(x) = \mathcal{B}\{y_{RGB}(x)\}, \tag{1.7}$$

where $\mathcal{B}\{\cdot\}$ is a Bayer sampling operator (Bayer, 1976)

$$\mathcal{B}\{y_{RGB}(x)\} = \begin{cases} G(x), & \text{at } x \in X_{G_1}, \\ G(x), & \text{at } x \in X_{G_2}, \\ R(x), & \text{at } x \in X_R, \\ B(x), & \text{at } x \in X_B. \end{cases} \tag{1.8}$$

Here, z is an output signal of the sensor, $y_{RGB}(x) = (R(x), G(x), B(x))$ is a true color RGB observation scene, $x \in X$, R (red), G (green), and B (blue) correspond to the

color channels. For two available green channels we will use notations $G_1(x)$, such that $x \in X_{G_1} = \{(x_1, x_2) : \ x_1 = 1, 3, ..., 2N-1, \ \ x_2 = 1, 3, ..., 2M-1\}$, and $G_2(x)$, such that $x \in X_{G_2} = \{(x_1, x_2) : \ x_1 = 2, 4, ..., 2N, \ \ x_2 = 2, 4, ..., 2M\}$. Spatial coordinates for the red $R(x)$ and blue $B(x)$ color channels are denoted $x \in X_R = \{(x_1, x_2) : \ x_1 = 1, 3, ..., 2N-1, \ \ x_2 = 2, 4, ..., 2M\}$ and $x \in X_B = \{(x_1, x_2) : \ x_1 = 2, 4, ..., 2N, \ x_2 = 1, 3, ..., 2M-1\}$, respectively.

Demosaicing attempts to invert $\mathcal{B}\{\cdot\}$ in order to reconstruct $R(x)$, $G(x)$, and $B(x)$ intensities from the observations $z(x)$. This problem is covered in Publications I, II.

1.2.3 Color Filter Array Interpolation of Noisy Bayer Data

In a single-sensor camera the light passes through the optical system and is focused on a digital sensor. The sensor is composed of photon-collection sites. Each site works as a photon-counter to measure the amount of light coming to it. The sensor produces a digital value for each site which corresponds to the intensity of the light at that position. This digital output of the sensor is called "raw data".

The general Bayer mask image formation model for the data corrupted by noise is considered as a combination of (1.1) and (1.7):

$$z(x) = \mathcal{B}\{y_{RGB}(x)\} + \sigma_{bayer}(x)\eta(x), \tag{1.9}$$

where the term $\eta(x)$ is an independent zero-mean noise with variance equal to one at every point x. Thus, $\sigma_{bayer}(x)$ is the standard deviation of $z(x)$. It is not necessarily invariant with respect to the spatial variable x. The problem is to reconstruct the true color high-resolution image y_{RGB} from the noisy subsampled data z.

In Publication I, III the techniques for integrated demosaicing and denoising into a single procedure are developed for the noise as in (1.3)-(1.5) targeted, in particular, the Poissonian Bayer data.

1.2.4 Deconvolution and Blind Deconvolution

Another type of distortions in digital cameras is caused by the optical system, relative motion between camera and object, imprecise focus, etc. Often, these distortions are called as blur.

Mathematically, image capturing is modelled by the Fredholm integral of the first kind in $\mathbb{R}^2$ space $z(x) = \int_X v(x,t)y(t)dt$ where $x, t \in X \subset \mathbb{R}^2$, v is a point-spread function (PSF) of a system, y is an image intensity function, and $z(x)$ is an observed image (Rushforth, 1987). A conventional simplification is that the PSF v is shift-invariant which leads to a convolution operation in the observation model. We assume that the convolution is discrete and noise is present. Hence, the observed image z is given in the following form:

$$z(x) = (y \circledast v)(x) + n(x), \tag{1.10}$$

where " $\circledast$ " denotes the convolution, x is defined on the regular $2N \times 2M$ lattice, $x \in X$, and $n(x)$ is the noise.

Usually, it is assumed that the noise is white Gaussian with zero-mean and variance σ^2, $n(x) \sim \mathcal{N}(0, \sigma^2)$ (it can be rewritten in the form (1.2-1.3)). However, the model (1.10) with Poissonian noise (1.4) is also used, for instance, in (Foi, 2006c).

Deconvolution aims to invert (1.10) and estimate the true signal $y(x)$ from the blurred noisy observation $z(x)$.

When the blurring operator v is unknown in (1.10), the image restoration becomes a blind deconvolution problem (Lagendijk, 1990; Giannakis, 2000; Harikumar, 1999a). The most popular approaches to blind deconvolution can be divided in two classes: a multi-channel deconvolution (Sroubek, 2005; Tico, 2006), and a single-channel one (Molina, 1997; Rekleitis, 1996; Rooms, 2004; Likas, 2004; Chen, 2005; Chen, 2006).

For a multi-channel blind deconvolution we consider a 2D single-input multiple-output (SIMO) linear spatially invariant imaging system. Such a system is appropriate for the model of multiple cameras, multiple focuses of a single camera, or acquisition of images from a single camera through a changing medium. The input to this system is an unknown image $y(x)$, $x \in X$. This image is distorted by unknown finite impulse response functions modeled by the PSFs $v_j(x)$, $j = 1, ..., L$. It is assumed that $v_j(x)$ are discrete spatially invariant. The discrete convolutions of the input $y(x)$ and the PSFs $v_j(x)$ are degraded by the additive white Gaussian noise to produce the observed output images:

$$z_j(x) = (y \circledast v_j)(x) + \sigma_j(x)\eta(x), \;\; j = 1, ..., L. \tag{1.11}$$

It is assumed that the noise in each channel is uncorrelated with the noise from other channels and $\eta(x)$ have the Gaussian distribution $\mathcal{N}(0, 1)$. The parameters σ_j are the standard deviations of the noise in the channels.

The problem is to reconstruct both the image y and the PSFs v_j from the observations $\{z_j(x) : x \in X, \; j = 1, ..., L\}$.

The problems (1.10)-(1.11) are considered in Publications V, VI, VII.

For 3D problems, model (1.10) may be reformulated in the form when $x \in \mathbb{R}^3$. The assumption that the PSF is shift-invariant in all three dimensions usually does not correspond to reality. A more natural assumption is that the PSF is shift-invariant with respect to two horizontal and vertical dimensions and varying with respect to the third depth dimension (Preza, 2004; Markham, 2001; Ng, 1996). This approach leads to the optical sectioning formalism originated in digital microscopy.

According to this technique the optical system is focused at some focal plane and an image is recorded, then it is refocused at another plane and another image is recorded, and so on. The focusing planes may differ from the planes of interests. Precise focusing is not needed for reconstruction. However, the spatial resolution depends on a number of recorded images.

Suppose that we wish to reconstruct a 3D image intensity function $y(\tilde{x})$, $\tilde{x} \in \mathbb{R}^3$, from its blurred and noisy observation $z(\tilde{x})$. In the argument $\tilde{x} = (x_1, x_2, x_3)$ the first two variables x_1 and x_2 define the pixel's coordinates of 2D image obtained from $y(\tilde{x})$ with the fixed depth coordinate x_3. The axe x_3 is parallel to the optical axe of the optical system and perpendicular to the 2D image plane.

We consider the discrete observation model in the following form:

$$z_i(x) = \sum_{j=1}^{m} (v_{i,j} \circledast y_j)(x) + \sigma_i(x)\eta(x), \;\; i = 1, ..., n, \tag{1.12}$$

where $x \in \mathbb{R}^2$, $x = (x_1, x_2)$, i is a discrete variable used for the depth variable x_3, and $\mathbf{v} = (v_{i,j})$ is an $n \times m$ matrix of the 2D PSFs. The PSF $v_{i,j}$ corresponds to the observation

of the object slice j from focusing at the position i. σ_j are the standard deviations of the noise in the channels.

Overall, when $n > m$ the system (1.12) is overdetermined, generally the least squares solution is applied. In the case if $n < m$ then the system (1.12) is underdetermined, and, therefore, we impose the assumption of smoothness on the solution. When $n = m$ the system (1.12) is consistent and the solution is unique. However, (1.12) is ill-posed with respect to PSF matrix $\mathbf{v}$ that results in high instability of the solution.

It is required to restore the 3D image (the slices of the object, which is described by $\mathbf{y}(x) = (y_1(x), ..., y_m(x)))$ from n blurred 2D projections $\mathbf{z}(x) = (z_1(x), ..., z_n(x))$. Optical sectioning problem is addressed in Publication IV.

1.3 Thesis Structure

The thesis is divided into the following parts. Chapter 2 is the introductory part where the basics of the LPA-ICI technique are presented. They are given in the form applicable for interpolation what makes it different from conventional use. This approach is used in most of our methods and algorithms.

In Chapter 3, methods to recover the true image from subsampled and noisy Bayer sensor data are considered. Firstly, we propose a novel CFAI technique. Secondly, we show that joint denoising and demosaicing of Bayer sensor data is more efficient than usual use of these independent cascaded operations. In this section we use Publications I-III. The principles of adaptive LPA-ICI denoising are used widely in the proposed techniques.

In Chapter 4 we consider the deconvolution problem. Firstly, deconvolution algorithm is explained for the optical sectioning problem (Section 4.1). It is assumed that the PSF of the optical system is known.

In Section 4.2 we show the filtering that was proposed to be robust with respect to both PSF (that was identified for a particular camera phone model) and noise misestimation.

In Sections 4.3 and 4.4, blind deconvolution techniques are presented, i.e. when the PSF is unknown (and practically cannot be measured). We consider multichannel and single channel approaches for blind deconvolution. For multichannel approach we exploit minimization of the energy criterion produced in frequency domain using a recursive gradient-projection algorithm. The proposed techniques are based on the adaptive LPA-ICI applied to the image and/or blur operators. This key element is used for filtering and regularization. For the single-channel deconvolution we used a neural network to identify the blur operator and its parameter.

Finally, in Section 4.5, techniques for selection of the varying regularization parameter are given. It is different from conventional approach to select the regularization parameter to be invariant for the image.

The Publications IV-VII are related to this chapter.

Chapter 2

Spatially Adaptive Filtering

One of the most crucial parts in many image processing applications is a filtering performed in a signal-adaptive (which is unknown in practice) way. In particular, the spatial (temporal) adaptivity is used in denoising in order to avoid smoothing of edges. For this purpose the LPA-ICI technique is used efficiently in many applications like denoising (Katkovnik, 2002), deblurring (Katkovnik, 2005, Publications IV-VII), CFAI (Publications I-III), bispectrum filtering (Totsky, 2006), etc. More details of the approach and a variety of its applications can be found in (Katkovnik, 2006b).

The general idea of the approach can be explained as follows. Let us consider a simplified model and assume that the image to be restored $y(x)$ in (1.1) is a piece-wise constant function. Let us assume that the signal $y(x)$ has constant value on a region I (Fig.2.1a), and also that it has a different constant value outside of this region. The best unbiased estimate for all given but also not given points in this region is the sample mean of $z(x)$ within this region (Katkovnik, 2006b). The idea is trivial, but the problem to determine this region is not.

The spatially adaptive filtering used in this work includes the following components:

1. Directional linear filters design,

2. Adaptive window-size selection,

3. Aggregation of directional estimates.

We use directional sectorial estimates for every point in I in order to find the approximation of this region (Fig.2.1b). The LPA is used to design directional linear filters, while the ICI is used to select the close to optimal size in data-driven manner. The obtained directional data-adaptive estimates are fused into a single final estimate of the true image.

In some applications, for instance as in (1.7) or (1.9), observations $z(x)$ are available not for all points (considering a specific R, G, or B color channels) (Fig.2.1c).

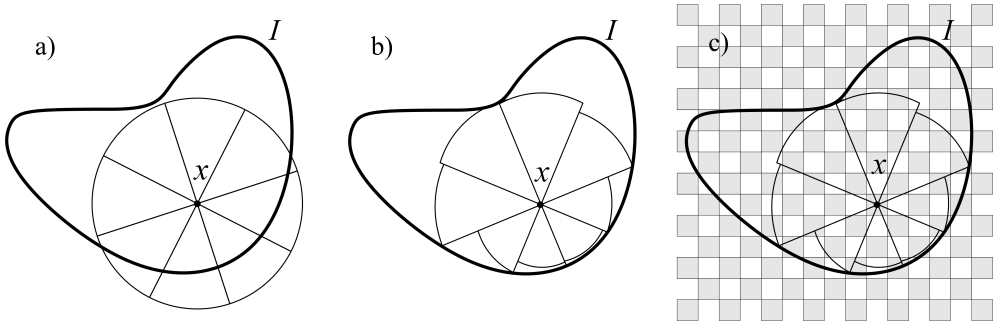

Figure 2.1: Directional (sectorial) LPA-ICI.

2.1 Design of Directional Linear Filters and Interpolators in Polynomial Basis

We introduce two sets of coordinates. Let $\tilde{X} \subseteq X \subset \mathbb{R}^2$ be a domain of coordinates $\tilde{x} \in \tilde{X}$ where the observations $z(\tilde{x})$, $\tilde{x} \in \tilde{X}$, are given, and $\bar{X} = X/\tilde{X}$ where the observations are not given. For $\tilde{x} \in \tilde{X}$ we aim to perform denoising and for $\bar{x} \in \bar{X}$ we aim to perform interpolation. Note that it is different from conventional use of LPA.

Particularly, if the domain of processing is not subsampled then $\tilde{X} = X$ that is typical for denoising problems (1.1)-(1.4). For interpolation (1.7) and (1.9), the coordinates for green channel are $\tilde{X} = X_{G_1} \cup X_{G_2}$. For red and blue we have $\tilde{X} = X_R$ and $\tilde{X} = X_B$, respectively. It can be used to design interpolation kernels. The interpolation should be produced for the missed pixels $\bar{X} = X/\tilde{X}$ if the data is downsampled $\bar{X} \neq \varnothing$.

It is emphasized that the sets $\bar{X}$ and $\tilde{X}$ are different. The set $\bar{X}$ is a collection of the "missed" points where there are no observations and the signal should be interpolated for these points. Contrary to it the set $\tilde{X}$ is a set of the observed points where values of the signal true or noisy are given.

It is assumed that $y(x)$ is a piece-wise smooth function which locally can be well approximated by polynomials (monomials)

$$\frac{1}{i!j!}x_1^i x_2^j,\ i = 0, ..., m_1,\ j = 0, ..., m_2.$$

Here, $m = (m_1, m_2)$ is the order of this set of polynomials. The maximal number of the linear independent polynomials of the order m is equal to $M = (m_1 + 1)(m_2 + 1)$.

Let $\boldsymbol{\phi}(x)$ be a set of these linear independent polynomials $\phi_k(x)$ presented as a vector-function

$$\boldsymbol{\phi}(x) = \left(\phi_0(x), \phi_1(x), ..., \phi_M(x)\right)^T,$$

where the symbol "T" denotes the transpose operation.

The polynomials in this vector are ordered according to their power defined for $x_1^i x_2^j$ as $i + j$. For instance

$$\begin{aligned}
\phi_0 &= 1, \text{ for } i+j=0,\\
\phi_1 &= x_1, \phi_2 = x_2, \text{ for } i+j=1,\\
\phi_3 &= \frac{x_1^2}{2}, \phi_4 = \frac{x_2^2}{2}, \phi_5 = x_1 x_2, \text{ for } i+j=2,\\
\phi_6 &= \frac{x_1^3}{6}, \phi_7 = \frac{x_2^3}{6}, \phi_8 = \frac{x_1^2 x_2}{2}, \phi_9 = \frac{x_1 x_2^2}{2}, \text{ for } i+j=3.
\end{aligned}$$

The LPA of $y(x)$ at the point $x \in X$ is of the form

$$\hat{y}(x, \tilde{x}) = \mathbf{C}^T \boldsymbol{\phi}(x - \tilde{x}), \tag{2.1}$$

where $\mathbf{C} = (C_0, C_1, ..., C_M)^T$ are the coefficients of this expansion to be found.

In order to find the vector $\mathbf{C}$ in (2.1) we use the weighted residual quadratic criterion:

$$J_s(x) = \sum_{\tilde{x} \in \tilde{X}} w_s(x - \tilde{x})(z(\tilde{x}) - \mathbf{C}^T \boldsymbol{\phi}(x - \tilde{x}))^2, \ x \in X \tag{2.2}$$

where $w_s(x)$ is a window function with a scaling parameter s defining the neighborhood size and the residual weights in the LPA.

In particular, typically we use the non-symmetric uniform window of the length s_1 and the width s_2 to design denoising kernels:

$$w_s(x) = \begin{cases} \frac{1}{s_1(s_2-1)}, \text{ for } 0 \le x_1 < s_1, \ |x_2| < \frac{s_2}{2}, \\ 0, \text{ otherwise,} \end{cases} \tag{2.3}$$

where $x \in \tilde{X}$, s_2 is even, $s_1 \ge 2$ and $s_2 \ge 2$. We use symmetric uniform window

$$w_s(x) = \begin{cases} \frac{1}{(s_1-1)(s_2-1)}, \text{ for } |x_1| < \frac{s_1}{2}, \ |x_2| < \frac{s_2}{2}, \\ 0, \text{ otherwise,} \end{cases} \tag{2.4}$$

to design the interpolation kernels for $x \in \bar{X}$, where $s_1 = s_2$, $s_1 \ge 2$ and $s_2 \ge 2$, for instance in Publications I,II,III. In (Paliy, 2006b), the use of directional smoothing kernels for downsampled data is considered.

Particularly, these types of windows were chosen from empirical considerations, since they showed the best performance. Other types of window functions $w_s(x)$ may be found in (Katkovnik, 2006b).

The estimates of $\mathbf{C}$ are found by minimization of (2.2)

$$\hat{\mathbf{C}}(x, s) = \arg\min_{\mathbf{C}} J_s(x).$$

The minimum condition

$$\frac{\partial J_s(x)}{\partial \mathbf{C}^T} = -2 \sum_{\tilde{x} \in \tilde{X}} w_s(x - \tilde{x})(z(\tilde{x}) - \mathbf{C}^T \boldsymbol{\phi}(x - \tilde{x}))\boldsymbol{\phi}^T(x - \tilde{x}) = 0$$

gives a system of the normal equations

$$\sum_{\tilde{x} \in \tilde{X}} w_s(x - \tilde{x}) z(\tilde{x}) \boldsymbol{\phi}^T(x - \tilde{x}) = \mathbf{C}^T \sum_{\tilde{x} \in \tilde{X}} w_s(x - \tilde{x}) \boldsymbol{\phi}(x - \tilde{x}) \boldsymbol{\phi}^T(x - \tilde{x}). \tag{2.5}$$

with the solution

$$\hat{\mathbf{C}}(x,h) = \sum_{\tilde{x}\in\tilde{X}} w_s(x-\tilde{x})\boldsymbol{\Phi}_s^{-1}\boldsymbol{\phi}(x-\tilde{x})z(\tilde{x}), \tag{2.6}$$

$$\boldsymbol{\Phi}_h = \sum_{\tilde{x}\in\tilde{X}} w_s(x-\tilde{x})\boldsymbol{\phi}(x-\tilde{x})\boldsymbol{\phi}^T(x-\tilde{x}). \tag{2.7}$$

Substituting $\hat{\mathbf{C}}(x,s)$ into (2.1) we obtain the polynomial estimate of the signal $\hat{y}_s(x,\tilde{x}) = \boldsymbol{\phi}^T(x-\tilde{x})\hat{\mathbf{C}}(x,s)$ valid in a neighborhood of the point $x \in X$. According to the idea of the LPA we use this model only for the center of the LPA, i.e. for $x = \tilde{x}$.

Then the estimate $\hat{y}_s(x,\tilde{x})$ is transformed to the final form

$$\hat{y}_s(x) = \hat{y}_s(x,x) = \hat{\mathbf{C}}^T(x,s)\boldsymbol{\phi}(0) = \sum_{\tilde{x}\in\tilde{X}} w_s(x-\tilde{x})\boldsymbol{\phi}^T(x-\tilde{x})\boldsymbol{\Phi}_s^{-1}\boldsymbol{\phi}(0)z(\tilde{x}).$$

This interpolation estimate can be rewritten in the form of convolution

$$\hat{y}_s(x) = \sum_{\tilde{x}\in\tilde{X}} g_s(x-\tilde{x})z(\tilde{x}),\ x \in X, \tilde{x} \in \tilde{X}, \tag{2.8}$$

with the convolution kernel

$$g_s(x) = w_s(x)\boldsymbol{\phi}^T(x)\boldsymbol{\Phi}_s^{-1}\boldsymbol{\phi}(0), \tag{2.9}$$

because the window $w_s(x) = 0$ for $x = \bar{x}$. Thus, the kernel $g_s(x)$ is also equal to 0 for $x = \bar{x}$, $g_s(\bar{x}) = 0$.

Using the directional windows $w_{s,\theta}$ in (2.3), (2.4) we obtain directional kernels $g_{s,\theta}$ (Katkovnik, 2006b).

In the case of interpolation, the kernels (2.9) are essentially different from the standard LPA kernels (Katkovnik, 2006b) by zeros used to fill the kernel support at the positions of the missed observations.

Note that the kernels g_s essentially depend on a given interpolation grid.

2.2 Adaptive Window-Size Selection

2.2.1 Motivation

The estimate of y in (1.1) is found in the form:

$$\hat{y}_s(x) = (z \circledast g_s)(x),$$

where s is the scale parameter of the filter (2.9).

The quadratic error between the true and estimated signal as a function of the scale s

$$J(s) = \|y - \hat{y}_s\|_2^2.$$

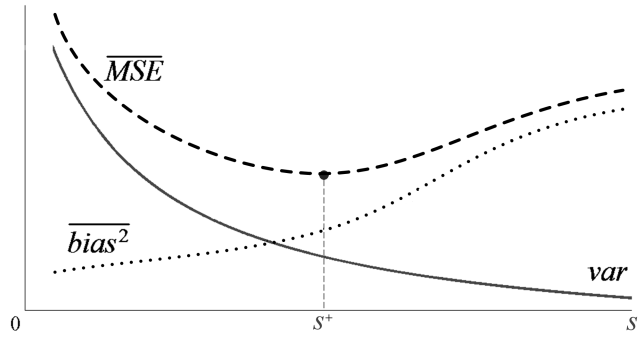

Figure 2.2: MSE, bias, and variance as a function of the scale parameter.

The expectation of J may be rewritten as the sum of quadratic bias and variance:

$$\begin{aligned} E\left[J(s)\right] &= E\left[\sum_{x\in X}\left(y-g_s\circledast\left(y+n\right)\right)^2\right]= \\ &= \sum_{x\in X}E\left[\left(y-g_s\circledast\left(y+n\right)\right)^2\right]= \\ &= \sum_{x\in X}E\left[\left(\left(y-g_s\circledast y\right)-g_s\circledast n\right)^2\right]= \\ &= \sum_{x\in X}\left(y-g_s\circledast y\right)^2+\sum_{x\in X}E\left[\left(g_s\circledast n\right)^2\right]= \\ &= \sum_{x\in X}\left(y-g_s\circledast y\right)^2+\sum_{x\in X}g_s^2\circledast\sigma^2=\mathrm{bias}^2\left(s\right)+\mathrm{var}\left(s\right). \end{aligned} \tag{2.10}$$

Here, $\mathrm{bias}^2\left(s\right)=\left\|y-g_s\circledast y\right\|_2^2$ is the systematic error which is an increasing function of s, and $\mathrm{var}\left(s\right)=\sum_{x\in X}g_s^2\circledast\sigma^2$ is the stochastic error which is a decreasing function of s.

The natural idea is to find such a scale s^+ that minimizes the global quadratic error (2.10). Different approaches were proposed and tested in (Hurvich, 1998; Katkovnik, 1985; Simonoff, 1998) in order find to such optimal scale s^+.

Contrary to that, we aim to find such a scale $s^+(x)$ that minimizes (2.10) in a pointwise manner:

$$\begin{aligned} E\left[J(x,s)\right] &= E\left[\left(y(x)-\left(g_s\circledast z\right)\left(x\right)\right)^2\right]= \\ &= \left(y(x)-\left(g_s\circledast y\right)\left(x\right)\right)^2+\left(g_s^2\circledast\sigma^2\right)\left(x\right)= \\ &= \mathrm{bias}^2\left(x,s\right)+\mathrm{var}\left(x,s\right) \end{aligned} \tag{2.11}$$

at every $x\in X$. Here, $\mathrm{bias}\left(x,s\right)=y(x)-\sum_{t\in X}g_s(t)y(x-t)$ is an increasing function of s and $\mathrm{var}\left(x,s\right)=\sum_{t\in X}g_s^2(t)\sigma^2(x-t)$ is a decreasing function of s (Katkovnik, 2006b) at every point x, as it is shown in Fig.2.2.

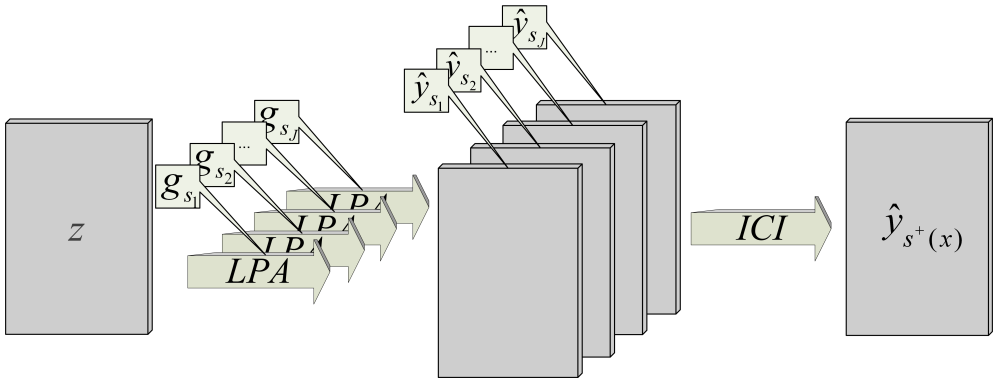

Figure 2.3: Selection of point-wise adaptive estimates by the LPA-ICI.

Various developments of this idea and statistical rules for adaptation can be found in (Klemela, 2001; Lepski, 1997; Nemirovski, 2000; Polzehl, 2000). Using the point-wise scale selection showed significant improvement in quality of restoration comparing it with the invariant scale selection. Larger review of this type of methods can found in (Katkovnik, 2006b).

In our works we used point-wise scale selection by statistical multiple hypothesis testing based on the intersection of confidence intervals (the ICI rule).

2.2.2 Multiple Hypothesis Testing based on Confidence Intervals

A set of the image estimates of different scales s and different directions θ are calculated by the convolution

$$\widehat{y}_{s,\theta}(x) = (z \circledast g_{s,\theta})(x), \tag{2.12}$$

for $s \in S = \{s_1, s_2, ..., s_J\}$, where $s_1 < s_2 < ... < s_J$, and $\theta \in \Theta$ (see Fig.2.3).

The ICI rule is the algorithm for selection of the scale (close to the optimal least-square value) for every pixel x. This algorithm uses a sequence of confidence intervals

$$D_{i,\theta} = \left[\widehat{y}_{s,\theta}(x) - \Gamma\sigma_{\widehat{y}_{s,\theta}},\, \widehat{y}_{s,\theta}(x) + \Gamma\sigma_{\widehat{y}_{s,\theta}}\right],\ s \in S, \tag{2.13}$$

where $\Gamma > 0$ is a threshold parameter for the ICI, $\widehat{y}_{s,\theta}$ is the estimate of y, $\sigma_{\widehat{y}_{s,\theta}}$ is the standard deviation of this estimate, and i is the index of s in S (Fig.2.4).

The ICI rule defines the adaptive scale as the largest s^+ of those scales in S whose estimate does not differ significantly from the estimates corresponding to the smaller window sizes. This rule is stated as follows: consider the intersection of the confidence intervals $I_{i_s} = \bigcap_{i=1}^{i_s} D_{i,\theta}$ and let i_s^+ be the largest of the indices of s for which I_{i_s} is non-empty (Fig.2.4). Then the optimal scale s^+ is defined as $s^+ = s_{i_s^+}$ and, as result, the optimal scale estimate is $\widehat{y}_{s^+,\theta}(x)$ (Fig.2.3).

The parameter Γ is a key element of the algorithm as it says when a difference between estimate deviations is large or small. Too large value of this parameter leads to signal oversmoothing and too small value leads to undersmoothing. Theoretical aspects about the value of this parameter can be found in (Katkovnik, 2006b). However, usually in practice, this parameter is treated as a fixed design parameter.

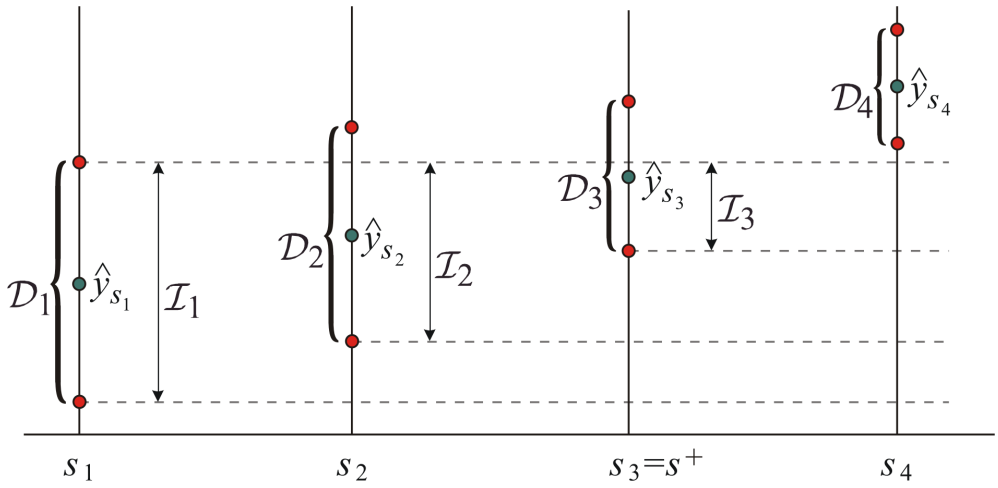

Figure 2.4: Illustration of the ICI rule principle.

The ICI rule provides mean-square convergence of the adaptive estimates to the true signal values as the number of observations increases (as it is shown in (Lepski, 1997; Goldenshluger, 1997; Katkovnik, 2006b, Chapter 6)).

Note that in the standard form of the ICI the standard deviation of the estimate is calculated according to (2.11):

$$\sigma_{\hat{y}_{s,\theta}}(x) = \sqrt{(\sigma^2 \circledast g^2_{s,\theta})(x)}, \tag{2.14}$$

where σ is a given standard deviation of the additive observation noise in the model (1.1).

This approach was used for filtering the noise of the models (1.3)-(1.5).

However, there are applications where either standard deviation or model of noise are unknown. For instance, in Publications I,III, we deal with the data where the noise is only a convenient form for modeling of the interpolation errors that are actually nonrandom. Thus, the standard deviation of the estimate $\widehat{y}_{s,\theta}$ is estimated at every position x over the directional local area. It is calculated as the weighted mean of the squared errors between the estimate and the observations in the directional neighborhood of the pixel x :

$$\sigma_{\hat{y}_{s,\theta}}(x) = \sqrt{((z - \hat{y}_{s,\theta})^2 \circledast g^2_{s,\theta})(x)}, \tag{2.15}$$

where the weights are defined by $g_{s,\theta}$ used in (2.12).

Equation (2.15) gives the results close to (2.14) assuming that the LPA estimates $\hat{y}_{s,\theta}$ fit to the underlying data and that squared difference is mainly due to error variance (and not bias). This approach is used only in demosaicing problems where we do not impose any prior for the noise.

2.3 Aggregation of Directional Estimates

This optimization of s for each of the directional estimates yields the adaptive scales $s^+(\theta)$ for each direction θ. The union of the supports of $g_{s^+(\theta),\theta}$ is considered as an approximation of the best local vicinity of x in which the estimation model fits the data. The final estimate is calculated as a linear combination of the obtained adaptive directional estimates $\widehat{y}_{s^+,\theta}(x)$.

The final LPA-ICI estimate $\widehat{y}(x)$ combined from the directional ones is computed as the weighted mean

$$\hat{y}(x) = \sum\nolimits_{\theta\in\Theta} \hat{y}_{s^+,\theta}(x) w_\theta,\ w_\theta = \frac{\sigma^{-2}_{\hat{y}_{s^+,\theta}}}{\sum_{\theta\in\Theta} \sigma^{-2}_{\hat{y}_{s^+,\theta}}}, \tag{2.16}$$

with the variance $\sigma^2_{\hat{y}}$ of the final estimate $\hat{y}(x)$ computed for simplicity as

$$\sigma^2_{\hat{y}} = \left(\sum\nolimits_{\theta\in\Theta} \sigma^{-2}_{\hat{y}_{s^+,\theta}}\right)^{-1}. \tag{2.17}$$

The weights in (2.16) follow from the maximum likelihood (ML) estimation provided that the estimates $\hat{y}_{s^+,\theta}(x)$ with variances $\sigma^2_{\hat{y}_{s^+,\theta}}$ are unbiased and independent. If these conditions are fulfilled then for Gaussian noise this fusing gives minimal mean square error.

It is convenient to treat this complex LPA-ICI multidirectional algorithm as an adaptive filter with the input z and the output $\hat{y}$. The input-output equation can be written as

$$\hat{y} = \mathcal{LI}\{z\} \tag{2.18}$$

by denoting the calculations imbedded in this algorithm as an $\mathcal{LI}$ operator.

Chapter 3

Demosaicing of Data Acquired by CCD/CMOS Sensor of Digital Camera

This chapter is based on Publications I, II, III, where the problem of demosaicing is considered for both the noiseless and noisy data. A novel CFAI technique was proposed in Publications I, II, that outperforms many well-known state-of-the-art techniques by both objective numerical and subjective visual criteria evaluation. Also, an integrated CFAI and denoising approach was proposed in Publications I, III. In Publication I we showed its efficiency and applicability for real digital imaging sensor data where the photon-counting noise model (among others) was taken into consideration as an important intrinsic degradation of data. We showed that this approach is more efficient than conventional divide-and-conquer one when the denoising and demosaicing are considered as two independent problems. The efficiency of this approach was shown by both artificial and real data simulations.

3.1 Problem Formulation

The common approach in single-chip digital cameras is to use a CFA to sample different spectral components like red, green, and blue. The sensor records one value per pixel location. The resulting image is a gray-scale mosaic-like one. Demosaicing algorithm interpolates sets of complete red, green, and blue values for each pixel, to make an RGB image. Independent interpolation of color channels usually leads to drastic color distortions. The way to effectively produce a joint color interpolation plays a crucial role for demosaicing.

Modern efficient algorithms exploit several main facts. The first is the high correlation between the red, green, and blue channels for natural images. As a result all three color channels are very likely to have the same texture and edge locations. The second fact is that digital cameras use the CFA in which the green channel is sampled at the higher rate than the red and blue channels. Therefore, the green channel is less likely to be aliased, and details are preserved better in the green channel than in the red and blue

channels (Gunturk, 2002). Also, the CFA is a crucial element in design of single-sensor digital cameras. Different characteristics in design of CFA affect both performance and computational efficiency of the demosaicking solution (Lukac, 2004e; Adams, 1998a). The fundamentals about digital color image acquisition with single-sensor can be found in (Lukac, 2006b; Parulski, 2002).

Considering the fact that the Bayer CFA (Bayer, 1976) (see Fig.1.2a) is one of the most often exploited today, in this work we focus on techniques for this particular CFA.

3.1.1 Correlation Models in Demosaicing

There are two basic interplane correlation models: the color difference rule (Laroche, 1994; Hamilton, 1997) and the color ratio rule (Kimmel, 1999; Lukac, 2004a). The first model asserts that intensity differences between red, green, and blue channels are slowly varying, that is the differences between color channels are locally nearly-constant (Adams, 1998b; Laroche, 1994; Hamilton, 1997; Li, 2005; Hirakawa, 2005a; Zhang, 2005; Lukac, 2004b; Lukac, 2005b). Thus, they contain low-frequency components only, making the interpolation using the color differences easier (Hirakawa, 2005a).

The second correlation model is based on the assumption that the ratios between colors are constant over some local regions (Kimmel, 1999; Lukac, 2004a). This hypothesis follows from the Lambert's law that if two colors have equal chrominance then the ratios between the intensities of three color components are equal (Hirakawa, 2005a; Kimmel, 1999).

The first difference-based correlation model is found to be more efficient than the ratio-based model and, therefore, exploited more often in practice. Moreover, the color-difference rule can be implemented with a lower computational cost and better fits linear interpolation modeling (Li, 2005).

Other correlation models used in the demosaicing literature can be found in (Keren, 1999; Lukac, 2004c; Lukac, 2006a).

3.1.2 Demosaicing Methods

Many demosaicing algorithms (Laroche, 1994; Hamilton, 1997; Kimmel, 1999; Lukac, 2004d) incorporate edge directionality in interpolation. Interpolation along object boundaries is preferable versus interpolation across these boundaries for most of the models.

We will classify the demosaicing techniques into two categories: noniterative (Adams, 1998b; Laroche, 1994; Hamilton, 1997; Malvar, 2004; Zhang, 2005; Menon, 2007; Taubman, 2000; Pei, 2003), and iterative (Gunturk, 2002; Kimmel, 1999; Lukac, 2004a; Li, 2005; Hirakawa, 2005a). There are also alternative ways of this classification, for instance considered in (Gunturk, 2005).

Noniterative demosaicing techniques basically rely on the idea of edge-directed interpolation. In a variety of color demosaicing techniques the gradient estimates analysis plays a central role in reconstructing sharp edges. The exploitation of intraplane correlation typically is done by estimating local gradients under the main assumption that locally the difference between colors is nearly constant. Directional filtering is the most popular approach for color demosaicing that produces competitive results. The best known directional interpolation scheme is perhaps the method proposed by Hamilton and Adams (Hamilton, 1997). The authors use the gradients of blue and red channels

as the correction terms to interpolate the green channel. Similar idea is exploited effectively in (Laroche, 1994; Malvar, 2004; Wu, 2004a) but with a different aggregation of vertical and horizontal estimates. Directional filtering with a posteriori decision is also effectively exploited for demosaicing in (Menon, 2007). A novel efficient data adaptive filtering concept in conjunction with the refined spectral models is proposed in (Lukac, 2005a) for demosaicing.

In addition, there are approaches based on: pattern recognition (Cok, 1994), restoration algorithms (Taubman, 2000; Trussel, 2005), sampling theory (Adams, 1998b) (see (Gunturk, 2005) for more details), the regularization theory (Keren, 1999), the Bayesian approach (Brainard, 1994; Vega, 2005), demosaicing in frequency domain (Alleyson, 2005; Alleysson, 2002; Dubois, 2005). Taubman (Taubman, 2000) proposed an efficient preconditioned approach of Bayesian demosaicing that is used in some digital cameras today.

A number of iterative demosaicing techniques have been proposed recently (Gunturk, 2002; Kimmel, 1999; Lukac, 2004a; Li, 2005; Hirakawa, 2005a). It has been observed that iterative demosaicing techniques often demonstrate higher quality restoration than noniterative ones at the price of increased computational cost. The refinement of green pixels and red/blue pixels are mutually dependent and jointly beneficial to each other. An iterative strategy is exploited in (Li, 2005) in order to handle this correlation.

A new idea has been proposed and effectively used in the recent papers (Li, 2005; Zhang, 2005), where the differences between initial directional interpolated estimates of color intensities are filtered. In the paper (Zhang, 2005) the concept of directional "demosaicing noise" was introduced for the interpolation errors. A filtering procedure is exploited to remove this noise and obtain the improved estimates of the differences between the chrominance and luminance channels as result of denoising procedure.

Our approach is motivated by the work (Zhang, 2005) where the demosaicing is reformulated as the denoising problem. The differences between color channels are considered as noisy signals and the term noise is used for interpolation errors. We use a directional anisotropic scale-adaptive denoising technique to remove the errors, instead of the fix-length filter used in (Zhang, 2005). The exploited technique is based on the LPA. The adaptivity to data is provided by the multiple hypothesis testing based on the ICI rule which is applied to select varying scales (window sizes) of LPA (Katkovnik, 1999; Katkovnik, 2002; Katkovnik, 2006b). The main problem that appears is that the LPA-ICI requires a priori knowledge about the variance of the noise. However, the "demosaicing noise" cannot be considered as a stationary one and its statistics are unknown, since the errors strongly depend on the signal. For instance, its variance near edges may be significantly higher than at smooth areas and, therefore, it is estimated locally. In such a way, we aim to improve results with a filtering that is adaptive to image irregularities, e.g. edges.

3.1.3 Demosaicing of Noisy Sensor Data

In many applications the observed data is noisy. In particular, it is known that the raw data from the sensor is corrupted by signal-dependant noise (Hirakawa, 2005b; Foi, 2007a; Foi, 2006b) (for details see Section 1.2.1).

The problem is to restore the true observation scene from the noisy subsampled data. The conventional approach used in image restoration chains for raw sensor data

exploits successive independent denoising and demosaicing steps. Denoising aims to remove the noise, and demosaicing performs interpolation of missing colors assuming that the processed data is noiseless.

In case of treating the original noisy observed data the denoising done first was proven to be more efficient. Some post-CFAI and pre-CFAI denoising techniques are compared in (Kalevo, 2002). The authors show the possibility to reduce more noise with the pre-CFAI denoising than with the post-CFAI denoising. Also, the computational costs can be lower with the pre-CFAI denoising than with the post-CFAI one. The model of noise plays a crucial role in image denoising, which is known before CFAI but not after CFAI.

Noting that image interpolation and image denoising are both estimation problems, the papers (Hirakawa, 2005b; Hirakawa, 2005c) propose a unified approach to performing demosaicing and image denoising jointly, where the noise is modeled as multiplicative Gaussian. The multi-colored demosaicing/denoising problem was simplified to a single-color denoising problem. The authors verified that performing demosaicing and denoising jointly is more effective than treating them independently (Hirakawa, 2005b). Ramanath and Snyder (Ramanath, 2003) proposed a bilateral filtering based scheme to denoise, sharpen and demosaic the image simultaneously.

Most denoising techniques are designed for stationary Gaussian-distributed noise. We propose a technique specially designed for filtering not only Gaussian but also more general signal-dependant noise. It is natural to adopt the CFAI proposed for noiseless case to the noisy one since it already considers demosaicing as a denoising problem. The crucial difference is that here all pixels have to be either denoised or interpolated from noisy observations. Therefore, filtering only the difference between directional interpolated estimates of color intensities is not sufficient and thus we decorrelate them by calculating both sum and difference, and then apply the LPA-ICI denoising to these pairs of components. The advantage of this approach is that different color channels are used for both denoising and interpolation, filtering also "demosaicing noise" that is present implicitly on the image. The proposed technique results in better utilization of data, in better performance and quality of image restoration, and lower complexity of implementation. These issues are of crucial importance especially for small mobile devices, where the impact of noise is particularly severe because of the constrained power and hardware.

3.2 Proposed Demosaicing Based on the Adaptive LPA-ICI

In this section we consider image formation model (1.7). Here, only the exploited idea is shown while all the details can be found in Publications I, II.

As in (Zhang, 2005), our algorithm consists of the following steps: initialization, filtering, and interpolation. At the initialization, the approximate color estimates are obtained and directional differences between $G - R$ and $G - B$ are calculated. These differences are considered as degraded by noise and filtered. The modified version of the LPA-ICI algorithm is used for this filtering. Finally, the obtained estimates are exploited to calculate missing color values at each pixel.

Firstly we calculate the directional (horizontal and vertical) estimates of the green channel at every point $(x_1, x_2) \in X$ following the rules of Hamilton-Adams algorithm (Hamilton, 1997). Interpolation of G at R positions $(x_1, x_2) \in X_R$ is done as follows:

$$\tilde{G}_h(x_1,x_2) = \frac{1}{2}\left(G(x_1+1,x_2)+G(x_1-1,x_2)\right)+ \tag{3.1}$$
$$+\frac{1}{4}\left(-R(x_1-2,x_2)+2R(x_1,x_2)-R(x_1+2,x_2)\right),$$
$$\tilde{G}_v(x_1,x_2) = \frac{1}{2}\left(G(x_1,x_2+1)+G(x_1,x_2-1)\right)+ \tag{3.2}$$
$$+\frac{1}{4}\left(-R(x_1,x_2-2)+2R(x_1,x_2)-R(x_1,x_2+2)\right).$$

Here h and v stand for horizontal and vertical estimates. Similarly to (3.1)-(3.2), the initial directional estimates for the red channel R at the green positions G ($(x_1,x_2)\in X_{G_1}$ or $(x_1,x_2)\in X_{G_2}$) are interpolated as:

$$\tilde{R}_h(x_1,x_2) = \frac{1}{2}\left(R(x_1+1,x_2)+R(x_1-1,x_2)\right)+ \tag{3.3}$$
$$+\frac{1}{4}\left(-G(x_1-2,x_2)+2G(x_1,x_2)-G(x_1+2,x_2)\right),$$
$$\tilde{R}_v(x_1,x_2) = \frac{1}{2}\left(R(x_1,x_2+1)+R(x_1,x_2-1)\right)+ \tag{3.4}$$
$$+\frac{1}{4}\left(-G(x_1,x_2-2)+2G(x_1,x_2)-G(x_1,x_2+2)\right).$$

As a result of (3.1)-(3.2) and (3.3)-(3.4) we obtain at the every horizontal line of red and green values two sets of true (from data) and estimated (interpolated) green and red values:

$$\begin{array}{cccccccc} ... & \tilde{G}_h & G & \tilde{G}_h & G & \tilde{G}_h & ... \\ ... & R & \tilde{R}_h & R & \tilde{R}_h & R & ... \end{array}.$$

Similar calculations are produced for the vertical lines.

Let us denote the spatial coordinates as $x=(x_1,x_2)$. At every point the differences between the true values $R(x)$ and $G(x)$, and the directional estimates $\tilde{G}_h(x)$ and $\tilde{R}_h(x)$, are calculates as follows:

$$\tilde{\Delta}^h_{g,r}(x) = G(x)-\tilde{R}_h(x),\ x\in X_{G_1}, \tag{3.5}$$

and

$$\tilde{\Delta}^h_{g,r}(x) = \tilde{G}_h(x)-R(x),\ x\in X_R, \tag{3.6}$$

for the horizontal direction. For the vertical direction the analogous computations are:

$$\tilde{\Delta}^v_{g,r}(x) = G(x)-\tilde{R}_v(x),\ x\in X_{G_2}, \tag{3.7}$$

and

$$\tilde{\Delta}^v_{g,r}(x) = \tilde{G}_v(x)-R(x),\ x\in X_R. \tag{3.8}$$

As in (Zhang, 2005), we assume for further filtering that these differences between the intensities of different color channels can be presented as the sums of the true values of the underlying differences and errors:

$$\tilde{\Delta}^h_{g,r}(x) = \Delta_{g,r}(x)+\varepsilon^h_{g,r}(x), \tag{3.9}$$
$$\tilde{\Delta}^v_{g,r}(x) = \Delta_{g,r}(x)+\varepsilon^v_{g,r}(x), \tag{3.10}$$

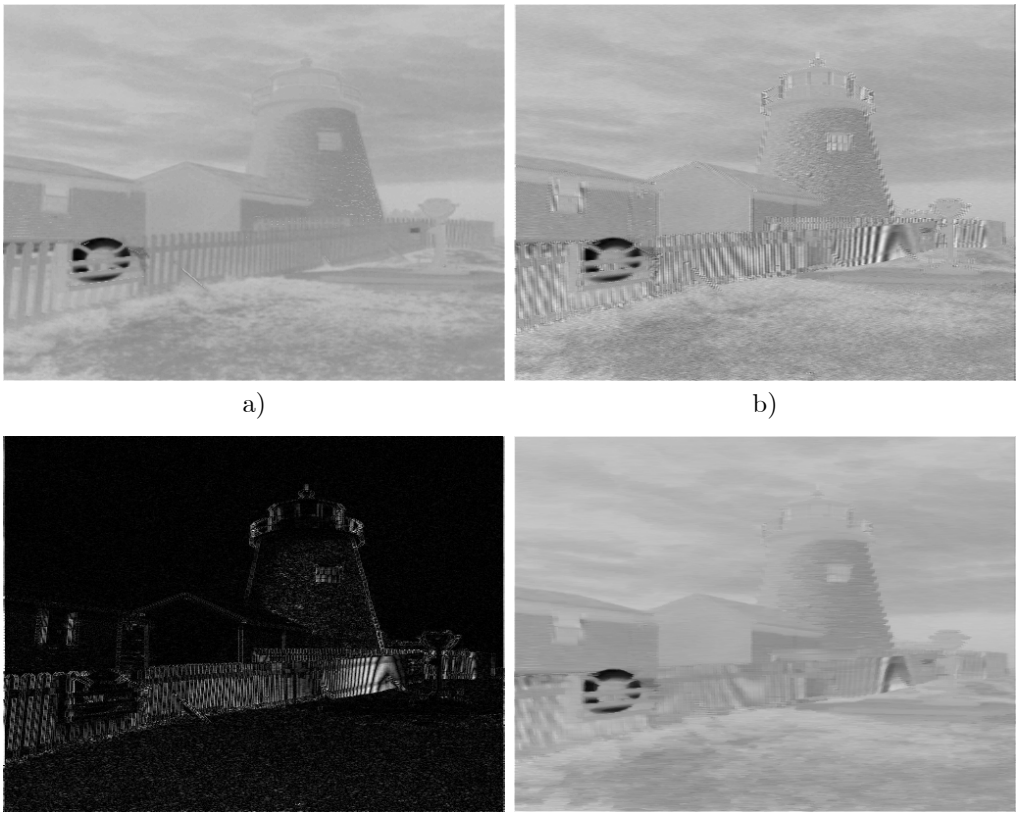

a) b)

c) d)

Figure 3.1: The horizontal difference between G and R colors: a) The true difference between the values R and G; b) The difference $\tilde{\Delta}^h_{g,r}$ between the true values R and G, and the directional color estimates G_h and R_h; c) The absolute values of the errors $\varepsilon^h_{g,r}$; d) The filtered difference $\tilde{\Delta}^v_{g,r}$ with LPA-ICI in horizontal direction.

where $\varepsilon_h(x)$ and $\varepsilon_v(x)$ are considered as random demosaicing noise; $\Delta_{g,r}(x)$ is the true difference between green and red color channels.

The blue channel B is treated in the same way and we calculate the directional differences $\tilde{\Delta}^h_{g,b}(x)$ and $\tilde{\Delta}^v_{g,b}(x)$.

In such way the problem of interpolation is reformulated into the denoising one.

The LPA-ICI filtering is used for all noisy estimates $\tilde{\Delta}^h_{g,r}(x)$, $\tilde{\Delta}^v_{g,r}(x)$ for R, and $\tilde{\Delta}^h_{g,b}(x)$, $\tilde{\Delta}^v_{g,b}(x)$ for B. We consider this input data in the form (1.1) in order to use this filtering in the form applicable for any input data as the adaptive filter $\mathcal{LI}\{\cdot\}$ (2.18) with the input z and the output $\hat{y}$. The input-output equation can be written as $\hat{y} = \mathcal{LI}\{z\}$ by denoting the calculations imbedded in this algorithm as an $\mathcal{LI}$ operator. It results in obtaining the following estimates $\hat{\Delta}^h_{g,r} = \mathcal{LI}\left\{\tilde{\Delta}^h_{g,r}\right\}$, $\hat{\Delta}^v_{g,r} = \mathcal{LI}\left\{\tilde{\Delta}^v_{g,r}\right\}$, $\hat{\Delta}^h_{g,b} = \mathcal{LI}\left\{\tilde{\Delta}^h_{g,b}\right\}$, and $\hat{\Delta}^v_{g,b} = \mathcal{LI}\left\{\tilde{\Delta}^v_{g,b}\right\}$. The final RGB image is restored from these

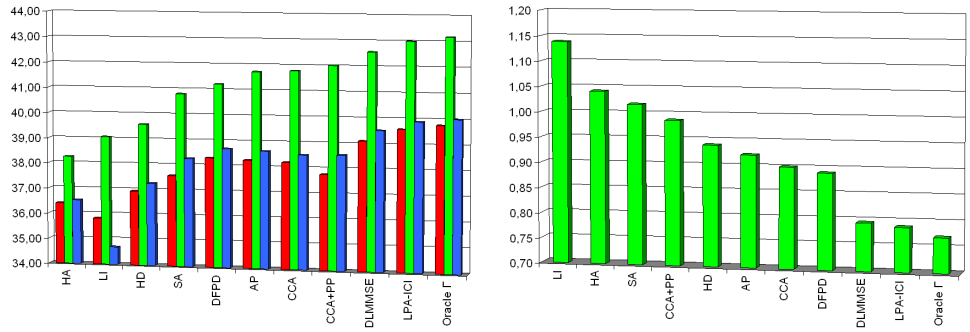

Figure 3.2: Mean values of PNSR (left) and S-CIELAB (right) for the Kodak test set of 24 images. The following techniques are compared: HA (Hamilton, 1997), LI (Malvar, 2004), HD (Hirakawa, 2005a), SA (Li, 2005), DFPD (Menon, 2007), AP (Gunturk, 2002), CCA (Lukac, 2004d), CCA+PP is a demosaicing approach (Lukac, 2004d) with postprocessing (Lukac, 2004a), DLMMSE based interpolation (Zhang, 2005), proposed LPA-ICI interpolation, "Oracle Γ" is the proposed LPA-ICI interpolation with the optimal threshold parameter Γ.

filtered estimates (see Publications I, II).

It is essential that the standard deviations of estimates of (3.9)-(3.10) for the ICI are estimated locally as in (2.15).

Fig.3.1 illustrates the difference $\tilde{\Delta}^h_{g,r}$ between the horizontal estimates of green and red color channels for the Lighthouse test image. It is clearly seen that $\tilde{\Delta}^h_{g,r}$ (Fig.3.1b) drastically suffers from aliasing comparing it to the true $G-R$ color difference, calculated at G, R lines only (Fig.3.1a). The largest errors are near edges and image details (Fig.3.1c). We aim to remove these errors by an adaptive filtering using the LPA-ICI in particular (for details see Chapter 2).

Our study shows that the "demosaicing noise" is not white and strongly localized. At different parts of an image the power of noise is different. It justifies the use of the local estimates of the variance in (2.15). As a result, suppression of color distortions becomes much better in terms of both numerical and visual evaluation.

In our example, the filtered difference $\hat{\Delta}^h_{g,r}$ is shown in Fig. 3.1d.

3.3 Adaptation of Color Filter Array Interpolation to Noisy Data

For the demosaicing of noisy data we consider the model (1.9) with the noise term as in (1.3)-(1.5). Details of the algorithm can be found in Publications I, III while here we focus on the difference in initialization part of the demosaicing for noiseless data.

Let $z(x)$ be a sampled noisy observation signal (1.9). Considering the fact that not only interpolation has to be performed in order to reconstruct y_{RGB} but also denoising at every point, the initialization differs from the one presented in Section 1.2.3. One way is to exploit a denoising before CFAI and then perform interpolation treating the obtained data as noiseless. This approach is trivial but may be significantly improved. We aim to perform both denoising and interpolation exploiting the high correlation between color

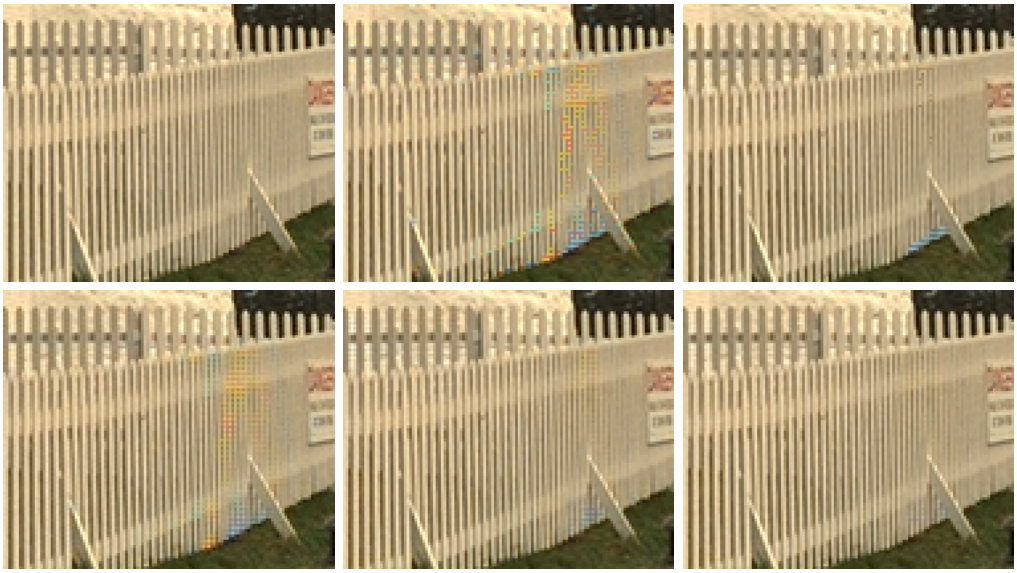

Figure 3.3: Fragment of the Lighthouse test image (from left to right and from top to bottom): True image; HA (Hamilton, 1997) PSNR=(36.67 38.34 37.09); HD (Hirakawa, 2005a) PSNR=(37.60 39.51 37.09); AP (Gunturk, 2002) PSNR=(38.70 42.12 39.80); DLMMSE based interpolation (Zhang, 2005) PSNR=(39.83 42.77 40.93); Proposed LPA-ICI based interpolation PSNR=(40.32 43.36 41.48).

channels and consider not only the differences between color channels but also their sums. Hence, the initialization (3.5)-(3.8) is transformed in the following way, where knowledge about σ_{bayer} plays crucial role.

Assuming that the color channels are correlated, we decorrelate them using the following summation and differentiation linear operators working in the horizontal direction which is different from (3.5)-(3.8):

$$\begin{pmatrix} \tilde{\Phi}^h_{g,r}(x) \\ \tilde{\Delta}^h_{g,r}(x) \end{pmatrix} = \begin{pmatrix} 1 & 1 \\ 1 & -1 \end{pmatrix} \begin{pmatrix} z(x) \\ \tilde{R}_h(x) \end{pmatrix}, \ (x) \in X_{G_1}, \tag{3.11}$$

and

$$\begin{pmatrix} \tilde{\Phi}^h_{g,r}(x) \\ \tilde{\Delta}^h_{g,r}(x) \end{pmatrix} = \begin{pmatrix} 1 & 1 \\ 1 & -1 \end{pmatrix} \begin{pmatrix} \tilde{G}_h(x) \\ z(x) \end{pmatrix}, \ (x) \in X_R. \tag{3.12}$$

For the vertical directions, the corresponding $\hat{\Phi}^v_{g,r}(x)$ and $\hat{\Delta}^v_{g,r}(x)$ are calculated as follows:

$$\begin{pmatrix} \tilde{\Phi}^v_{g,r}(x) \\ \tilde{\Delta}^v_{g,r}(x) \end{pmatrix} = \begin{pmatrix} 1 & 1 \\ 1 & -1 \end{pmatrix} \begin{pmatrix} z(x) \\ \tilde{R}_v(x) \end{pmatrix}, \ (x) \in X_{G_2}, \tag{3.13}$$

and

$$\begin{pmatrix} \tilde{\Phi}^v_{g,r}(x) \\ \tilde{\Delta}^v_{g,r}(x) \end{pmatrix} = \begin{pmatrix} 1 & 1 \\ 1 & -1 \end{pmatrix} \begin{pmatrix} \tilde{G}_v(x) \\ z(x) \end{pmatrix}, \ (x) \in X_R. \tag{3.14}$$

Here, $\tilde{R}_h, \tilde{G}_h, \tilde{R}_v, \tilde{G}_v$ are calculated similarly to (3.1)-(3.4) for the noisy data (1.9). Let us stress that in (3.1)-(3.4) G and R notations are used because $z(x) = G(x)$, $x \in X_{G_1} \cup X_{G_2}$, and $z(x) = R(x)$, $x \in X_R$.

We assume for further filtering that the directional differences between the green and red signals $\tilde{\Delta}^h_{g,r}(x)$, $\tilde{\Delta}^v_{g,r}(x)$ can be presented as the sums of the true values of these differences and the errors including the random observation noise in (1.9) and what has been called the "directional demosaicing noise" (Zhang, 2005):

$$\tilde{\Delta}^h_{g,r}(x) = \Delta^h_{g,r}(x) + \varepsilon^{\Delta,h}_{g,r}(x),\ x \in X_R \cup X_{G_1}, \tag{3.15}$$

$$\tilde{\Delta}^v_{g,r}(x) = \Delta^v_{g,r}(x) + \varepsilon^{\Delta,v}_{g,r}(x),\ x \in X_R \cup X_{G_2}, \tag{3.16}$$

where $\varepsilon^{\Delta,h}_{g,r}(x)$ and $\varepsilon^{\Delta,v}_{g,r}(x)$ are the errors and $\Delta^h_{g,r}(x)$ and $\Delta^v_{g,r}(x)$ are the true values of the corresponding differences.

The same modeling with the additive errors is assumed for the sums $\tilde{\Phi}^h_{g,r}(x)$ and $\tilde{\Phi}^v_{g,r}(x)$:

$$\tilde{\Phi}^h_{g,r}(x) = \Phi^h_{g,r}(x) + \varepsilon^{\Phi,h}_{g,r}(x),\ x \in X_R \cup X_{G_1}, \tag{3.17}$$

$$\tilde{\Phi}^v_{g,r}(x) = \Phi^v_{g,r}(x) + \varepsilon^{\Phi,v}_{g,r}(x),\ x \in X_R \cup X_{G_2}, \tag{3.18}$$

where $\Phi^h_{g,r}(x)$ and $\Phi^v_{g,r}(x)$ are the true values of the sums and $\varepsilon^{\Phi,h}_{g,r}(x), \varepsilon^{\Phi,h}_{g,r}(x)$ are the errors.

It can be verified that (3.11)-(3.14) can be computed as a convolution of $z(x)$ with the linear 1D FIR filters $f_\Phi = (-1, 2, 6, 2, -1)/4$ and $f_\Delta = (-1, 2, -2, 2, -1)/4$. For calculations of the variance of the sums $\tilde{\Phi}^h_{g,r}, \tilde{\Phi}^v_{g,r}$, and differences $\tilde{\Delta}^h_{g,r}, \tilde{\Delta}^v_{g,r}$ in (3.11)-(3.14) we assume that the random observation noise *is dominant* in the errors in (3.15)-(3.18). Then the observation noise from (1.9) gives the following standard deviations for the sums $\tilde{\Phi}^h_{g,r}, \tilde{\Phi}^v_{g,r}$ (3.17),(3.18):

$$\sigma_{\tilde{\Phi}^h_{g,r}}(x) = \sqrt{\left(\sigma^2_{bayer} \circledast f^2_\Phi\right)(x)},\ x \in X_R \cup X_{G_1}, \tag{3.19}$$

$$\sigma_{\tilde{\Phi}^v_{g,r}(x)} = \sqrt{\left(\sigma^2_{bayer} \circledast \left(f^T_\Phi\right)^2\right)(x)},\ x \in X_R \cup X_{G_2}, \tag{3.20}$$

where the symbol "^{T}" denotes the transpose operation and $\sigma_{bayer}(x)$ is the noise standard deviation in (1.9). The standard deviations for the differences $\tilde{\Delta}^h_{g,r}, \tilde{\Delta}^v_{g,r}$ corresponding to the observation noise are computed as

$$\sigma_{\tilde{\Delta}^h_{g,r}}(x) = \sqrt{\left(\sigma^2_{bayer} \circledast f^2_\Delta\right)(x)},\ x \in X_R \cup X_{G_1}, \tag{3.21}$$

$$\sigma_{\tilde{\Delta}^v_{g,r}(x)} = \sqrt{\left(\sigma^2_{bayer} \circledast \left(f^T_\Delta\right)^2\right)(x)},\ x \in X_R \cup X_{G_2}. \tag{3.22}$$

The blue channel B is treated in the same way in order to calculate the directional sums and differences $\tilde{\Delta}^h_{g,b}$, $\tilde{\Delta}^v_{g,b}$, $\tilde{\Phi}^h_{g,b}$, $\tilde{\Phi}^v_{g,b}$ for $(G - B)$ and $(G + B)$.

The spatially adaptive LPA-ICI filtering $\mathcal{LI}\{\cdot\}$ (2.18) is exploited to denoise $\tilde{\Delta}^h_{g,r}$, $\tilde{\Delta}^v_{g,r}$, $\tilde{\Phi}^h_{g,r}$, $\tilde{\Phi}^v_{g,r}$ for R color channel, and $\tilde{\Delta}^h_{g,b}$, $\tilde{\Delta}^v_{g,b}$, $\tilde{\Phi}^h_{g,b}$, $\tilde{\Phi}^v_{g,b}$ for B color channel.

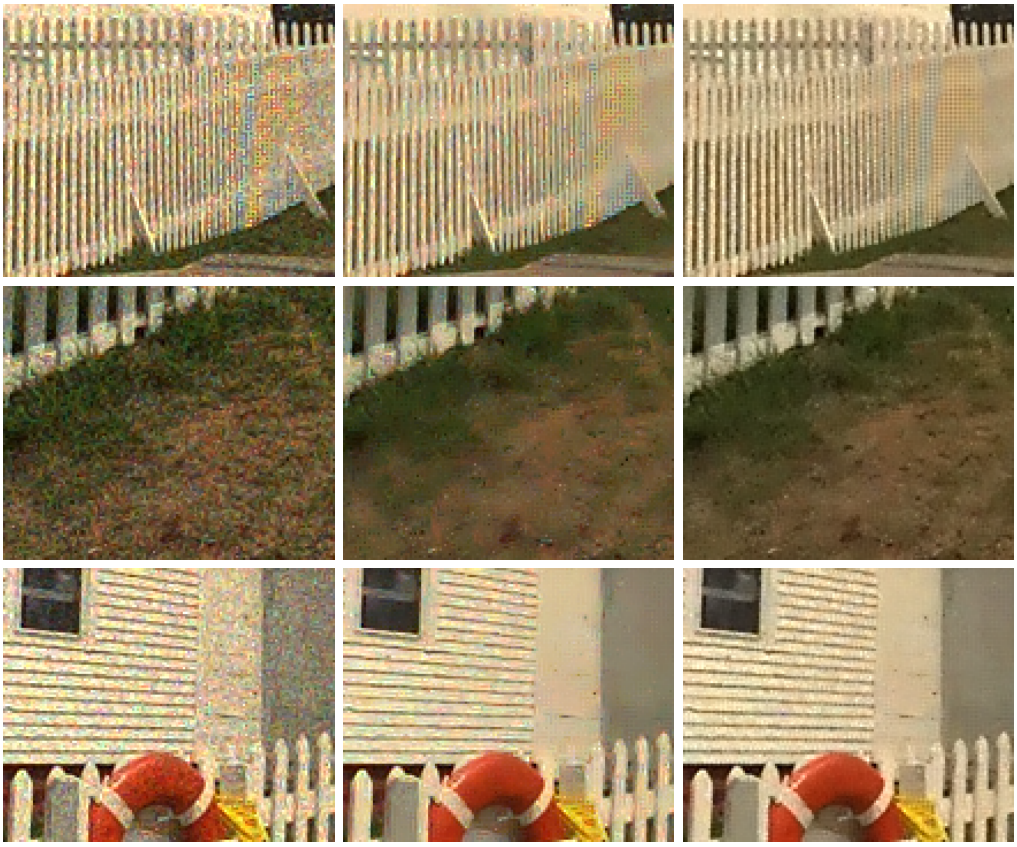

Figure 3.4: Restoration of the Lighthouse test image corrupted by Poissonian noise. Columns are enumerated from left to right: interpolated noisy image by HA (Hamilton, 1997) CFAI; restoration by HA (Hamilton, 1997) CFAI with iterative LPA-ICI denoising (Foi, 2005) at the prefiltering step, PSNR=(28.17, 29.07, 28.61); proposed LPA-ICI based integrated interpolation with denoising, PSNR=(29.39, 30.13, 30.15).

The standard deviation of directional estimates inside of the LPA-ICI is calculated as in (2.14).

The final RGB image is restored from the obtained filtered estimates (for details see Publications I, III).

3.4 Experiments with Artificial and Real Sensor Data

The efficiency of the proposed approaches was demonstrated on the standard database of Kodak set of color test-images in terms of both numerical and visual criteria evaluation. The diagram of mean PSNR values for each color channel is shown in Fig.3.2. The PSNR values are calculated excluding 15 border pixels in order to eliminate the boundary effects.

The threshold Γ in (2.13) is an important design parameter of the ICI rule. With small Γ the ICI selects only the estimates with the smallest scale s, while with large Γ

Figure 3.5: Fragment of the restored Window (7) and Parrots (23) test images corrupted by noise with $\sigma = k_0 + k_1\mathcal{B}\{y_{RGB}\}$ (Hirakawa, 2005b; Hirakawa, 2005c) where $k_0 = 10, k_1 = 0.1$. Columns are enumerated from left to right: interpolated by HA (Hamilton, 1997) CFAI noisy image; restoration by joint denoising and demosaicing technique (Hirakawa, 2005b; Hirakawa, 2005c); restoration by proposed technique.

only the estimates with the largest scale s. The best selection of Γ for each image can be found only if the original images are known. We call these best values of Γ "Oracles". They show the potential of the developed adaptive algorithm provided the best selection of Γ. The corresponding PSNR values are given in the column "Oracle Γ" of Fig.3.2. It can be seen that these oracle results are significantly better than the results for all other methods.

We have found an empirical formula giving the image dependent Γ with the values close to the oracle ones. Let σ_f be standard deviation of high frequency components of G channel calculated as median absolute deviation (MAD) (Donoho, 1995). Then nearly oracle values of the threshold parameter can be calculated as $\Gamma = 0.05\sigma_f + 0.33$. The results with this value of Γ are shown in the "LPA-ICI" column of Fig.3.2.

The proposed technique ("LPA-ICI" column) gives about 0.4 dB better mean PSNR value than DLMMSE method (Zhang, 2005) demonstrated the best performance among the reviewed CFAI methods. Analyzing the diagram in Fig.3.2 (left) we can see that this improvement is significant.

The results in terms of average S-CIELAB[1] (Zhang, 1997) metric for color images are shown in the diagram in Fig.3.2 (right). It shows actual ordering of the methods as the S-CIELAB performance is improving. It is seen that the proposed technique provides the best performance for the majority of the test images.

As an example, demosaicing of the well-known benchmark Lighthouse image is demonstrated in Fig.3.3. It is clearly seen that the color artifacts are removed almost completely

[1]The MATLAB code for the S-CIELAB metric is available following the link: `http://white.stanford.edu/~brian/scielab/scielab.html`

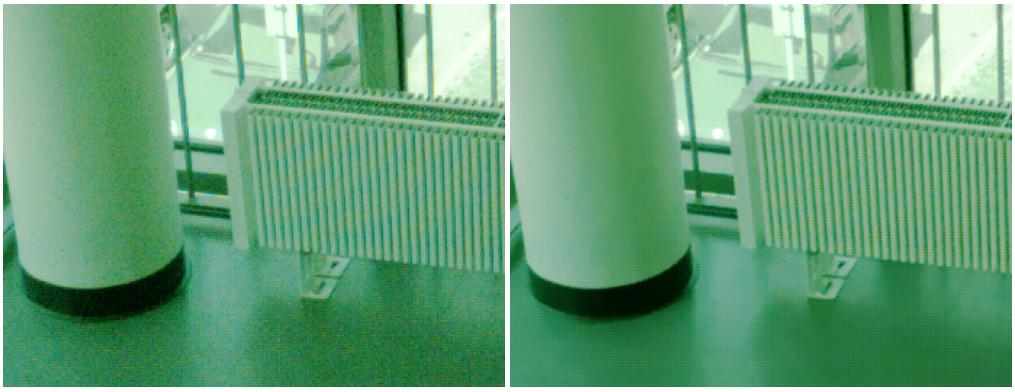

Figure 3.6: Restoration of raw sensor data taken by cameraphone: HA (Hamilton, 1997) interpolation (left); The proposed integrated denoising and interpolation (right) for noisy data.

by the proposed method (Fig.3.3 bottom right image). It is done significantly better than by other methods.

Detailed numerical and visual simulations for the proposed demosaicing for all images from the testing set and for a variety of well-known demosaicing techniques can be found in Publications I, II.

Similarly, performance of the demosaicing of noisy data is illustrated in Fig.3.4-3.6.

Fig.3.4 illustrates some difficult parts of the restored Lighthouse test-image with imposed Poissonian noise (1.4). Left column illustrates the noisiness of the test image where Hamilton-Adams (HA) CFAI was used to interpolate noisy data. Second column illustrates processing by the LPA-ICI denoising and DLMMSE CFAI (Zhang, 2005) performed independently for each color channels. As a result, the final image visually looks oversmoothed and suffers from color artifacts visible especially near edges, even for very advanced CFAI techniques. In combination with aliasing problem (noticeable at the fence and wall regions of the Lighthouse image) the color artifacts become visible significantly. It is seen that the proposed technique (right column) provides significantly better performance also at the regions that contain small details and textures difficult for restoration.

The LPA-ICI denoising embedded into the interpolation procedure helps to avoid or reduce the mentioned above problems. As a result, numerical and visual quality evaluation show better performance. The high frequency regions difficult for denoising like the grass region are preserved significantly better and color artifacts are reduced. As a result, the restored image looks more natural. Detailed numerical and visual simulations for the proposed technique for different images can be found in Publications I, III.

In Publications I, III, we also showed the efficiency of the proposed technique for other noise models like stationary (1.3) and nonstationary (1.5) Gaussian noise. As an example of the technique's performance, the visual comparison on the Window and Parrots test images is given in Fig.3.5 for $k_0 = 10$, $k_1 = 0.1$ for the noise model (1.5). The HA CFAI (Hamilton, 1997) was used in order to visualize the noisiness of the simulated noisy Bayer data (Fig.3.5, first column). The second column contains restored fragments by (Hirakawa, 2005b; Hirakawa, 2005c) and the third column corresponds to the results

obtained by the proposed technique. The proposed technique provides less color artifacts that is supported by the better S-CIELAB values provided in Publication I. The difference is significant especially for the Window test image.

Also, it is very important that we demonstrate the restoration of real noisy Bayer data directly from the sensor of a cameraphone (Fig.3.6). The noise model and its parameters were identified exactly in the same way how it is done in (Foi, 2007a; Foi, 2006b). The left image was interpolated by HA CFAI (Hamilton, 1997) and the right by the proposed CFAI for noisy data. The histograms for both of them were equalized in order to improve visual perception in print. No other color correction steps, pre- and postfiltering were done in these experiments.

Chapter 4

Deconvolution Methods

Usually blur refers to the low-pass distortions introduced into an image. It can be caused, e.g., by the relative motion between the camera and the original scene, by the optical system which is out of focus, by atmospheric turbulence (optical satellite imaging), aberrations in the optical system, etc. (Pratt, 1992). Any type of blur, which is spatially invariant, can be expressed by the convolution kernel in the integral equation (Nagy, 1998; Rushforth, 1987). Hence, deblurring (restoration) of a blurred image is an ill-posed inverse problem, and regularization is commonly used when solving this problem (Tikhonov, 1977).

There exists a variety of sophisticated and efficient deblurring techniques such as deconvolution based on Wiener filtering (Pratt, 1992, Katkovnik, 2005), nonparametric image deblurring using local polynomial approximation with spatially-adaptive scale selection based on the intersection of confidence intervals rule (Katkovnik, 2005), Fourier-wavelet regularized deconvolution (Neelamani, 2003), expectation-maximization algorithm for wavelet-based image deconvolution (Figueiredo, 2003), etc. All these techniques assume a prior knowledge of the blurring kernel or PSF, and its parameter.

When the blurring operator is unknown, the image restoration becomes a blind deconvolution problem (Lagendijk, 1990; Giannakis, 2000; Harikumar, 1999a).

This chapter is dedicated to solution of some of the mentioned problems. It is based on Publications IV-VII. We start from the 3D deconvolution for optical sectioning (Publication IV) which is a generalized form of the technique based on LPA-ICI filtering proposed in (Katkovnik, 2003; Katkovnik, 2005). A special iterative Landweber deconvolution with LPA-ICI post-filtering is considered with application to mobile devices (Trimeche, 2005). D. Paliy was a co-author of this publication and, in part, the obtained results have been used for further works. Similarly, the adaptive LPA-ICI post-filtering applied to the iterative gradient-projection minimization was effectively used in Publication V for multi-channel blind deconvolution.

A different principle for blind deconvolution was used in Publication VI where this problem was considered from the classification point of view. A neural network was exploited for the PSF identification. The multi-layer neural network based on multi-valued neurons (MLMVN) was used as an efficient classifier having only single observation. We showed its efficiency for this particular problem. After the PSF was identified, the blind deconvolution was reduced to a conventional deconvolution for which the LPA-ICI based

technique (Katkovnik, 2005) was used.

As a part of the considered problems, the problem of the regularization parameter selection was considered in Publication VII.

In such a way, we aimed to cover the deconvolution for imaging in a comprehensive manner.

4.1 Deconvolution for Optical Sectioning

In Publication IV we propose a novel nonparametric approach to reconstruction of three-dimensional (3D) objects from 2D blurred and noisy observations. This is the problem of computational optical sectioning. This approach is based on an approximate image formation model which takes into account depth varying nature of blur described by a matrix of shift-invariant 2D PSF of an optical system (1.12). The proposed restoration scheme incorporates the matrix regularized inverse and matrix regularized Wiener inverse algorithms in a combination with a novel spatially adaptive denoising. This technique is based on special statistical rules for selection of the adaptive size and shape neighborhood used for the local polynomial approximation of the 2D image intensity.

In general, images suffer from degradation due to the out-of-focus areas contributing to the in-focus areas. For instance, in an observation of specimen in a microscope there is only one portion that appears in focus. However, usually a specimen is not flat but is a 3D structure. Therefore, some portions are out of focus. Nevertheless, these out-of-focus structures are in the field of view and thus obscure the in-focus plane. In order to obtain a deblurred 3D image of a specimen, it is common to use the optical sectioning method. The microscope is focused at a given focal plane and the image is recorded. This image is an optical slice. Then, the microscope is refocused and another image is recorded. This process is repeated until the whole specimen is covered (Preza, 2004). The restoration of a scene from its multiple degraded observations is typical also for conventional photography. This is often considered as a multichannel image restoration problem. Usually, this problem exploits methods of a single-image restoration to degraded multi-channel images to recover the original scene (Kubota, 2005). The 3D optical sectioning equipped with digital deblurring algorithms is a powerful modern tool for visualization of specimens in biology, medicine, mineralogy, etc. Computational restoration methods applied to slice images are quite an efficient and promising tool.

The 3D PSF is the main factor describing how a point source of light is being distributed laterally and across the focal planes. It plays a crucial role in image formation and its reconstruction. 3D inverse is a problem of object restoration from its observations using a known PSF of optical system. It is an ill-posed problem (Tikhonov, 1977). It means that small perturbations in initial data (observed image and inaccuracy in the used PSF model) result in large changes in the solution. For solving the deconvolution problem with a given PSF, a number of approaches were proposed since the mid 1970s under various idealizations of the PSF and noise model.

In microscopy there are two approaches to reduce out-of-focus contributions: optical and computational. In the optical approach a confocal microscope is used that reduces the contribution from the out-of-focus fluorescence. The recorded images are all in-focus and are an optical equivalent of a series of microtome slices allowing the 3D reconstruction of the specimen.

In the computational approach, image processing is applied to process the set of 2D optical slices in order to reduce the out-of-focus interferences. This method is based on information about the processes of image formation. The most severe degradation is often caused by diffraction at objective and condenser lenses. This degradation is modeled by the PSF of the microscope optical system.

Image deconvolution has become an established technique to improve both resolution and signal-to-noise ratio of serially sectioned three-dimensional images (Schaefer, 2001). The reconstruction of 3D objects by means of optical sectioning is very popular in fluorescence microscopy imaging. A number of techniques was proposed for optical sectioning based on the iterative expectation-maximization approach (Preza, 2004; Markham, 2001). Using the expectation-maximization formalism, algorithms for maximum-likelihood image restoration were developed using a depth-variant model for the optical sectioning microscopy. Theoretical analysis of properties for proposed techniques is an advantage. However, these methods are efficient but computationally expensive. Other works which exploit iterative inverse schemes can be seen also in (Zhu, 2004; McNally, 1999). A good review of non-linear image restoration techniques for fluorescence microscopy and theoretical background for mathematical modeling can be found in (VanKempen, 1999).

The iterative solution presented by a combination of the conjugate gradient method with the Tikhonov regularization is proposed in (Schaefer, 2001). The conjugate gradient iteration scheme was used considering either Gaussian or Poisson noise models. For the regularization, the standard Tikhonov method was modified. However, the generic design of the algorithm allows for more regularization approaches. To determine the regularization parameter, the generalized cross-validation method is used. Tests produced for both simulated and experimental fluorescence wide-field data show reliable results.

Linear non-iterative methods for deconvolution of 3D images in computational optical sectioning microscopy are proposed in (Homem, 2004). The authors consider also Gaussian and Poissonian noise formation models. An approach using complex-valued wavelet transform to obtain extended depth-of-focus for multi-channel microscopy images is proposed in (Forster, 2004). However, this method does not take into account the image acquisition model.

Knowledge about image formation is an important issue in the restoration techniques. The PSF of an optical system as the main factor plays a crucial role. We assume that the PSF is known a priori. For example, modeling and estimation of PSF are done in (Preza, 2004; Li, 1995) for optical system of a microscope or in (Kubota, 2005) for a photo-camera. The reconstruction of all-in-focus image from two arbitrarily focused images is proposed in (Kubota, 2005). The true scene is supposed to have the background and foreground regions only. The authors propose a method for PSF estimation from degraded observed images and use the inverse filter to obtain an original scene. However, the image formation model does not assume the presence of noise.

We focus on the noniterative method of reconstruction and generalize the spatially adaptive 2D deblurring algorithm developed in (Katkovnik, 2005; Katkovnik, 2006b) to the 3D imaging. It incorporates the regularized inverse and regularized Wiener filters. The noise model considered in this paper is Gaussian. The scale-adaptive denoising technique is used to remove it effectively.

The simulations done for a realistic phantom image show the efficiency of the proposed technique.

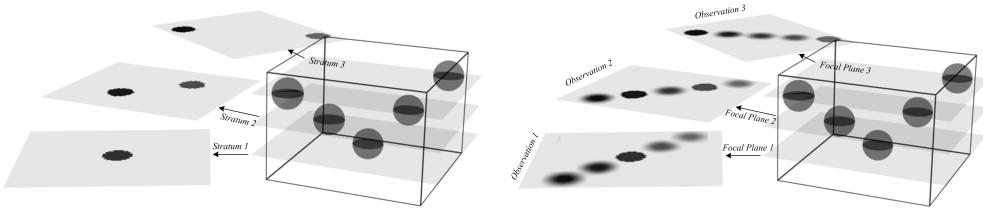

a) b)

Figure 4.1: 3D object consisted of 5 spheres: a) strata of the object; b) observation of each stratum focusing preciselly at stratum 1, stratum 2, and stratum 3.

We consider the problem as the formal modeling given in the form (1.12). Speculations on formalities of the problem addressed are given in Section 1.2.4.

Let $Z_i(\omega)$ be the discrete 2D Fourier transform of $z_i(x)$, $Z_i = \mathcal{F}\{z_i\}$, $\mathcal{F}\{\cdot\}$ is the discrete Fourier transform (DFT) operator, and $x \in X \subset \mathbb{R}^2$ as in (1.1). Here $\omega \in W = \{(\omega_1, \omega_2), \omega_1 = 1, ..., 2N, \omega_2 = 1, ..., 2M\}$ is the 2D normalized discrete frequency. Then, equation (1.12) in the frequency domain can be written as follows:

$$\begin{pmatrix} Z_1 \\ ... \\ Z_n \end{pmatrix} = \begin{pmatrix} V_{11} & ... & V_{1m} \\ ... & ... & ... \\ V_{n1} & ... & V_{nm} \end{pmatrix} \begin{pmatrix} Y_1 \\ ... \\ Y_m \end{pmatrix} + \begin{pmatrix} \varepsilon_1 \\ ... \\ \varepsilon_n \end{pmatrix}, \tag{4.1}$$

where $V_{ij} = \mathcal{F}\{v_{ij}\}$, $Y_j = \mathcal{F}\{y_j\}$, and $\varepsilon_i = \mathcal{F}\{\varepsilon_i\}$. Here, ε_i corresponds to the noise term in (1.12). Speculations on the given image formation model are given in Section 1.2.4.

Finally, the collected 3D observation $\mathbf{Z} = (Z_1, ..., Z_n)^T$ is a set of blurred 2D images. In order to find the true object $\mathbf{Y} = (Y_1, ..., Y_m)^T$ we need to solve the system of linear equations (4.1).

We obtain for (4.1) the following vector-matrix representation defined in the 2D frequency domain:

$$\mathbf{Z}(\omega) = \mathbf{V}(\omega)\mathbf{Y}(\omega) + \boldsymbol{\varepsilon}(\omega). \tag{4.2}$$

We develop the technique which is a vector-matrix generalization of the regularized inverse (RI) and regularized Wiener inverse (RWI) adaptive scale deblurring algorithms proposed in (Katkovnik, 2003; Katkovnik, 2005). The ICI rule (Katkovnik, 1999) is exploited for the adaptive scale filtering of the reconstructed 2D slices of the 3D object function $\mathbf{y}(x)$. The algorithm consists of two stages. At the first stage the RI filter and adaptive LPA with the ICI rule are used in order to obtain the estimate $\hat{\mathbf{y}}^{RI}(x)$ exploited at the second stage as a reference signal. The second stage incorporates the RWI filter and LPA-ICI to obtain the final result $\hat{\mathbf{y}}^{RWI}(x)$ (Fig.4.2).

Fig.4.1 illustrates the setting of the problem. Let us consider as an example the 3D object that consists of 5 spheres. The object slices called *strata* (Preza, 2004) lie in the planes perpendicular to the optical axis. It is assumed that the thickness of the strata is small and variation of the PSF with respect to the coordinate x_3 in one stratum is insignificant. The object in Fig.4.1 is discretized to $m = 3$ strata. In observations of

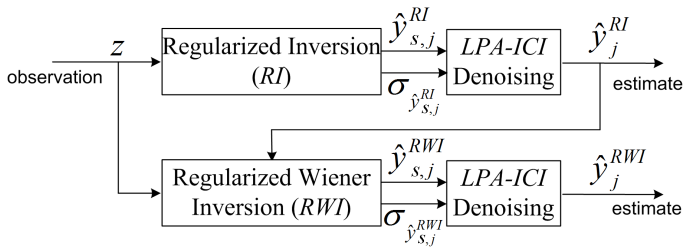

Figure 4.2: The proposed restoration scheme includes RI step with adaptive LPA-ICI denoising in order to obtain a pilot signal for the RWI filter.

this object one can see clearly only the strata which are in the focal planes while others are blurred (Fig.4.1b). The aim is to reconstruct the original strata Fig.4.1a from their $n = 3$ observations Fig.4.1b.

4.1.1 Regularized Inverse

The RI filter is obtained by minimization of the penalized quadratic residual function which for the problem (4.2) is given in the form:

$$\begin{aligned} J &= \|\mathbf{Z} - \mathbf{V}\mathbf{Y}\|_2^2 + r_{RI}^2 \|\mathbf{Y}\|_2^2 = \\ &= \sum_{\omega} (\mathbf{Z}(\omega) - \mathbf{V}(\omega)\mathbf{Y}(\omega))^H (\mathbf{Z}(\omega) - \mathbf{V}(\omega)\mathbf{Y}(\omega)) + r_{RI}^2 \sum_{\omega} \mathbf{Y}^H(\omega)\mathbf{Y}(\omega), \end{aligned} \tag{4.3}$$

where r_{RI}^2 is a regularization parameter and the superscript "H" denotes the Hermitian transpose.

In order to justify the choice of the residual function (4.3), let us firstly consider the residual function for (1.12) in the signal domain:

$$J = n \cdot 2N \cdot 2M \left(\|\mathbf{z} - \mathbf{v} \circledast \mathbf{y}\|_2^2 + r_{RI}^2 \|\mathbf{y}\|_2^2 \right), \tag{4.4}$$

whose minimization, exploiting the Parseval's theorem, is equivalent to minimization of (4.3), which refers to the well-known method of Lagrange multipliers of constrained optimization and the Tikhonov regularization (Tikhonov, 1977). Here, the term $\|\mathbf{z} - \mathbf{v} \circledast \mathbf{y}\|_2^2$ corresponds to the fidelity between estimate and observation signal. However, due to the ill-posedness of the problem, the solution is highly unstable and, therefore, the term $\|\mathbf{y}\|_2^2$ imposes bounds on the power of the estimate.

The minimum of J is achieved when $\partial J / \partial \mathbf{Y}^H = 0$. Calculation of this derivative gives the estimate:

$$\widehat{\mathbf{Y}}^{RI}(\omega) = (\mathbf{V}^H(\omega)\mathbf{V}(\omega) + r_{RI}^2 \mathbf{I}_{m\times m})^{-1} \mathbf{V}^H(\omega)\mathbf{Z}(\omega), \tag{4.5}$$

where $\mathbf{I}_{m\times m}$ is the $m \times m$ identity matrix.

Following the technique developed in (Katkovnik, 2003; Katkovnik, 2005) we introduce the filtered RI estimate as follows:

$$\widehat{\mathbf{Y}}_s^{RI}(\omega) = G_s(\omega)\widehat{\mathbf{Y}}^{RI}(\omega), \tag{4.6}$$

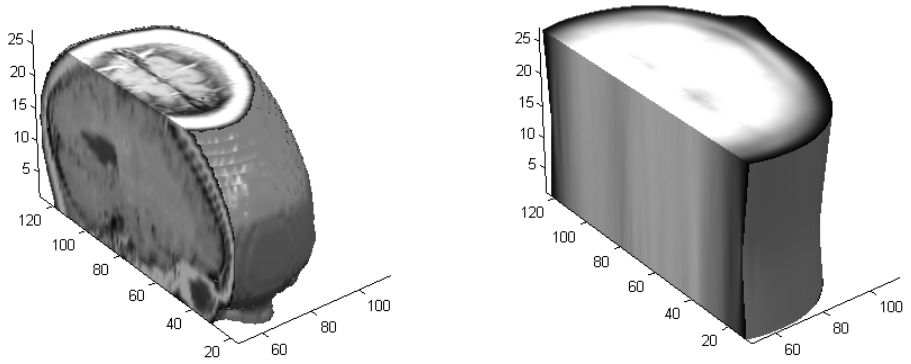

Figure 4.3: The phantom 3D MRI object used in simulations: a) A subvolume of the true object; b) A corresponding subvolume of blurred and noisy observations.

where G_s is a low-pass filter generated by LPA (see details in Section 2.1). This filter is the same for all components of the vector $\widehat{\mathbf{Y}}^{RI}(\omega)$.

Here, s is an important scale-parameter of the filter which is selected adaptively by the ICI rule. In spatial domain $\hat{y}^{RI}_{s,j} = \mathcal{F}^{-1}\left\{\hat{Y}^{RI}_{s,j}\right\}$, $j = 1, ..., m$, where $\mathcal{F}^{-1}\{\cdot\}$ denotes inverse discrete Fourier transform (IDFT).

Using formulas (4.2), (4.5), (4.6), and Parseval's theorem the variance at every point of the estimate $\hat{y}^{RI}_{s,j}(x)$, $j = 1, ..., m$, is computed as

$$\sigma^2_{\hat{y}^{RI}_{s,j}(x)} = var\{\hat{y}^{RI}_{s,j}(x)\} = \frac{1}{2N \cdot 2M} \sum_{\omega} (\mathbf{Q}_{RI}(\omega)\boldsymbol{\sigma}^2\mathbf{Q}^H_{RI}(\omega))_{j,j},\ j = 1, ..., m. \tag{4.7}$$

Here, $\mathbf{Q}_{RI}(\omega)$ is a transfer matrix of (4.6)

$$\mathbf{Q}_{RI}(\omega) = G_s(\omega)(\mathbf{V}(\omega)^H\mathbf{V}(\omega) + r^2_{RI}\mathbf{I}_{m\times m})^{-1}\mathbf{V}^H(\omega)$$

and $\boldsymbol{\sigma}^2 = diag(\sigma^2_1, ..., \sigma^2_n)$ is a diagonal matrix of the variances of observations $\mathbf{z}(x) = (z_1(x), ..., z_n(x))$.

The variance of noise for every observation can be different. The variances $\sigma^2_{\hat{y}^{RI}_{s,j}(x)}$ are used in the ICI rule for the adaptive selection of the scale s.

4.1.2 Regularized Wiener Inverse

Looking for an optimal linear estimate $\hat{y}_j(x) = (q^{WI}_{j,i} \circledast z_i)(x)$, $i = 1, ..., n$, $j = 1, ..., m$, of a smoothed signal $y_{s,j}(x) = (g_s \circledast y_j)(x)$ we come to the Wiener inverse filter $\mathbf{Q}_{WI} = \left(\mathcal{F}\{q^{WI}_{j,i}\}\right)$ by minimizing criterion function

$$J = E\left\{\left\|\mathbf{Y}_s - \widehat{\mathbf{Y}}\right\|^2_2\right\} = E\left\{\|G_s\mathbf{Y} - \mathbf{Q}_{WI}\mathbf{Z}\|^2_2\right\}.$$

Solution of $\partial J/\partial \mathbf{Q}_{WI}^H = 0$ gives us the transfer matrix for the Wiener filter:

$$\mathbf{Q}_{WI} = G_s \mathbf{Y}\mathbf{Y}^H \mathbf{V}^H (\mathbf{V}\mathbf{Y}\mathbf{Y}^H \mathbf{V}^H + 2N \cdot 2M\boldsymbol{\sigma}^2)^{-1}. \tag{4.8}$$

Inserting the regularization parameter r_{RWI}^2 into (4.8) we obtain the regularized Wiener inverse (RWI) filter:

$$\mathbf{Q}_{RWI} = G_s \mathbf{Y}\mathbf{Y}^H \mathbf{V}^H (\mathbf{V}\mathbf{Y}\mathbf{Y}^H \mathbf{V}^H + 2N \cdot 2M r_{RWI}^2 \boldsymbol{\sigma}^2)^{-1}. \tag{4.9}$$

The filtered RWI estimate similarly to the (4.6) has the following form:

$$\widehat{\mathbf{Y}}_s^{RWI}(\omega) = \mathbf{Q}_{RWI}(\omega)\mathbf{Z}(\omega). \tag{4.10}$$

In spatial domain $\hat{y}_{s,j}^{RWI} = \mathcal{F}^{-1}\left\{\hat{Y}_{s,j}^{RWI}\right\}$, $j = 1, ..., m$. The variances for the estimate (4.10) are:

$$\begin{aligned} \sigma^2_{\hat{y}_{s,j}^{RWI}(x)} &= var\{\hat{y}_{s,j}^{RWI}(x)\} = \\ &= \frac{1}{2N \cdot 2M} \sum_{\omega} (\mathbf{Q}_{RWI}(\omega)\boldsymbol{\sigma}^2 \mathbf{Q}_{RWI}^H(\omega))_{j,j},\ j = 1, ..., m, \end{aligned} \tag{4.11}$$

and they are used in the following LPA-ICI post-processing.

4.1.3 Experiments

We use a 3D body modeling of an MRI datascan of a human cranium as a complex phantom for simulations of 3D object. This numerical model is available within MATLAB. The image file *mri.tif* presents 27 slices of 128×128 cross-section images of a cranium. We use this model in order to imitate observation data for the considered 3D inverse imaging. Intensity values are in the range from 0 to 1, $y_j(x) \in [0, 1]$. It consists of 27 object slices enumerated from 1 to 27, $x_3(j) = j$, $j = 1, ..., 27$. A corresponding subvolume of the true object is visualized in Fig.4.3a. A subvolume of 27 noisy and blurred observations is shown in Fig.4.3b as they are recorded by focusing one after another at each object slice.

We set the additive noise variances σ_i^2 in such a way that the BSNR for each observation

$$\mathrm{BSNR}_i = 10 \log_{10} \left(\frac{\left\| \sum_j (v_{i,j} \circledast y_j) - \frac{1}{2N \cdot 2M} \sum_x \left(\sum_j (v_{i,j} \circledast y_j)(x) \right) \right\|_2^2}{2N \cdot 2M \cdot \sigma_i^2} \right)$$

equals 40 dB, which is significant level of the noise for inverse problems. It is strongly visible on the reconstructed by RI technique strata (e.g. Fig.4.4c). The adaptive LPA-ICI technique is exploited to remove it.

In experiments we run the following test in order to reconstruct the true object strata shown in Fig.4.4a. Let the observations $z_i(x)$ consist of 9 strata $y_j(x)$, $j = 1 + \triangle k$, where $\triangle = 3$ and $k = 0, ..., 8$, of the MRI object by focusing precisely at the positions j, i.e. $i = j$. Applying the proposed technique, we reconstruct this object at positions j. The results of the RI reconstruction only are shown in Fig.4.4c. The slices are reconstructed and the object is clearly visible but the noise is significant.

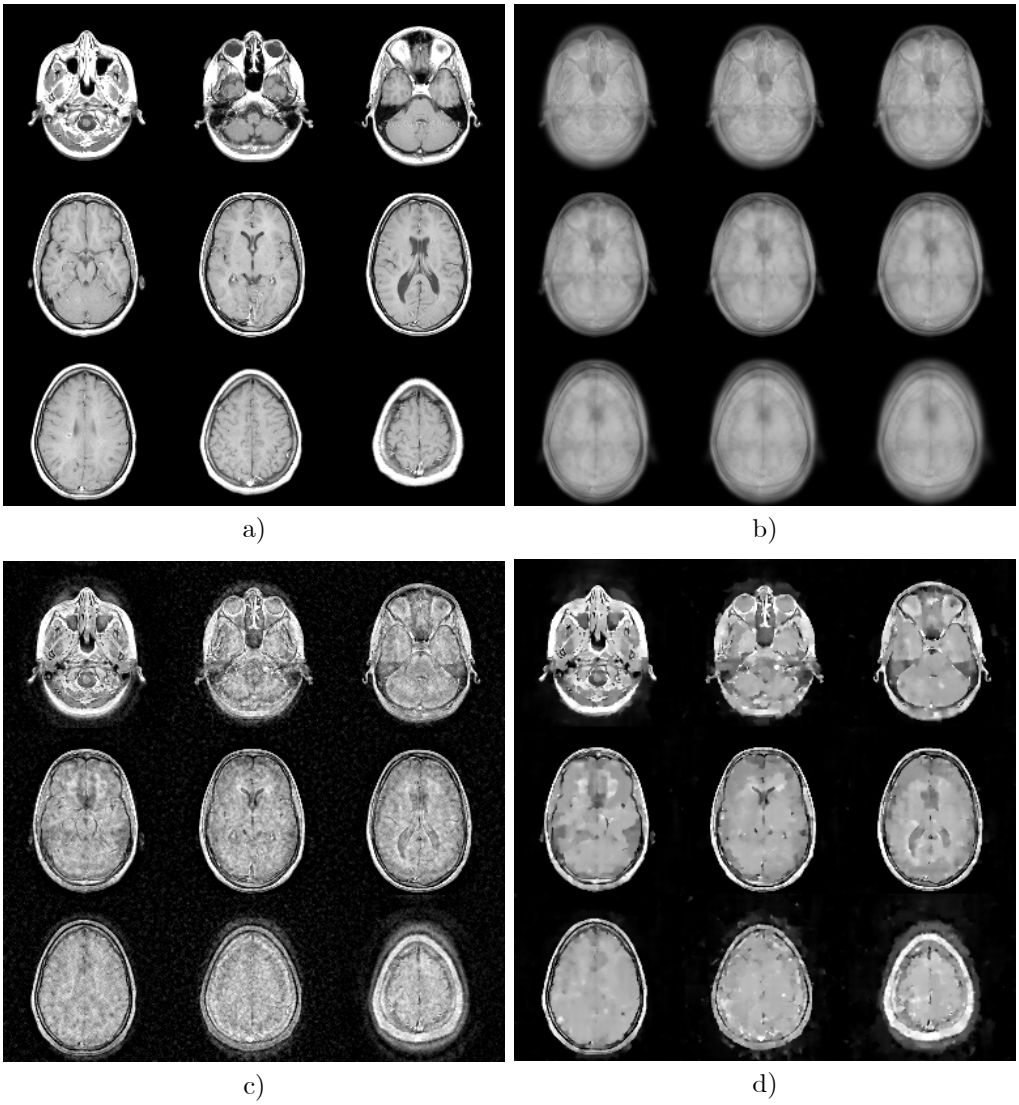

Figure 4.4: The reconstruction of the true MRI object: a) True object strata (j=1,4,...,26); b) Observations made by focusing at the positions of the true strata given in (a); c) RI reconstruction of (a) using observations (b); d) RWI reconsruction with LPA-ICI denoising of (a) using observations (b).

The adaptive LPA-ICI denoising technique significantly improves the quality of reconstruction visually and numerically. This can be seen in Fig.4.4d, where the images after the RWI reconstruction with the LPA-ICI filtering are shown. The level of noise is lower and small details are better preserved.

Other simulations can be found in Publication IV. With this publication we showed efficiency of the proposed approach to the optical sectioning problem.

In the proposed approach the important fact is that the PSF (practically PSFs for all observations) are assumed to be known. However, it is difficult to achieve this in practice. In (Trimeche, 2005) the PSF of a camera phone was estimated. It was possible since its optical system is significantly less complex than optical system of a microscope. The authors proposed a deblurring procedure robust to misestimation of PSF and noise. The adaptive LPA-ICI filtering was effectively used as a post-filtering procedure (a regularizator) for the iterative Landweber deconvolution scheme (Trimeche, 2005). Further, similar approach was applied to gradient-projection method for multi-channel blind deconvolution (Publication V).

4.2 Deconvolution for Mobile Devices

In the paper (Trimeche, 2005) a novel multi-channel image restoration algorithm was presented as a result of collaboration of Tampere University of Technology (TUT) and Nokia Research Center (NRC).

The main intention was to develop practical approaches to reduce optical blur from noisy observations produced by the sensor of a digital camera. In this method, an iterative deconvolution is applied separately to each color channel directly on the raw data. A modified iterative Landweber algorithm was used combined with the adaptive LPA-ICI denoising technique. In order to avoid a false coloring due to independent component filtering in RGB space, we have integrated a novel saturation control mechanism that smoothly attenuates the high-pass filtering near saturated regions. It is shown by simulations that the proposed filtering is robust with respect to both errors in PSF and approximated noise models. Experimental results show that the proposed processing technique produces significant improvement in perceived image resolution.

4.2.1 Overview

Image restoration requires knowledge of the degradation process in order to solve the consequent inverse problem. This inverse problem is generally ill-posed (Bertero, 1998), that is, if the direct solution is considered, a small perturbation in the input can result in an unbounded output. Several algorithms have been proposed to solve the ill-posed inverse problem by introducing a regularization step that suppresses over-amplification of the solution. For example, a directional adaptive regularization was proposed to avoid over-smoothing of the solution (Lee, 2003). Another method suggests the use of spatially adaptive intensity bounds in the framework of gradient projection method (May, 2003) in order to regularize the problem.

The specific problem of restoring noisy and blurred color images has been investigated in the literature since the mid-eighties. Several algorithms (Molina, 2002; Katsaggelos, 1988; Tekalp, 1989) have been proposed to restore the color images by utilizing the inter-channel correlation between the different color components. However, most techniques approach the problem as a post-processing problem, that is, the processing is applied after the image is captured, processed, and stored. Our approach is inherently different. We consider the application of the image restoration algorithm directly (and separately) on the raw color image data, so that the deblurring and denoising are at the first step of the image reconstruction chain. In other words, we apply the restoration as a pre-processing operation which gives benefits for the cascaded algorithms in the imaging chain, such

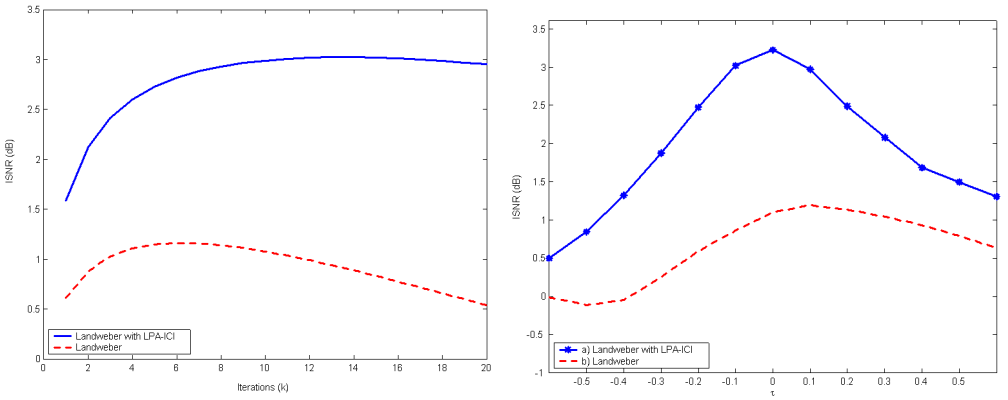

Figure 4.5: a) Landweber technique with LPA-ICI denoising (solid line) compared with the standard Landweber technique without denoising (dashed line). b) Simulation of the sensitivity of the iterative deblurring methods to possible errors in PSF estimates (v_i). We used Gaussian PSF with parameter $\sigma_{blur} = 1 \pm \Delta_\sigma$, where Δ_σ is an error that is deliberately introduced.

as AWB and CFAI (typically non-linear operations). Applying the image restoration as a pre-processing step also minimizes the non-linearities that are accumulated in the image gathering process. A similar processing paradigm was proposed earlier (Na, 1995) in order to reduce color cross-talk and to decorrelate the different color components. However, the processing was carried out after color conversion which may introduce the cross-talk itself. The restoration was proposed without consideration of the difference in the blur of the different color channels. In our work, we use separate processing of the raw RGB color components measured by the camera sensor, and we restore separately each channel according to the estimated optical blur. In fact, the optical blur in each color channel is different, since the focal length depends on the wavelength of the incoming light (Hecht, 2002).

Another key issue in our proposed solution is the use of a modified iterative Landweber algorithm which includes adaptive denoising filter LPA-ICI (Katkovnik, 1985; Katkovnik, 1999; Katkovnik, 2006b). This combination gives us estimates that are robust to errors in the estimation of the PSF and in noise parameters. The direct inverse methods such as the RI and RWI deconvolution techniques (Katkovnik, 2005; Katkovnik, 2006b) are effective methods, but sensitive to modelling errors. On the other hand, the iterative methods are more robust (Liang, 2003; Jiang, 2003; Biggs, 1997a; Biggs, 1997b) and, hence, more interesting for practical implementations.

4.2.2 Proposed Approach

Let us consider image formation model (1.10). This model is considered for every color component of the Bayer pattern. Therefore, the observed image can be modelled as:

$$z_i(x) = (v_i * y_i)(x) + n_i(x),\ i = 1, ..., 4 \tag{4.12}$$

where z_i is the measured color component image, y_i is the original color component, v_i is the corresponding PSF in that component, and n_i is an i.i.d. additive Gaussian noise term as in (1.3). The index $i = \{1, 2, 3, 4\}$ denotes respectively the data corresponding to the Red, Green1, Green2, and Blue color channels, those are measured according to the Bayer matrix sampling pattern (1.8). Note that each of these images has a quarter oh the size of the final output image. The restoration problem can be stated as recovering the original image y_i from its degraded observation z_i.

Iterative methods have shown to be an attractive alternative for implementing the inverse solution of image deblurring, especially when the blurring parameters can exhibit some modelling errors. The standard Landweber method (Liang, 2003; Jiang, 2003) to solve for y_i from the observations z_i in equation (4.12) is given by the following iterative process:

$$y_i^{(0)} = 0, \tag{4.13}$$

$$y_i^{(k+1)} = y_i^{(k)} + \mu_i \cdot v_i^T * (z_i - v_i * y_i^{(k)}),\ k = 0, 1, ...,\ i = 1, ..., 4, \tag{4.14}$$

where μ_i is the update parameter, $v_i^T(t) = v_i(-t)$. If the image formation model (4.12) is noise-free, $\eta_i(t) = 0$, the iterative process described above converges to the true signal (Jiang, 2003).

Another aspect of the Landweber method in equation (4.14) is the fact that it is designed to solve a problem $z_i(t) = (v_i * y_i)(t)$. As a result, the obtained solution is sub-optimal in presence of noise. We propose to use the following modifications in order to incorporate a noise filtering stage and to enhance convergence:

$$\widetilde{y}_i^{(0)} = 0, \tag{4.15}$$

$$y_i^{(k+1)} = \widetilde{y}_i^{(k)} + \mu_i \cdot d_i * v_i^T * (z_i - v_i * \widetilde{y}_i^{(k)}), \tag{4.16}$$

$$\widetilde{y}_i^{(k+1)} = \mathcal{LI}\{y_i^{(k+1)}\},\ k = 0, 1, ...,\ i = 1, ..., 4 \tag{4.17}$$

where d_i is an impulse response of high-pass linear filter that is used to accelerate the convergence of the solution. The choise $d_i = \mathcal{F}^{-1}\left\{1/|V_i|^2\right\}$ gives 1 step convergence but requires inverse for the PSF which can be ill-conditioned. The Laplacian filter for d_i is used in some applications.

We used LPA-ICI denoising in this work $\mathcal{LI}\{\cdot\}$ (2.18) which is an intermediate filtering operator that is intended to enhance the robustness of the solution.

It can be considered as a separate regularization step. It is interesting to note that in the context of expectation-maximization (EM) methods (Figueiredo, 2003), in the iterative process described above, the E-step coincides with equation (4.16), and M-step corresponds to filtering stage in equation (4.17).

The operator $\mathcal{LI}\{\cdot\}$ can be, for example, a simple averaging filter, or any other sophisticated filter that takes into consideration the local signal statistics. We have chosen to plug-in an adaptive LPA-ICI denoising filter in order to preserve the image details from over-smoothing. This adaptive denoising technique plays an important role in our proposed solution because it preserves image details and ensures also efficient noise removal, which is difficult to achieve using filters operating on fixed data support.

a) b)

Figure 4.6: a) Image taken from Nokia 6600 phone; b) Image (a) processed by the proposed iterative Landweber with LPA-ICI technique after 3 iterations.

It is worth to note that an adaptive technique provides more accurate and robust estimates against misestimations in the noise model.

Importance of the introduced step is illustrated in Fig.4.5. For studying properties of this proposed method we used the Cameraman test image that was corrupted by a Gaussian PSF with σ_{blur} equal to one. We further degraded the blurred image with an additive white Gaussian noise (variance equals to 0.02). The restoration results obtained with the standard Landweber method were compared against the proposed method with the LPA-ICI filtering. It can be seen from the improvement in signal-to-noise ratio (ISNR) values (Fig.4.5a) that the proposed denoising step significantly enhances the performance of the restoration process.

Also important that, in practice, it is rarely possible to have precise estimates for the PSF. Therefore, it is essential to have restoration algorithms that are robust against deviations in PSF. In Fig.4.5b, we compared the proposed technique (solid line) with the standard Landweber method (dashed line). In our experiments, we used Gaussian PSF with parameter $\sigma_{blur} = 1 \pm \Delta_\sigma$, where $\Delta_\sigma \in \{0, 0.1, ..., 0.6\}$ is the assumed estimation error. It is clear from the ISNR curves that the proposed solution is more robust against possible errors in PSF, since the performance was consistently better than the standard Landweber method for all the values of Δ_σ that were used.

This approach showed also its efficiency for real data. Fig.4.6 illustrates the final result that is obtained when we applied the proposed multichannel restoration algorithm in the reconstruction chain of a real camera system. The processing was carried out on the raw pictures captured with Nokia 6600 camera-phone. The PSF was estimated for this particular camera.

It is not always possible to estimate the PSF of optical system. Therefore, it is reasonable to consider the problem when the PSF is unknown, i.e. the blind deconvolution problem. Further, two approaches are proposed for its solution.

4.3 Multi-Channel Blind Deconvolution

The most popular approaches to blind deconvolution considered in the scientific literature can be divided in two classes: a multi-channel deconvolution (Sroubek, 2005; Katkovnik, 2006a; Tico, 2006, Yuan, 2007), and a single-channel one (Molina, 1997; Rekleitis, 1996; Rooms, 2004; Likas, 2004; Chen, 2006; Chen, 2005).

The multi-channel blind deconvolution assumes that several observations of a single scene are available for restoration. The problem is to restore the true scene from these noisy, differently-blurred data having no preliminary knowledge about the distortion (smoothing) operators (Katkovnik, 2006a). Multi-channel deblurring of spatially misaligned images has been considered in (Sroubek, 2005). Restoration from two observations where one of them is very noisy (for instance, taken by the camera phone with short exposition time), and one is less noisy but blurred (taken with long exposition time) was proposed in (Tico, 2006; Yuan, 2007).

The single channel blind deconvolution usually assumes preliminary knowledge on the model of blur. For instance, it can be defocus, Gaussian, motion models, etc. After this, having one observation of a scene and knowing the type of distortion operator, the problem is to estimate the parameters of this model that can be described mathematically (e.g., variance for the Gaussian blur, extent for motion blur, etc.). For instance, restoration from data destroyed with motion blur was considered in (Rekleitis, 1996). The parameter for Gaussian model of blur is determined efficiently by wavelet decomposition in (Rooms, 2004). Single-channel blind deconvolution within Bayesian framework is considered in (Likas, 2004). Camera shake removal from a single photograph is proposed in (Fergus, 2006).

The known size of PSF support may simplify the problem significantly (Chen, 2006). Parametric solution where a prior imposed on PSF takes into account multiple classes is proposed in (Chen, 2005).

Image processing based on multiple observations of one scene aims to enhance comprehensive restoration quality, often when knowledge about image formation is incomplete. Classical fields of application are the astronomy, remote sensing, medical imaging, etc. Multisensor data of different spatial, temporal, and spectral resolutions are exploited for image sharpening, improvement of registration accuracy, feature enhancement, and improved classification. Other examples can be seen in digital microscopy, where the same specimen may be recorded at several different focus settings; or in multispectral radar imaging through a scattering medium which has different transfer functions at different frequencies.

Image restoration is an inverse problem which assumes having a prior information about the formation model. This model includes all sorts of distortions related to the image degradation. For instance, the atmospheric turbulence, the relative motion between an object and the camera, the out-of-focus camera, the variations in optical and electronic imaging components, etc.

Conventionally, the image acquisition is modelled by the convolution with the PSF and noise (1.10). The PSF introduces low-pass distortions into an image which are called often as blur. When the blur is unknown, the image restoration becomes a blind inverse problem or blind deconvolution. For multiple observations of one scene, it is a multiframe, or multichannel, blind inverse problem.

A theoretical breakthrough on the blind and non-blind deconvolution techniques has

Figure 4.7: Illustration of Cameraman image restoration (lower row) from its three blurred noisy observations (upper row).

been done in works on perfect blur and image reconstruction. With the blur functions satisfying certain co-primeness requirements the existence and uniqueness of the solution is guaranteed under quite unrestrictive conditions, i.e. both the blur and the original image can be determined exactly in the absence of noise, and stably estimated in its presence (Harikumar, 1999a; Harikumar, 1999b; Giannakis, 2000).

A number of works have been done to deal with noisy data. In particular, the blind deconvolution based on the Bussgang filters is proposed in (Panci, 2003). The inverse filter is build as a nonlinear approximation of the optimal Wiener deconvolution filter. This approach is used efficiently for both multi-channel and single-channel blind deconvolution in (Campisi, 2007, pp. 43-93).

Blind noise-resistant deconvolution algorithms based on the least square method have been proposed in (Sroubek, 2003). The criterion includes the standard quadratic fidelity term as well as a quadratic term of the cross-channel balance. Overall, the criterion is nonquadratic as the total variation and Mumford-Shah energy functionals are used as the regularizators. These nonquadratic terms, or penalty functions, of the criterion result in a nonlinear edge-preserving filtering (Rudin, 1992; Mumford, 1989; Chan, 2001). It is shown in (Sroubek, 2003) that the proposed algorithm using this sort of regularization performs quite well.

The novel approach obtained as a further development of (Sroubek, 2003) was pro-

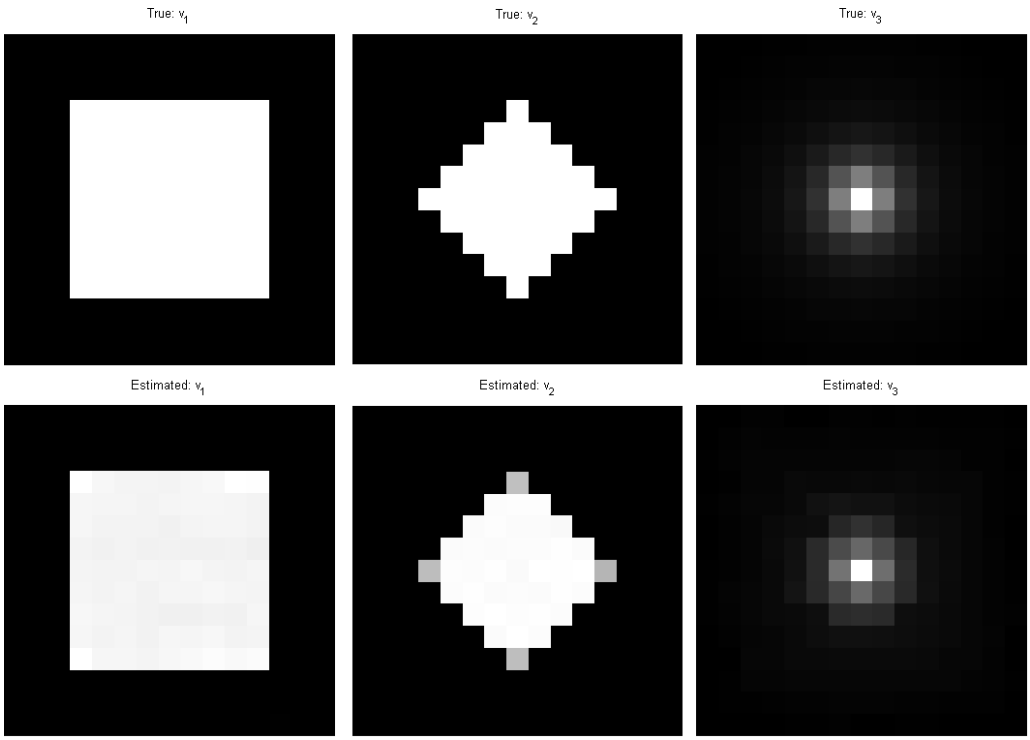

Figure 4.8: The used three PSFs (upper row) and their estimates (lower row).

posed in the recent paper (Sroubek, 2005). The main emphasise of this work is done on multichannel deblurring of spatially misaligned images. The proposed algorithm does not require the accurate size of supports of the blur functions, and the observed images are not assumed to be perfectly spatially aligned.

Many state-of-the-art works on image blind deconvolution can found in the recent book (Campisi, 2007) dedicated to this problem.

The technique proposed in Publication V is based on the frequency domain representation of the observation model. One of the benefits of this approach concerns the ability to work with large images and with large supports of PSFs.

4.3.1 Gradient-Projection Algorithm

Let us present briefly the formal approach to solve the problem (1.11). The blind deconvolution is ill-posed with respect to both the image and the blurring operators. Therefore, a joint regularization technique is commonly used in order to regularize both v_j and y (Campisi, 2007, Chapter 3).

In order to estimate v_j and y, let us consider the problem of minimization of the

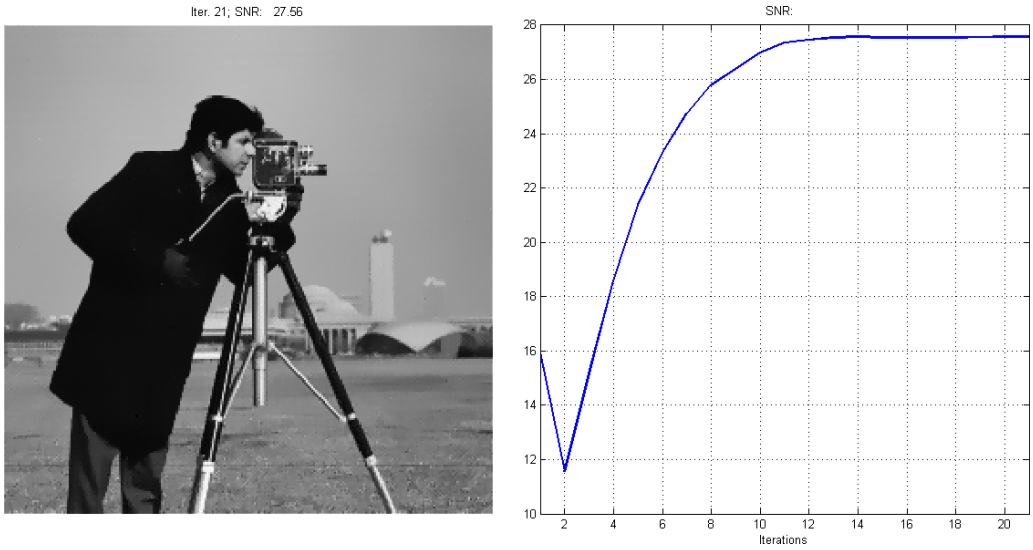

Figure 4.9: The result of restoration of Cameraman (left) after 20 iterations and the plot illustrating improving SNR criterion vs. iterations (right).

following non-negative functional:

$$\min_{y,v_j,j=1,\ldots,L} J = \sum_{j=1}^{L} \frac{1}{\sigma_j^2} \sum_x \left(z_j - y \circledast v_j\right)^2 + \lambda_2 \sum_x y^2 + \lambda_1 \sum_{i,j=1}^{L} d_{ij} \sum_x \left(z_i \circledast v_j - z_j \circledast v_i\right)^2 + \lambda_3 \sum_{j=1}^{L} \sum_x v_j^2, \tag{4.18}$$

where the first term corresponds to the fidelity between estimate and observation signal, the terms $\sum_x y^2$ and $\sum_{j=1}^{L} \sum_x v_j^2$ impose boundedness on the solution. The normalization factor $1/\sigma_j^2$ follows from the observation model as $E\left\{\left(z_j(x) - (y \circledast v_j)(x)\right)^2\right\} = \sigma_j^2$. Since the fidelity term corresponds to multiple observations, the normalization is applied to each of them.

An important difference between (4.18) and conventional approaches in regularization, for instance as Tikhonov regularization, is the cross-term $\sum_{i,j=1}^{L} d_{ij} \sum_x \left(z_i v_j - z_j v_i\right)^2$ that is equal to 0 if the given data is noiseless ($z_j = y \circledast v_j$):

$$z_j \circledast v_i = (y \circledast v_j) \circledast v_i = (y \circledast v_i) \circledast v_j = z_i \circledast v_j. \tag{4.19}$$

This term serves as a measure of divergence between true PSFs and their estimates.

Analogously to the fidelity term, the normalization factor d_{ij} is calculated exploiting (4.19) as

$$\begin{aligned} E\left\{\left(z_i \circledast v_j - z_j \circledast v_i\right)^2\right\} &= E\left\{\left((\sigma_i \eta_i \circledast v_j) - \left(\sigma_j \eta_j \circledast v_i\right)\right)^2\right\} = \\ &= \sigma_i^2 \sum_x v_j^2 - \sigma_j^2 \sum_x v_i^2, \end{aligned}$$

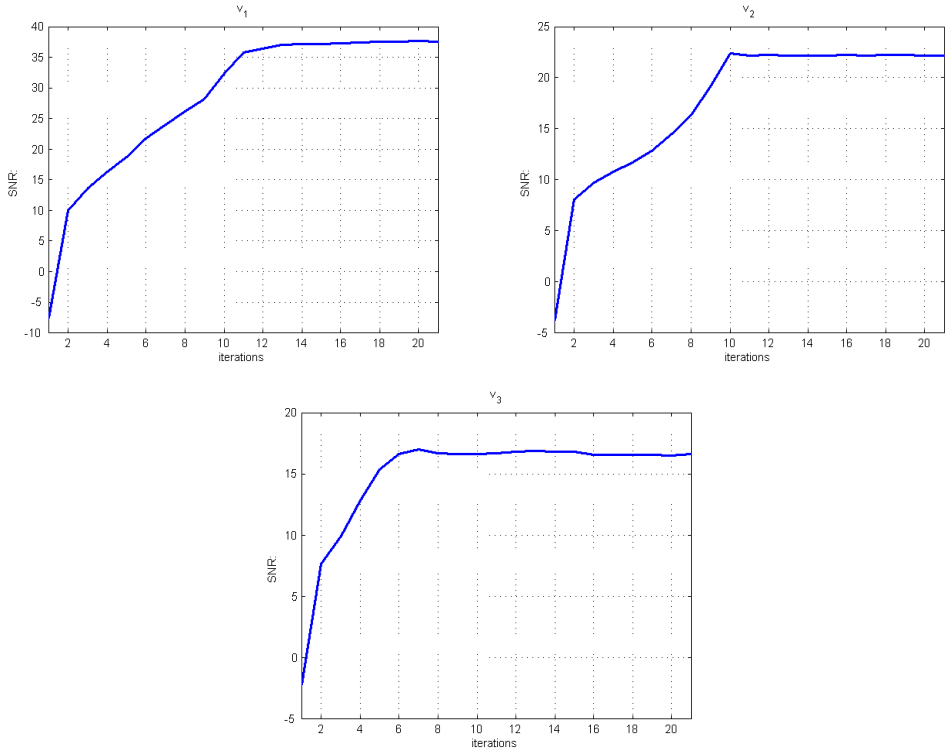

Figure 4.10: Improving the SNR criterion vs number of iterations for restoration of the Cameraman and three PSFs.

where η_i and η_j denote different realizations of the noise in order to avoid possible confusion comparing to (1.11). Here, σ_i and σ_j are the standard deviations of the Gaussian noise and they are constant over the observations z_i and z_j. Hence, $d_{ij} = \frac{1}{\sigma_i^2 \sum_x v_j^2 - \sigma_j^2 \sum_x v_i^2}$.

Using the Parseval's theorem, $\sum_x y^2(x) = \sum_\omega |Y(\omega)|^2/(2N \cdot 2M)$, minimization of (4.18) is equivalent to minimization of the functional

$$J = \sum_{j=1}^{L} \frac{1}{\sigma_j^2} \sum_\omega |Z_j - YV_j|^2 + \lambda_2 \sum_\omega |Y|^2 + \tag{4.20}$$
$$\lambda_1 \sum_{i,j=1}^{L} d_{ij} \sum_\omega |Z_i V_j - Z_j V_i|^2 + \lambda_3 \sum_{j=1}^{L} \sum_\omega |V_j|^2,$$

where

$$d_{ij} = \frac{2N \cdot 2M}{\sigma_i^2 \sum_f |V_j|^2 + \sigma_j^2 \sum_f |V_i|^2}. \tag{4.21}$$

Here, Z_j, Y, and V_j are the Fourier transforms (FTs) of the signals z_j, y, and v_j, respectively. For the sake of simplicity, we do not show in the formulas the frequency argument ω.

The estimates of the signal and of the PSFs are the solutions of the following problem:

$$(\hat{y}, \hat{v}_j) = \text{argmin}_{y \in Q_y, v_j \in Q_{v_j}} J, \tag{4.22}$$

where the admissible convex sets Q_y for y and Q_{v_j} for v_j are defined as $Q_y = \{y : 0 \le y \le 1\}$, $Q_{v_j} = \{v_j : \sum_x v_j(x) = 1, v_j(x) \ge 0, v_j(x) = 0 \text{ if } |x_1| > \Delta, |x_2| > \Delta\}$. The sets Q_{v_j} impose the positivity and normalized mean value assumptions on PSFs v_j. The parameter $\Delta > 0$ defines the size of the support of $v_j(x)$.

The recursive projection-gradient algorithm is used for solution of (4.22). Firstly, the values $Y^{(k)}$ and $V_j^{(k)}$ are calculated:

$$Y^{(k)} = Y^{(k-1)} - \alpha_k \partial_{Y^*} J(Y^{(k-1)}, V^{(k-1)}), \tag{4.23}$$

$$V_j^{(k)} = V_j^{(k-1)} - \beta_k \partial_{V_j^*} J(Y^{(k)}, V^{(k-1)}), \tag{4.24}$$

where $k = 1, ...$; $\alpha_k > 0$ and $\beta_k > 0$ are step-size parameters.

Secondly, $Y^{(k)}$, $V_j^{(k)}$ are projected onto the sets Q_y, Q_{v_j}:

$$P_{Q_y}\{y\} = \max\{0, \min(1, y)\}, \tag{4.25}$$

$$P_{Q_{v_j}}\{v_j\} = v_j / \sum_x v_j(x), \ v_j \ge 0, \tag{4.26}$$

$$v_j(x) = 0 \text{ if } |x_1| > \Delta, \ |x_2| > \Delta.$$

The ill-conditioning of the considered inverse problem means that the criterion J has different scale behavior for different frequencies. In order to enable stable iterations for all frequencies the step-sizes α_k and β_k should be small and, as result, the partial convergence rates on $Y^{(k)}$ and $V_j^{(k)}$ can be very slow.

The convergence of the algorithm on the variables Y and V_j is defined mainly by the second-order derivative $H_{Y^*Y} = \partial_Y \partial_{Y^*} J$ for Y and the Hessian matrix $H_{V^*V^T} = \left(\partial_{V_i} \partial_{V_j^*} J\right)_{i,j}$ for V.

The final solution is obtained as:

$$Y^{(k)} = P_{Q_y}\left\{(1-\alpha_k) Y^{(k-1)} + \alpha_k \frac{\sum_j Z_j V_j^{*(k-1)} / \sigma_j^2}{\sum_j |V_j^{(k-1)}|^2 / \sigma_j^2 + \lambda_2}\right\}, \tag{4.27}$$

$$V_j^{(k)} = P_{Q_{v_j}}\left\{(1-\beta_k) V_j^{(k-1)} + \right. \tag{4.28}$$

$$\left. \beta_k \frac{Z_j Y^{*(k-1)} / \sigma_j^2 + \lambda_1 Z_j \sum_{i, i \ne j} d_{ij}^{(k-1)} V_i^{(k-1)} Z_i^*}{|Y^{(k)}|^2 / \sigma_j^2 + \lambda_1 \sum_{i, i \ne j} d_{ij}^{(k-1)} |Z_i|^2 + \lambda_3}\right\},$$

where $d_{ij}^{(k-1)}$ are calculated in (4.21) for $V_j = V_j^{(k-1)}$.

Some of the restrictions defining Q_y and Q_{v_j} (e.g., $0 \le y \le 1$) are not principal and are imposed only to improve the convergence and the accuracy of the algorithm.

The recursive procedure endowed with the spatially-adaptive LPA-ICI filters works as a spatially-adaptive regularizator for the blur-operator inversion. It is applied to $y^{(k)}, v_j^{(k)}$

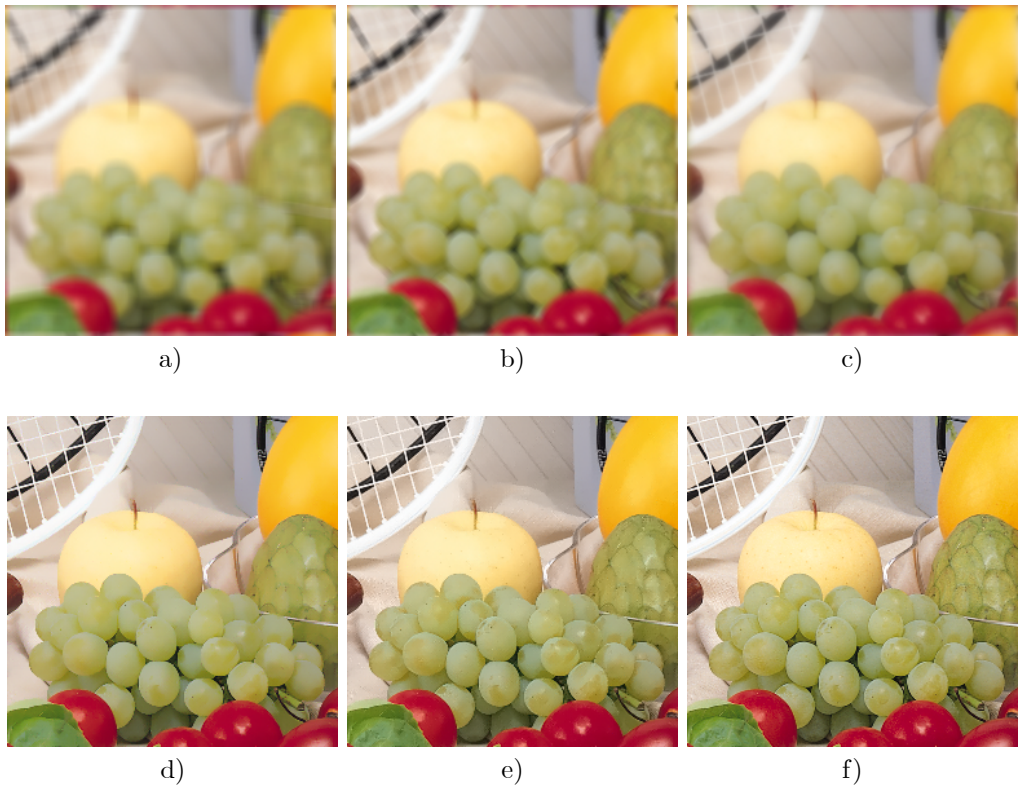

Figure 4.11: The three blurred noisy observations: a) blurred with boxcar 9×9 PSF; b) blurred with rotated by 45^0 boxcar 7×7 PSF; c) blurred with inverse-quadratic 7×7 PSF. Blind reconstruction estimate in: d) RGB color space; e) Opponent color space. The true *Fruits* image is illustrated in (f).

according to the algorithm:

$$\begin{aligned} y^{(k)} &\triangleq \mathcal{LI}\left\{y^{(k)}\right\}, \\ v_j^{(k)} &\triangleq \mathcal{LI}\left\{v_j^{(k)}\right\}, \ j = 1, ..., L. \end{aligned}$$

The details of algorithm derivation and implementation are given in Publication V.

4.3.2 Experiments

Simulation experiments show the efficiency of the restoration algorithm which demonstrates good convergence and high quality image restoration. The algorithm is quite robust with respect to the support sizes used in the PSF estimation.

The simulations for the Cameraman test image are given in Fig.4.7-4.10. We consider three channel observations with the following different PSFs: Box-car 9×9 uniform; Box-car 7×7 uniform rotated by 45^0; "Inverse-quadratic" $v\left(x_1, x_2\right) = \left(1 + x_1^2 + x_2^2\right)^{-1}$,

$x_1, x_2 = -7, \ldots, 7$ (Fig.4.8). The level of noise in the observations z_j, $j = 1, 2, 3$, is such that BSNR

$$\mathrm{BSNR}_j = 10 \log_{10} \left(\frac{1}{\sigma^2} \left\| v_j \circledast y - \frac{1}{2N \cdot 2M} \sum_{x \in X} (v_j \circledast y)(x) \right\|_2^2 \right)$$

is equal to 40 dB. The obtained observations and the restored image are shown in Fig.4.7. Similarly, the true simulated PSFs and their restored estimates are illustrated in Fig.4.8.

Improvement of the SNR criterion versus iteration number is illustrated for the observation z in Fig.4.9 and three PSFs v_j in Fig.4.10.

As a test image for blind deconvolution of color images we used 256×256 RGB Fruits image (Fig.4.11f). We assume that blurring operator v_j for a single observation $z_j = (R, G, B)$ is the same for all color R (red), G (green), and B (blue) channels. The PSFs v_j used are the same as for grayscale images experiments provided in the previous section. The level of noise is set to be 40 dB for each channel. The observations z_j obtained are illustrated in Fig.4.11a-c.

The restored image when the proposed technique was applied to the three color channel independently is shown in Fig.4.11d. However, usually natural color images are highly correlated. We use the opponent color space transformation in order to decorrelate these color signals (Plataniotis, 2000).

The results of image restoration are illustrated in Fig.4.11e that looks significantly more natural. Evaluation in terms of the SNR showed about 1 dB higher values then those for straightforward restoration in RGB color space.

As it was mentioned above, some of the restrictions imposed on the signal and the PSFs (Q_y and Q_{v_j}) are not principal. However, they may help to improve the convergence and the accuracy of the algorithm. Stronger assumptions, for instance assumptions imposed of the size and the model of PSFs v_j, may lead to the general single-channel blind deconvolution approach, where a single observation is enough to restore the true image y.

4.4 Single-Channel Blind Deconvolution

Recently, applications of neural networks in image restoration became very popular. In (Da Rugna, 2006), a neural network is used for segmentation. The authors propose an approach to find and classify areas in one photo image that are blurred and in-focus. In (Qiao, 2006) a support-vector machine (SVM)-based method is used for blind super-resolution image restoration.

In Publication VI, we proposed a novel approach to blind deconvolution when the PSF and its parameter are identified by a classifier. The multilayer neural network based on multi-valued neurons (MLMVN) was used for this purpose, whose precise identification is of crucial importance for the image deblurring.

We proposed to identify a blur model and its parameters from the finite number of multiple models and the corresponding parameters using single observed blurred image. The proposed solution is a one step process, which is significantly different from typical single-channel blind deconvolution.

Preliminary results in (Aizenberg, 2006a; Aizenberg, 2006b) showed efficiency of this approach. The MLMVN was exploited for identification of a type of blur among six

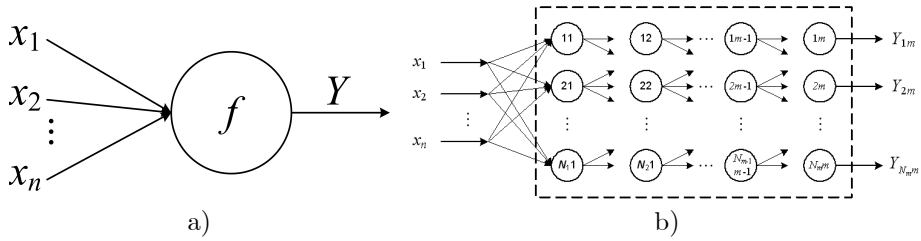

Figure 4.12: a) A neural element with n inputs and activation function f; b) A neural network with n inputs, m layers, and N_m outputs.

trained blurs and their parameters. The functionality of the MLMVN is higher than the ones of the traditional feedforward neural networks and a variety of kernel-based networks (Aizenberg, 2006c). Its higher flexibility and faster adaptation to the mapping makes possible an accomplishment of complex problems using a simpler network. Therefore, the MLMVN can be used to solve those non-standard recognition and classification problems.

When the PSF is identified, the problem becomes conventional deconvolution. The adaptive LPA-ICI based deconvolution technique (Katkovnik, 2005) was used for this purpose.

4.4.1 Multilayer Neural Network Based on Multi-Valued Neurons as a Classifier

A multi-layered feedforward neural network (MLF) and a backpropagation learning algorithm for it are well studied from all points of view. It is possible to say that this is a classical example of a neural network. We can refer in this context to the hundreds of the papers and books. Let us refer, for example, to the book (Haykin, 1998). A multi-layer architecture of the network with a feedforward dataflow through nodes that requires full connection between consecutive layers and an idea of a backpropagation learning algorithm was proposed in (Rumelhart, 1986). It is well known (Haykin, 1998) that MLF can be used as a universal interpolator. It is also well known that MLF is traditionally based on the neurons with a sigmoid activation function. MLF learning is based on the backpropagation learning algorithm, when the error is being sequentially backpropagated form the "right hand" layers to the "left hand" ones (Fig.4.12b).

On the other hand, it is possible to use different neurons as the basic ones for a network with a feedforward architecture. We consider the MLMVN.

A multi-valued neuron (MVN) is based on the principles of the multiple-valued threshold logic over the field of the complex numbers. A comprehensive observation of MVN and its learning is presented in (Aizenberg, 2000). Different applications of MVN have been considered during the last years: MVN has been successfully used, for example, as a basic neuron in cellular neural networks (Aizenberg, 2000), as a basic neuron of neural-based associative memories (Aizenberg, 2000; Jankowski, 1996; Aoki, 2000; Muezzinoglu, 2003; Aoki, 2001) and as the basic neuron of pattern recognition systems (Muezzinoglu, 2003; Aoki, 2001).

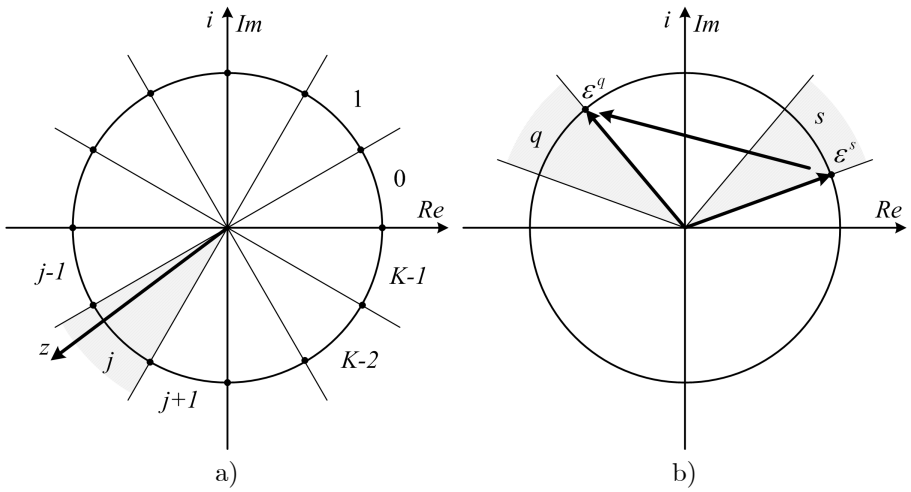

Figure 4.13: a) Geometrical interpretation of the MVN activation function; b) Geometrical interpretation of the MVN learning rule.

The mentioned successful applications of MVN make further extensions very attractive. Taking into account that a single MVN has a higher functionality than a single neuron with a sigmoid activation function and that learning of a single MVN is based on the simple linear error correction rule, it would be interesting to consider a neural network with a traditional feedforward architecture, but with MVN as a basic neuron.

MVN with discrete activation function

An MVN was introduced in (Aizenberg, 1992) as a neural element based on the principles of multiple-valued threshold logic over the field of complex numbers proposed in (Aizenberg, 1977). It was thoroughly analyzed in (Aizenberg, 2000), where its theory, basic properties, and learning were presented.

A single discrete-valued MVN performs a mapping between n inputs and a single output (Fig.4.12a). This mapping is described by a multiple-valued (K-valued) function of n variables $f(x_1, ..., x_n)$ with $n + 1$ complex-valued weights as parameters:

$$f(x_1, ..., x_n) = P(w_0 + w_1x_1 + ... + w_nx_n), \tag{4.29}$$

where $X = (x_1, ..., x_n)$ is an input vector (pattern vector) and $W = (w_0, w_1, ..., w_n)$ is a weighted vector. The function and variables are the K^{th} roots of unity: $\varepsilon^j = \exp(i2\pi j/K)$, $j = 0, ..., K-1$, where i is an imaginary unity. P is the activation function of the neuron:

$$P(z) = \exp(i2\pi j/K), \text{ if } 2\pi j/K \le \arg z < 2\pi(j+1)/K, \tag{4.30}$$

where $j = 0, ..., K-1$ are the values of K-valued logic, $z = w_0 + w_1x_1 + ... + w_nx_n$ is a weighted sum, $\arg z$ is the argument of the complex number z. Fig.4.13a illustrates the

idea behind (4.30). Function (4.30) divides a complex plane onto K equal sectors and maps the whole complex plane into a subset of points belonging to the unit circle. This is a set of K^{th} roots of unity.

Let ε^q be a desired output of the neuron (see Fig.4.13b) and $\varepsilon^s = P(z)$ be an actual output of the neuron. The most efficient MVN learning algorithm is based on the error-correction learning rule (Aizenberg, 2000):

$$W_{r+1} = W_r + \frac{C_r}{n+1}(\varepsilon^q - \varepsilon^s)\bar{X}, \tag{4.31}$$

where X is an input vector, n is the number of neuron's inputs, $\bar{X}$ is a vector with the components complex conjugated to the components of vector X, r is the index of iteration, W_r is the current weighted vector, W_{r+1} is a weighted vector after correction, C_r is a learning rate.

MVN with continuous activation function

The activation function (4.30) is discrete. As proposed in (Aizenberg, 2005b; Aizenberg, 2007b), the function (4.30) can be modified in order to generalize it for the continuous case in the following way: if $K \to \infty$ in (4.30) then the angle value of the sector approaches zero. Hence, the function (4.30) can be defined as follows:

$$P(z) = \exp(i(\arg z)) = e^{i\,\mathrm{Arg}\,z} = \frac{z}{|z|}, \tag{4.32}$$

where $\mathrm{Arg}\,z$ is the main value of the argument of the complex number z and $|z|$ is its modulo.

The function (4.32) maps the complex plane into a whole unit circle, while the function (4.30) maps a complex plane just into a discrete subset of the points belonging to the unit circle. Thus, the activation function (4.32) determines a continuous-valued MVN. The learning rule (4.31) is modified for the continuous-valued case in the following way (Aizenberg, 2005b; Aizenberg, 2007b):

$$W_{r+1} = W_r + \frac{C_r}{n+1}\left(\varepsilon^q - \frac{z}{|z|}\right)\bar{X}. \tag{4.33}$$

MVN-based Multilayer Feedforward Neural Network

A multilayer feedforward neural network (Rumelhart, 1986) (MLF, it is also often referred as a "multilayer perceptron") and backpropagation learning algorithm for it are well established. MLF learning is based on the algorithm of error backpropagation. The error is sequentially backpropagated from the "rightmost" layers to the "leftmost" ones. A crucial property of the MLF backpropagation is that the error of each neuron of the network is proportional to the derivative of the activation function.

As proposed in (Aizenberg, 2005b; Aizenberg, 2007b), MLMVN network has at least two principal advantages in comparison with an MLF: higher functionality, (i.e. an MLMVN with the smaller number of neurons outperforms an MLF with the larger number of neurons) and simplicity of learning.

As mentioned above for a single multi-valued neuron, the differentiability of the MVN activation function is not required for its learning. The MVN learning is reduced to the

movement along the unit circle and it is based on the error-correction rule. Hence, the correction of weights is completely determined by the neuron's error. The same property holds not only for the single MVN, but for an MVN-based feedforward neural network.

A backpropagation training algorithm for the MLMVN is analogous to training of a single MVN. Firstly, this algorithm for the MLMVN with a single output neuron and a single hidden layer has been derived in (Aizenberg, 2007b).

MLMVN is a multilayer neural network with standard feedforward architecture, where the outputs of neurons from the preceding layer are connected with the corresponding inputs of neurons from the following layer. The network contains one input layer, $m-1$ hidden layers and one output layer, the m^{th} one. Let us use here the following notations. Let T_{km} be a desired output of the k^{th} neuron from the m^{th} (output) layer; Y_{km} be an actual output of the k^{th} neuron from the m^{th} (output) layer (Fig.4.12b). Then the global error of the network taken from the k^{th} neuron of the m^{th} (output) layer is calculated as follows:

$$\delta^*_{km} = T_{km} - Y_{km}. \tag{4.34}$$

The square error functional for the s^{th} pattern $X_s = (x_1, ..., x_n)$ is as follows:

$$E_s = \sum_k \left(\delta^*_{km}\right)^2,$$

where δ^*_{km} is a global error of the k^{th} neuron of the m^{th} (output) layer, E_s is the square error of the network for the s^{th} pattern. It is fundamental that the error depends not only on the weights of the neurons from the output layer but on all neurons of the network.

The backpropagation of the global errors δ^*_{km} through the network is used (from the m^{th} (output) layer to the $m-1^{st}$ one, from the $m-1^{st}$ one to the $m-2^{nd}$ one, ..., from the 2^{nd} one to the 1^{st} one) in order to express the error of each neuron δ_{kj}, $j = 1, ..., m$ by means of the global errors δ^*_{km} of the entire network.

The errors of the m^{th} (output) layer neurons are:

$$\delta_{km} = \frac{1}{s_m}\delta^*_{km}, \tag{4.35}$$

where km specifies the k^{th} neuron of the m^{th} layer; $s_m = N_{m-1} + 1$, i.e. the number of all neurons on the preceding layer (layer $m-1$ which the error is propagated back to) incremented by 1.

The errors of the hidden layers neurons are computed as follows:

$$\delta_{kj} = \frac{1}{s_j}\sum \delta_{ij+1}\left(w_k^{ij+1}\right)^{-1}, \tag{4.36}$$

where kj specifies the k^{th} neuron of the j^{th} layer ($j = 1, \ldots, m-1$); $s_j = N_{j-1} + 1$, $j = 2, ..., m$ is the number of all neurons in the layer $j-1$ (the preceding layer j which error is backpropagated to) incremented by 1.

The MVN learning is reduced to the movement along the unit circle and it is based on the error-correction learning rule. Thus, the correction of the weights is completely determined by the neuron's error. The same property is true not only for the single MVN, but also for the whole MLMVN. The errors of all neurons from the MLMVN are completely determined by the global errors of the network (4.34).

The weights for neurons of the network are corrected after calculation of all errors. This can be done by using the learning rule (4.30) or (4.32) depending on the discrete-(4.30) or continuous-valued (4.32) model. Let $\bar{\bar{Y}}_{ij}$ be the complex conjugated output of the i^{th} neuron from the j^{th} layer after weights update in the current training step. Hence, the following correction rules are used for the weights (Aizenberg, 2005b; Aizenberg, 2007b):

$$\begin{aligned} \tilde{w}_i^{kj} &= w_i^{kj} + \frac{C_{km}}{N_m+1}\delta_{km}\bar{\bar{Y}}_{km-1},\ i=1,..,n, \\ \tilde{w}_0^{kj} &= w_0^{kj} + \frac{C_{km}}{N_m+1}\delta_{km}, \end{aligned}$$

for the neurons from the m^{th} (output) layer (k^{th} neuron of the m^{th} layer),

$$\begin{aligned} \tilde{w}_i^{kj} &= w_i^{kj} + \frac{C_{kj}}{(N_j+1)\,|z_{kj}|}\delta_{kj}\bar{\bar{Y}}_{ij-1},\ i=1,..,n, \\ \tilde{w}_0^{kj} &= w_0^{kj} + \frac{C_{kj}}{(N_j+1)\,|z_{kj}|}\delta_{kj}, \end{aligned}$$

for the neurons from the 2^{nd} till $m-1^{st}$ layer (k^{th} neuron of the j^{th} layer ($j=2,\ldots,m-1$), and

$$\begin{aligned} \tilde{w}_i^{kl} &= w_i^{kl} + \frac{C_{kl}}{(n+1)\,|z_{kj}|}\delta_{kl}\bar{x}_i,\ i=1,..,n, \\ \tilde{w}_0^{kj} &= w_0^{kj} + \frac{C_{kl}}{(n+1)\,|z_{kl}|}\delta_{kl}, \end{aligned}$$

for the neurons of the 1^{st} hidden layer, where C_{kj} is a constant part of the learning rate.

In general, the learning process should continue until the following condition is satisfied:

$$E = \frac{1}{N}\sum_{s=1}^{N}\sum_{k}(\delta_{km}^*)_s^2 \le \lambda, \tag{4.37}$$

where λ determines the precision of learning. In particular, in the case when $\lambda = 0$ the equation (4.37) is transformed to $\delta_{km}^* = 0$ for all k and all s.

The detailed derivation of this training algorithm is given in Publication VI.

4.4.2 Training and Testing Patterns

The considered neural network is used for training on the training set of pattern vectors as follows.

The observed image $z(x)$ is modeled as the output of a linear shift-invariant system (1.10) which is characterized by the PSF v. The PSF v, e.g. Gaussian, linear motion, and the boxcar blurs are considered in Publication VI, has its own specific frequency characteristics. Hence it is natural to use its spectral coefficients as features for both training and testing sets. Since originally the observation is not v (v is not known) but z, we use spectral coefficients of z as input training (and testing) vectors in order to identify the PSF v. Since this model in the frequency domain is the product of the true

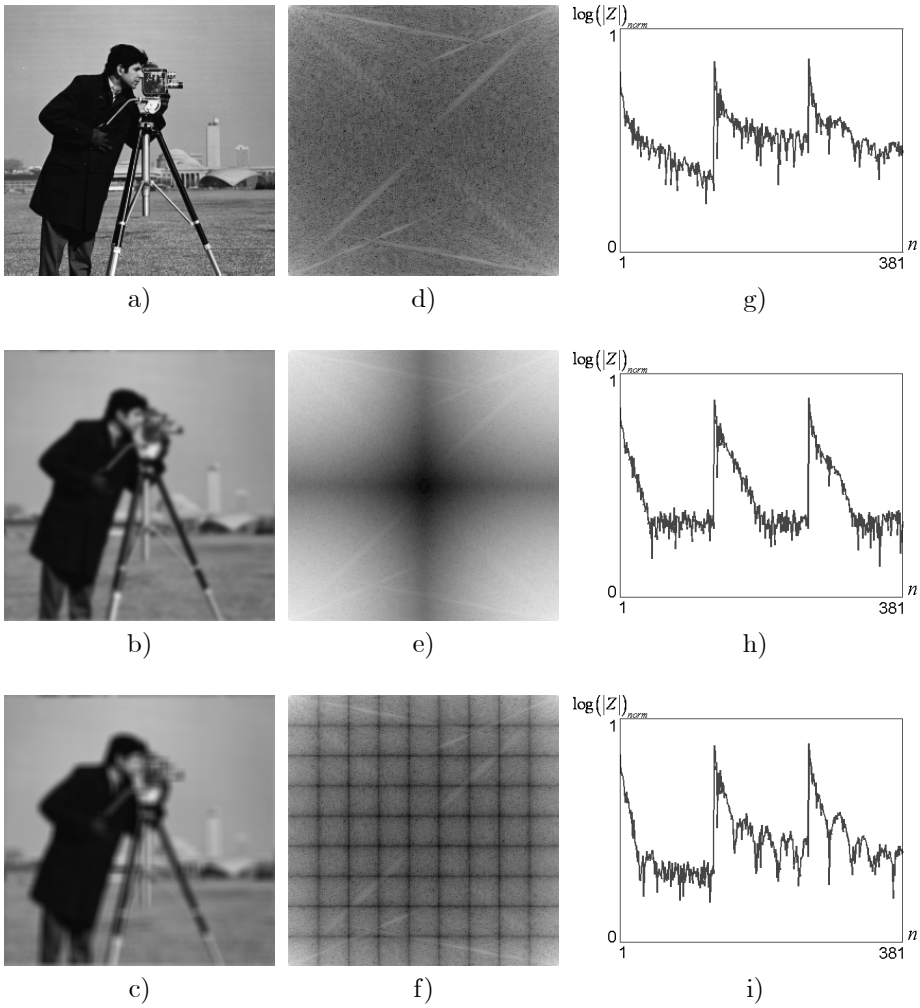

Figure 4.14: Illustration of pattern vectors selection for Cameraman test image: a) true image; b) image blurred with Gaussian PSF with variance 2; c) image blurred with rectangular boxcar PSF of the size 9x9. d) normalized $log|Z|$ of true image; e) normalized $log|Z|$ of image blurred with Gaussian PSF as in (b); f) normalized $log|Z|$ of image blurred with rectangular boxcar blur as in (c); g) the normalized $log|Z|$ values used as arguments to generate training vectors X obtained from the true image (a): h) training vectors X for image blurred with Gaussian blur as in (b); i) training vectors X for image blurred with rectangular boxcar blur as in (c).

object function Q and the PSF V, we state the problem as recognition of the shape of V and its parameter from the power-spectral density (PSD) of the observation Z, i.e. from $|Z|^2 = Z \cdot \overline{Z}$.

We use normalized log values of $|Z|$ for pattern vectors X in (4.29). Examples of X values are shown in Fig.4.14. The distortions of PSD for the test image Cameraman (Fig.4.14a) that are typical for each type of blur (Fig.4.14b,c) are clearly visible in

Fig.4.14e,f.

4.4.3 Blur Models

We consider Gaussian, motion, and rectangular (boxcar) blurs. We aim to identify both the blur, which is characterized by the PSF, and its parameter using a single network. Let us consider all these models and how they depend on the corresponding parameters.

The PSF v describes how the point source of light is spread over the image plane. It is one of the main characteristics of the optical system (Hecht, 2002). For a variety of devices, like photo or video camera, microscope, telescope, etc., PSFs are often approximated by the Gaussian function:

$$v(x) = \frac{1}{2\pi\sigma_{blur}^2} \exp\left(-\frac{x_1^2 + x_2^2}{\sigma_{blur}^2}\right), \tag{4.38}$$

where σ_{blur}^2 is a parameter of the PSF (the variance). Its Fourier transform V is also a Gaussian function.

Another source of blur is a uniform linear motion which occurs while taking a picture of a moving object relatively to the camera:

$$v\left(x\right) = \begin{cases} \frac{1}{h}, \sqrt{x_1^2 + x_2^2} < h/2, x_1 \cos\phi = x_2 \sin\phi, \\ 0, \text{ otherwise}, \end{cases} \tag{4.39}$$

where h is a parameter which depends on the velocity of the moving object and describes the length of motion in pixels, and ϕ is the angle between the motion orientation and the horizontal axis. Any uniform function like (4.39) is characterized by the number of slopes in the frequency domain.

The uniform rectangular blur is described by the following function:

$$v\left(x\right) = \begin{cases} \frac{1}{h^2}, |x_1| < \frac{h}{2}, |x_2| < \frac{h}{2}, \\ 0, \text{ otherwise}, \end{cases} \tag{4.40}$$

where parameter h defines the size of smoothing area.

4.4.4 Neural Network Structure

Below we consider the complex multiple-class identification problem where every class (blur model) also has a parameter to be identified. The number of neurons at the output layer N_m (see Section 4.4.1) equals to the number of classes to be identified (Fig.4.15a), and Ψ_i is a number of parameter's values for the i^{th} class, $i = 1, ..., N_m$. Each output neuron has to classify simultaneously blur, a parameter of the corresponding type of blur, and to reject other blurs (as well as an unblurred image) (Fig.4.15b).

4.4.5 Performance Evaluation

The MLMVN that we use here contains 5 neurons in the first hidden layer and 35 ones in the second hidden layer; this structure of the network has been selected experimentally.

The output level neuron has a specific structure (see Fig.4.15b). The range of values $[\exp\left(i \cdot 0\right) = 1, \exp\left(i \cdot 2\pi\right) = 1[$ of the activation function (4.32) is divided onto $\Psi_i + 1$

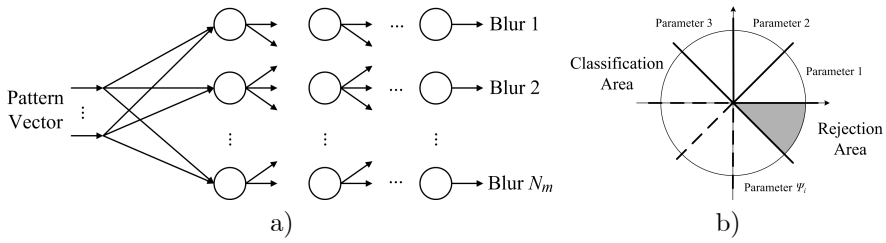

Figure 4.15: a) Structure of the feedforward neural network used for both blur model and its parameter identification; b) Structure of the neural element on the output layer of MLMVN.

intervals, each used for identification of the blur parameter value, and one more interval is used to reject other blurs and unblurred images.

As an example, let us consider performance of the MLMVN solving the problem of identification of the Gaussian PSF parameter. Thus, the structure of MLMVN is $5 \to 35 \to 1$. The Gaussian blur is considered with $\sigma_{blur} \in \{1, 1.33, 1.66, 2, 2.33, 2.66, 3\}$ (4.38), i.e. $\Psi_1 = 7$. The level of noise in (1.10) is selected to satisfy BSNR

$$\mathrm{BSNR} = 10 \log_{10} \left(\frac{1}{\sigma^2} \left\| v \circledast y - \frac{1}{2N \cdot 2M} \sum_{x \in X} (v \circledast y)(x) \right\|_2^2 \right) \tag{4.41}$$

to be equal to 40 dB.

We have used a database which consists of 150 greyscale images with sizes to generate the training and testing sets. 100 images are used to generate the training set and 50 other images are used to generate the testing set. The images with no blur and no noise were also included in both the training and testing set.

The trained network is used to perform classification on the testing set. The classification rate (CR) is computed as the number of correct classifications in terms of percentage (%):

$$CR = 100 \frac{N_{correct}}{N_{total}} \, (\%) \, ,$$

where N_{total} is a total number of pattern vectors X in the testing set, and $N_{correct}$ is a number pattern vectors correctly classified by the trained network.

The numerical results (given in Publication VI) for MLMVN showed CR close to 100%. Its performance was compared with such NN as support-vector machines (SVM), and MLF trained using the Fletcher-Reeves Conjugate Gradient and the Scaled Conjugate Gradient algorithms. The improvement in performance was significant.

For multiple models of blur, we provide the following two experiments. In the first experiment (Experiment 1) we consider six types of blur ($N_m = 6$) with the following parameters:

- the Gaussian blur $\sigma_{blur} \in \{1, 1.33, 1.66, 2, 2.33, 2.66, 3\}$, in (4.38), $\Psi_1 = 7$;
- the linear uniform horizontal $\phi = 0$ motion blur of the lengths 3, 5, 7, 9, in (4.39), $\Psi_2 = 4$;

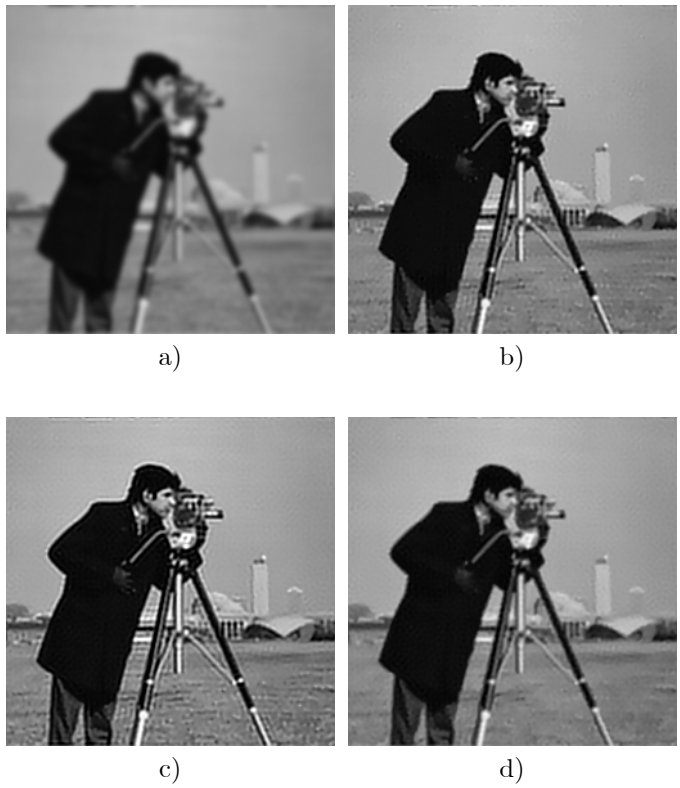

Figure 4.16: Experiments for Cameraman test image: a) noisy blurred image with Gaussian PSF $\sigma_{blur} = 2$; b) reconstructed using the regularization technique (Katkovnik, 2005) after the blur and its parameter has been identified as Gaussian PSF with $\sigma_{blur} = 2$ (ISNR=3.88 dB); c) the original image was blurred by the Gaussian PSF with $\sigma_{blur} = 1.835$ and then reconstructed using the regularization technique (Katkovnik, 2005) after the blur and its parameter has been identified as Gaussian PSF with $\sigma_{blur} = 2$ (ISNR=3.20 dB); d) the original Cameraman image was blurred by Gaussian PSF with $\sigma_{blur} = 2.165$ (This blurred image does not differ visually from the one in (a)) and then reconstructed using the regularization technique (Katkovnik, 2005) after the blur and its parameter has been identified as Gaussian PSF with $\sigma_{blur} = 2$ (ISNR=3.22 dB).

- the data corrupted by the linear uniform vertical $\phi = \pi/2$ motion blur of the length 3, 5, 7, 9, in (4.39), $\Psi_3 = 4$;

- the linear uniform diagonal motion from South-West to North-East blur $\phi = \pi/4$ of the lengths 3, 5, 7, 9, in (4.39), $\Psi_4 = 4$;

- the linear uniform diagonal motion from South-East to North-West blur $\phi = 3\pi/2$ of the lengths 3, 5, 7, 9, in (4.39), $\Psi_5 = 4$;

- rectangular has sizes 3×3, 5×5, 7×7, 9×9, in (4.40), $\Psi_6 = 4$.

Since we consider six types of blur ($N_m = 6$), the output layer contains six neurons. As mentioned above, the structure of the MLMVN is two hidden layers with 5 and 35 neurons, respectively and the output layer. Therefore, the structure of network is $5 \rightarrow 35 \rightarrow 6$.

Each neural element of the output layer has to classify a parameter of the corresponding type of blur, and reject other blurs, as well as the unblurred image. For instance, the first neuron is used to identify the Gaussian blur and to reject the non Gaussian ones. If the weighted sum for the 1^{st} neuron at the output (3^{rd}) layer hits the j^{th} interval, $j \in \{1, ..., 7\}$, then the input vector X corresponds to the Gaussian blur and its parameter is τ_j.

We have used the same initial database of 150 different greyscale images with sizes 256×256, which has been used to generate the training and testing sets. As well as above, 100 images are used to generate the training set and 50 other images are used to generate the testing set. The level of noise in (1.10) is selected satisfying BSNR (4.41) to be equal to 40 dB.

The trained network is used to perform the classification on the testing set. The CR is used as an objective criterion of classification. The results are presented in Publication VI.

The results of using the MLMVN classification for image reconstruction are shown in Fig.4.16 for the test Cameraman image. The adaptive deconvolution technique proposed in (Katkovnik, 2005) has been used after the blur and its parameter identified. The image was blurred by the Gaussian PSF (4.38) with $\sigma_{blur} = 2$. It is seen that if classified PSF coincides with the true PSF, then the value of ISNR criterion is 3.88 dB. If the image is blurred using $\sigma_{blur} = 2 - 0.33/2 = 1.835$ or $\tau = 2 + 0.33/2 = 1.835$ then the network classifies them as blurred with $\sigma_{blur} = 2$ and reconstruction is applied using the recognized value. Then, the error of reconstruction is approximately 0.6 dB below the accurate value in the case if reconstruction would be performed for original σ_{blur}.

In order to reduce this error we propose to consider Experiment 2. We are targeting here classification of a single Gaussian blur type, but with much higher precision. The grid of the blur's parameters is finer with significantly larger number of them in the same interval $\sigma_{blur} \in \{1 + 0.15\Delta : \Delta = 0, 1, ..., 14\}$ in (4.38), which makes the problem of classification more challenging. The output layer of the network contains in this case a single neuron, and the network structure is $5 \rightarrow 35 \rightarrow 1$.

The error of classification was formally higher, approximately by 10%. Nevertheless, it is very important that the reconstruction error for the similar experiment as shown in Fig.4.16 does not exceed 0.1 dB, which is a minor value in practice. During the reconstruction simulation we used the images that have been blurred with $\sigma_{blur} = 2 - 0.15/2 = 1.925$ and $\sigma_{blur} = 2 + 0.15/2 = 2.075$, while the reconstruction has been done as for $\sigma_{blur} = 2$.

4.5 Techniques to Select the Varying Regularization Parameter

The estimation of y from the observation z (1.10) is a removal of the degradation caused by the PSF v. Usually this problem is ill-posed which results in instability of the solution which, in particular, is very sensitive with respect to the additive noise.

In the 2D frequency domain for the circular convolution the model (1.10) takes a form:

$$Z(\omega) = V(\omega)Y(\omega) + n(\omega), \tag{4.42}$$

$Z = \mathcal{F}\{z\}$, $V = \mathcal{F}\{v\}$, $Y = \mathcal{F}\{y\}$, $n = \mathcal{F}\{n\}$, and $\omega \in W$, is the normalized 2D discrete frequency as in (4.1). $n(x)$ is the white Gaussian noise (1.3).

Stabilizing effects can be introduced by constraints imposed on the solution. A general approach to this kind of constrained estimation refers to the methods of Lagrange multipliers and the Tikhonov regularization (Tikhonov, 1977). The regularized (constrained) inverse (RI) filter can be obtained as a solution of the least square problem with a penalty term:

$$\hat{Y} = \arg\min_{Y} J = \|Z - VY\|_2^2 + r\,\|Y\|_2^2\,, \tag{4.43}$$

where $r \geq 0$ is a regularization parameter and $\|\cdot\|_2$ denotes Euclidean norm. Here, the first term $\|Z - VY\|_2^2$ evaluates the fidelity of the model VY to the available data Z and the second term $\|Y\|_2^2$ bounds the power of this estimate. The regularization parameter r balances these two terms in the criterion J. In (4.43), and further, we omit the argument ω in the Fourier transforms. We obtain the estimate of the image by minimizing (4.43):

$$\widehat{y}_r(x) = \mathcal{F}^{-1}\left\{\widehat{Y}\right\},\ \widehat{Y} = \frac{V^*}{|V|^2 + r} Z, \tag{4.44}$$

where $(^*)$ means the complex-conjugate variable.

The PSF v can be estimated for a particular optical system (e.g. as in Section 4.2), or can be estimated in blind manner as it was proposed in Section 4.3 and identified as in Section 4.4. The regularization parameter r is an important parameter that controls a trade-off between fidelity to data and smoothness of a solution adjusted by a regularization parameter. The problem to select the proper r plays a crucial role in any inverse regularization.

A proper selection of the regularization parameter r in (4.44) is a key point of the regularization technique overall. There are numerous publications concerning this problem.

Roughly speaking there are two types of methods: with a prior knowledge and without a prior knowledge about the noise variance σ^2 in (1.3). The L-curve method, sometimes also called the Tikhonov curve method, belongs to the group of methods with no information on the value of σ^2 (e.g. in (Miller, 1970), and (Tikhonov, 1977)). This technique uses a $\log - \log$ plot with the $\log \left\|Z - V\widehat{Y}\right\|_2^2$ as an abscissa and $\log \left\|\widehat{Y}\right\|_2^2$ as an ordinate, with r as a parameter along this curve. The transition between under- and over-regularization corresponds to the "corner" of the L-curve and the corresponding value of r is proposed as an optimal value of the regularization parameter that minimizes (4.43). Further, this idea was developed in (Hansen, 1992) where he has stipulated conditions when the corner exists. The corner is defined as the maximal curvature point of the $\log - \log$ plot. Methods for detection of this point can be seen in (Hansen, 1993; Oraintara, 2000).

Galatsanos and Katsaggelos in (Galatsanos, 1992) proposed a technique for selection of the asymptotically optimal regularization parameter provided that the variance of noise in (1.10) is known. This approach is based on calculation of the derivative of the mean squared error (MSE) functional. A similar idea is exploited by Neelamani et al.

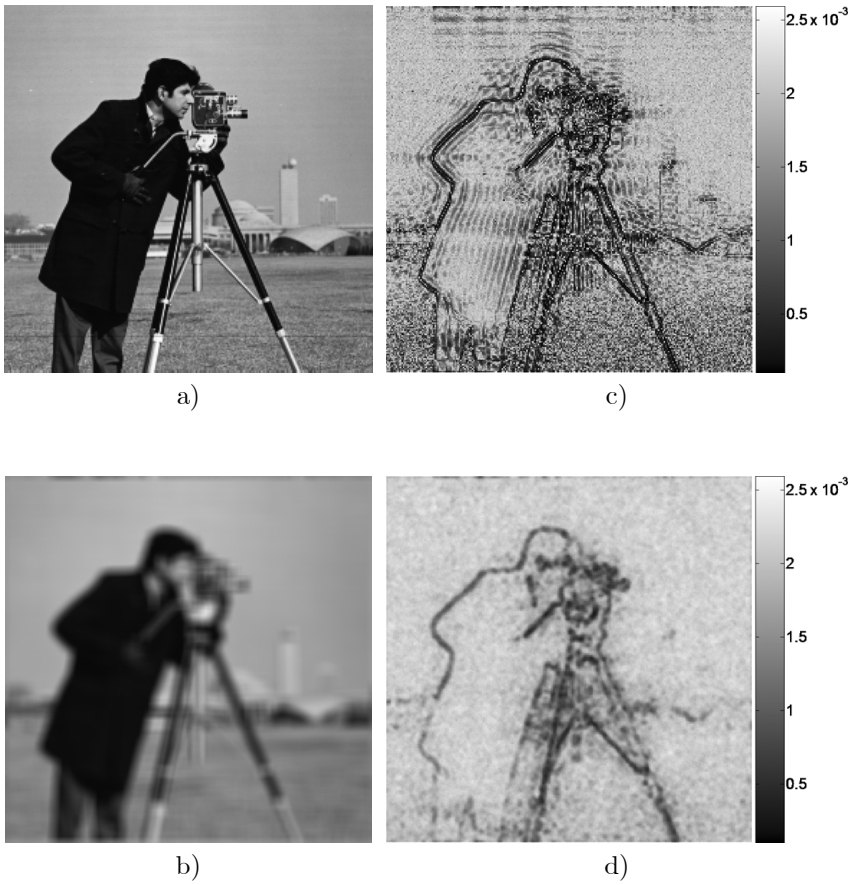

Figure 4.17: Results obtained by Monte-Carlo (100 runs) silmulations for Cameraman test image: a) true image; b) blurred with 9x9 boxcar PSF and noisy (white Gaussian noise) with BSNR=40dB; c) values of the varying *oracle* regularization parameters; d) varying regularization parameters obtained by the ICI rule.

in (Neelamani, 2003), where the optimal invariant regularization parameter is found by minimizing an upper bound of MSE calculated in the Fourier-Wavelet domain. The iterative constrained total least-square adaptive procedure is used in (Chen, 2000), and its stability and convergence are shown.

The review of the methods for invariant regularization parameter selection can be found in (Galatsanos, 1992; Thompson, 1991; Vogel, 2002).

In (Berger, 1999), authors propose a spatially varying regularization parameter selection and describe a method based on the local weighted standard deviation analyzing the difference signal of the estimate. Wu et al. in (Wu, 2004b) choose both the spatially adaptive regularization parameter and regularization operator by estimation of the local noise variance and detecting edges in the image.

In Publication VII we develop two methods based on minimization of the point-wise mean squared error. The first algorithm is based on estimation of the squared point-wise bias. The second algorithm is based on direct multiple statistical hypothesis testing for the estimates calculated with different regularization parameters. The estimates $\widehat{y}_r(x)$ are calculated for different r and those estimates are compared in a pixel-wise manner in order to select best r. The ICI rule is used in this testing (Katkovnik, 1999, Katkovnik, 2005) (see Chapter 2).

The algorithm based on the ICI rule demonstrated better performance than the algorithm using the bias estimate. Comparison of the proposed adaptive techniques' versus the optimal (oracle) invariant selection technique for various images showed that the proposed techniques performs better than the estimate with the best possible invariant regularization parameter.

The results are shown the Cameraman of the size 256×256 (Fig.4.17a) by the Monte-Carlo simulation (100 runs)

The blur is defined as the 9×9 boxcar PSF (mean filter). The level of the Gaussian noise is calculated as the BSNR (4.41) equals to 40 dB in our experiments.

We select the regularization parameter values from the set $R = \{r_1, r_2, ..., r_N\}$. In general, these optimal value depends on the image, the point-spread function and the noise level. The following construction defines the set R in the manner universally applicable for variety of scenarios:

$$r_i = \tau_i \cdot \frac{2N \cdot 2M \cdot \sigma^2 \left\|v(x)\right\|_1^2}{\sum_f \left|Z(f)\right|^2 - \sigma^2 \cdot 2N \cdot 2M}, \ i = 1, ..., 5,$$

where $\tau \in \{1.3,\ 2.3,\ 6.3,\ 9.6,\ 30\}$ and $\left\|v(x)\right\|_1^2 = \left(\sum_x |v(x)|\right)^2$. It is employed for all test images used in our simulation experiments and similar to implementation proposed in (Neelamani, 2003).

Visually the effects of point-wise regularization are demonstrated in Fig.4.17c,d, where the results of Monte-Carlo modeling are shown for the blurred Cameraman image (Fig.4.17b). These images show the mean values of the regularization parameters for different pixels of the Cameraman image. The varying oracle values of the regularization parameter are small near edges while larger values correspond to the smoother areas of the image (Fig.4.17c). The mean values of the varying adaptive regularization parameter selected by the ICI rule are shown in Fig.4.17d. Comparing the images Fig.4.17c and Fig.4.17d we note their similarity. In particular, the ICI rule gives smaller values of the regularization parameter near the edges and larger for smoother areas as the oracle estimator does. The adaptive values of the regularization parameter accurately delineate the edges of the image similarly to Fig.4.17c.

Conclusions

The demosaicing and deblurring are the problems studied in this thesis. The main results can be briefly finalized as follows.

We proposed a novel demosaicing technique based on spatially adaptive filtering of interpolation errors. These errors are treated as noise that is nonstationary and strongly depends on signal. The magnitude of errors is higher near edges of image details. We efficiently exploited the adaptive LPA-ICI denoising in order to remove these errors and preserve the edges. This idea was exploited for noiseless and noisy Bayer data considering signal-dependant noise natural for CCD/CMOS digital imaging sensors. The CFAI and denoising were integrated into a single procedure that showed significant improvement comparing it with the independent analogous denoising and CFAI. The efficiency and applicability of the proposed technique were shown by experiments for both artificial and real raw data (taken directly from the sensor of a cameraphone).

We considered several settings for the deconvolution problems. A novel technique was proposed for the computational optical sectioning with a good potential for high-resolution 3D image reconstruction and efficient noise suppression. The technique is a multi-channel generalization of the algorithms for 2D inverse imaging developed in (Katkovnik, 2005). Efficient deconvolution algorithms in combination with a point-wise adaptive denoising make this approach powerful tool for the visualization of 3D objects. It can be applied in microscopy, astronomy, or in digital photo-images. This approach requires precise knowledge about the image formation model, in particular the PSF. Further works are focused on the methods of restoration when the blurring operator is unknown, i.e. on the blind deconvolution problems.

We proposed an iterative multi-channel blind deconvolution algorithm. It is assumed that several degraded observations of a single scene (that is to be restored) are available. The technique proposed is based on the frequency domain representation of the observation model. This algorithm does not require the accurate size of supports of blur functions, and the observed images are not supposed to be perfectly spatially aligned. One of the benefits of this approach concerns the ability to work with large images and with large supports of PSFs. The recursive procedure completed by the spatially-adaptive LPA-ICI filters works as a spatially-adaptive regularizator for the blur-operator inversion. Simulations produced for both grayscale and color images showed high quality of restoration in terms of objective numerical criteria and subjective visual evaluation.

A prior information about the PSF may significantly simplify the restoration. We considered the single-channel blind deconvolution where it is assumed that the parametric model of PSF is known. As a particular example we considered Gaussian, motion, and boxcar PSFs. The PSF and its parameter were identified from a single image. For

this purpose we employed the MLMVN neural network that was trained for a database of images. The identification procedure is computationally fast and cheap. After identification any conventional deblurring technique can be used in order to restore an image. We used the LPA-ICI deconvolution technique (Katkovnik, 2005) and the obtained results have shown the efficiency of the proposed approach.

As a key element of deconvolution problem, we considered the problem to select the regularization parameter. Usually it is considered as invariant for the whole image. We proposed two techniques for selection of the varying regularization parameter. The first algorithm is based on the bias estimation and MSE minimization for every point of an image. The second one uses the statistical ICI rule. The last algorithm demonstrated better performance than the former one. Comparison of the proposed adaptive techniques' versus the ideal (oracle) invariant selection technique showed that the proposed techniques performs better than the estimate with the best possible invariant regularization parameter.

We intensively used the LPA-ICI adaptive to the signal filtering as an important part of the proposed techniques.

Overall, two kinds of nonparametric estimation are exploited in this thesis. The first one is an empirical fitting implemented in the LPA. It is used for filter design. The second one is closer to the conventional estimation theory based on statistical moments calculations. It is used in Wiener style estimators and in the ICI rule enabling the quality estimation close to the minimum squared error.

Bibliography

Adams, J., K. Parulski, and K. Spaulding, "Color processing in digital cameras", *IEEE Micro,* vol. 18, no. 6, pp. 20-30, 1998.

Adams Jr., J.E., "Design of color filter array interpolation algorithms for digital cameras", Part 2, IEEE Proc. Int. Conf. Image Processing 1, pp. 488–492, 1998.

Aizenberg, N.N., and Yu.L. Ivaskiv, *Multiple-Valued Threshold Logic*, Naukova Dumka Publisher House, Kiev, 1977 (in Russian).

Aizenberg, N.N., and I.N. Aizenberg, "CNN Based on Multi-Valued Neuron as a Model of Associative Memory for Gray-Scale Images", Proc. of the Second IEEE Int. Workshop on Cellular Neural Networks and their Applications, Technical University Munich, Germany October 14-16, pp.36-41, 1992.

Aizenberg, I., N. Aizenberg, and J.Vandewalle, *Multi-valued and universal binary neurons: theory, learning, applications*, Kluwer Academic Publishers, Boston/Dordrecht/London, 2000.

Aizenberg, I., N. Aizenberg, and C. Butakoff. "Neural Network Based on Multi-Valued Neurons: Application in Image Recognition, Type of Blur and Blur Parameters Identification", In: J. Mira, A. Prieto (eds.) Bio-inspired Applications of Connectionism. Lecture Notes in Computer Science, vol. 2085 Springer-Verlag, Berlin Heidelberg New York, pp. 254-261, 2001.

Aizenberg, I., Bregin T., and Paliy D. "Method for Impulsive Noise Detection and Its Applications to the Improvement of Impulsive Noise-Filtering Algorithms", SPIE Proceedings on Image Processing: Algorithms and Systems, vol. 4667, pp. 204-214, 2002.

Aizenberg, I., C. Butakoff, V. Karnaukhov, N. Merzlyakov, and O. Milukova, "Blurred Image Restoration Using the Type of Blur and Blur Parameters Identification on the Neural Network", SPIE Proceedings vol. 4667 Image Processing: Algorithms and Systems, pp. 460-471, 2002.

Aizenberg, I., Astola J., Bregin T., Butakoff C., Egiazarian K. and Paliy D. "Detectors of the impulsive noise and new effective filters for impulsive noise reduction", Proceedings of SPIE Electronic Imaging, Image Processing: Algorithms and Systems II, Santa Clara, California, USA, vol. 5014, pp. 419-428, Jan. 2003.

Aizenberg, I., Astola J., Butakoff C., Egiazarian K. and Paliy D. "Effective Detection and Elimination of Impulsive Noise with a Minimal Image Smoothing", International Conference on Image Processing, ICIP 2003, vol. 3, pp. III- 357-360, Sept. 2003.

Aizenberg, I., Butakoff C. and Paliy D. "Impulsive Noise Removal using Threshold Boolean Filtering based on the Impulse Detecting Functions", *IEEE Signal Processing Letters*, vol. 12, iss. 1, pp. 63- 66, Jan. 2005.

Aizenberg, I., C. Moraga, and D. Paliy, "A Feedforward Neural Network based on Multi-Valued Neurons", In Computational Intelligence, Theory and Applications. Advances in Soft Computing, XIV, (B. Reusch - Ed.), Springer, Berlin, Heidelberg, New York, pp. 599-612, 2005.

Aizenberg, I., Paliy D., and Astola J. "Multilayer Neural Network based on Multi-Valued Neurons and the Blur Identification Problem", 2006 IEEE World Congress on Computational Intelligence, Proceedings of the 2006 IEEE Joint Conference on Neural Networks, Vancouver, Canada, pp. 1200-1207, Jul. 2006.

Aizenberg, I., D. Paliy, C. Moraga, and J. Astola, "Blur Identification Using Neural Network for Image Restoration ", Proc. of Fuzzy Days 2006, Dortmund, pp. 441-455, Sept. 2006.

Aizenberg, I., C. Moraga and D. Paliy, "A Feedforward Neural Network Based on Multi-valued Neurons", Advances in Soft Computing: Computational Intelligence, Theory and Applications, Springer Berlin/Heidelberg, New York, pp. 599-612, 2006.

Aizenberg, I., D.V. Paliy, J.M. Zurada, J.T. Astola, "Blur Identification by Multilayer Neural Network based on Multi-Valued Neurons", *IEEE Trans. on Neural Networks*, (Accepted for publication).

Aizenberg, I. and C. Moraga, "Multilayer Feedforward Neural Network Based on Multi-Valued Neurons (MLMVN) and a Backpropagation Learning Algorithm", Soft Computing, vol. 11, no 2, pp. 169-183, Jan. 2007.

Alleysson, D., S. Susstrunk, J. Herault, Color demosaicing by estimating luminance and opponent chromatic signals in the Fourier domain, in Proc IS&T/SID 10th Color Imaging Conf, 331–336, 2002.

Alleysson, D., S. Susstrunk, J. Marguier, Linear demosaicing inspired by the human visual system, *IEEE Trans. on Image Procesing,* vol. 14, no. 4, 439-449, 2005.

Aoki, H. and Y. Kosugi "An Image Storage System Using Complex-Valued Associative Memory", Proc. of the 15th International Conference on Pattern Recognition, Barcelona, 2000, IEEE Computer Society Press, vol. 2, 626-629, 2000.

Aoki, H., E. Watanabe, A.Nagata and Y. Kosugi "Rotation-Invariant Image Association for Endoscopic Positional Identification Using Complex-Valued Associative Memories", In: J. Mira, A. Prieto (eds.) Bio-inspired Applications of Connectionism. Lecture Notes in Computer Science, Springer-Verlag, Berlin Heidelberg New York, vol. 2085, pp. 369-374, 2001.

Banham, M. and A. Katsaggelos, "Digital image restoration", *IEEE Signal Processing Magazine,* vol. 14, pp. 24-41, Mar 1997.

Bayer, B.E., "Color imaging array", U.S. Patent 3 971 065, 1976.

Berger, T., Stromberg, J.O., Eltoft, T., Adaptive regularized constrained least squares image restoration, *IEEE Trans. on Image Processing*, vol. 8, iss. 9, pp. 1191-1203, 1999.

Bertero, M., and P. Boccacci , *Inverse Problems in Imaging,* IOP Publishing, 1998.

Bovik, A., *Handbook of Image and Video Processing*, New York: Academic, 2000.

Biggs, D., M. Andrews, "Acceleration of iterative image restoration algorithms", *Applied optics*, vol. 36, no. 8, pp. 1766-1775, Mar. 1997.

Biggs, D., M. Andrews, "Iterative blind deconvolution of extended objects", International Conference on Image Processing, IEEE Proceedings, vol. 2 , pp. 454-457, Oct. 1997.

Brainard, D.H., Bayesian method for reconstructing color images from trichromatic samples, IS&T's 47th Annual Conference/ICSP, pp. 375-380, 1994.

Campisi, P., and K. Egiazarian, *Blind Image Deconvolution: Theory and Applications*, Edited by Campisi P., and K. Egiazarian, CRC Press, 2007.

Chan, T., S. Osher, J. Shen, "The digital TV filter and nonlinear denoising," *IEEE Trans. Image Processing*, vol. 10, no. 10, pp. 231-241, 2001.

Chan, R.H., C.-W. Ho, M. Nikolova, "Salt-and-Pepper Noise Removal by Median-Type Noise Detectors and Detail-Preserving Regularization", *IEEE Trans. on Image Processing*, vol. 14, no. 10, pp. 1479-1485, Oct. 2005.

Chen, W., Chen, M., Zhou, J., Adaptively regularized constrained total least-squares image restoration, *IEEE Trans. on Image Processing*, vol. 9, iss. 4, pp. 588-596, 2000.

Chen, L., and K.-H. Yap, "A soft double regularization approach to parametric blind image deconvolution," *IEEE Trans. Image Processing*, vol. 14, iss. 5, pp. 624-633, May 2005.

Chen, L., and K.-H. Yap, "Efficient discrete spatial techniques for blur support identification in blind image deconvolution," *IEEE Trans. Signal Processing*, vol. 54, no. 4, pp. 1557-1562, Apr. 2006.

Cok, D.R., Reconstruction of CCD images using template matching, IS&T's 47th Annual Conference/ICPS, pp. 380-385, 1994.

Da Rugna, J., and H. Konik, "Blur Identification in Image Processing", IEEE World Congress on Computational Intelligence, IJCNN 2006, Vancouver, pp. 4843-4848, Jul 2006.

Donoho, D.L., De-noising by soft-thresholding, *IEEE Trans. Inform Theory,* vol. 41, no. 3, pp. 613-627, 1995.

Dubois, E., Frequency-domain methods for demosaicking of Bayer-sampled color images, *IEEE Signal Processing Letters,* vol. 12, no. 12, 847-850, 2005.

Fergus, R., Singh, B., Hertzmann, A., Roweis, S.T., Freeman W.T., Removing Camera Shake from a Single Photograph, ACM Transactions on Graphics (TOG), Proceedings of ACM SIGGRAPH 2006, vol. 25, iss. 3, pp. 787-794, July 2006.

Figueiredo, M., R. Nowak, "An EM algorithm for wavelet-based image restoration", *IEEE Trans. on Image Processing*, vol. 12, iss. 8, pp. 906 - 916, Aug. 2003.

Foi, A., R. Bilcu, V. Katkovnik, and K. Egiazarian, "Anisotropic local approximations for pointwise adaptive signal-dependent noise removal", Proc XIII European Signal Process Conf, EUSIPCO 2005.

Foi, A., V. Katkovnik, D. Paliy, K. Egiazarian, M. Trimeche, S. Alenius, R. Bilcu, M. Vehvilainen, Apparatus, method, mobile station and computer program product for noise estimation, modeling and filtering of a digital image", U.S. Patent Application No. 11/426,128, 2006.

Foi, A., S. Alenius, M. Trimeche, and V. Katkovnik, "Adaptive-size block transforms for Poissonian image deblurring", Proc. Int. TICSP Workshop Spectral Meth. Multirate Signal Process., SMMSP 2006, Florence, Sept. 2006.

Foi, A., S. Alenius, V. Katkovnik, and K. Egiazarian, Noise measurement for raw-data of digital imaging sensors by automatic segmentation of non-uniform targets, *IEEE Sensors J.*, 2006, (to be pulished September-October 2007).

Foi, A., M. Trimeche, V. Katkovnik, and K. Egiazarian, "Practical Poissonian-Gaussian noise modeling and fitting for single image raw-data", *submitted for publication to IEEE Trans. Image Processing*, 2007 (in review).

Forster, B., Van De Ville D., Berent J., Sage D., Unser M., Extended depth-of-focus for multi-channel microscopy images: a complex wavelet approach, IEEE International Symposium on Biomedical Imaging, vol. 1, pp. 660-663, Apr. 2004.

Galatsanos, N.P., Katsaggelos, A.K.: Methods for choosing the regularization parameter and estimating the noise variance in image restoration and their relation. *IEEE Trans. on Image Processing*, vol. 1, iss. 3, pp. 322-336, 1992.

Giannakis, G.B., and R. W. Heath, "Blind identification of multichannel FIR blurs and perfect image restoration", *IEEE Trans. on Image Processing*, vol. 9, no 11, pp. 1877-1896, Nov. 2000.

Goldenshluger ,A., and A. Nemirovski, "On spatial adaptive estimation of nonparametric regression," *Math. Meth. Statistics*, vol. 6, pp.135-170, 1997.

Gunturk, B.K., Y. Altunbasak, R.M. Mersereau, "Color plane interpolation using alternating projections", *IEEE Trans. on Image Processing,* vol. 11, iss. 9, pp. 997-1013, 2002.

Gunturk, B.K., J. Glotzbach, Y. Altunbasak, R. Schafer, R.M. Mersereau, Demosaicking: color filter array interpolation, *IEEE Signal Processing Magazine*, pp. 44-54, 2005.

Hamilton Jr., J.F. and J.E. Adams, "Adaptive color plane interpolation in single color electronic camera", U.S. Patent 5 629 734, May 1997.

Hansen, P.C., Analysis of discrete ill-posed problems by menas of the L-curve, *SIAM Rev.*, vol. 34, 561-580, 1992.

Hansen, P.C., O'Leary, D.P., The use of the L-curve in the regularization of discrete ill-posed problems, *SIAM J. Sci.Comput.*, vol. 14, no. 6, 1487-1503, 1993.

Harikumar G. and Y. Bresler, Perfect blind restoration of images blurred by multiple filters: Theory and efficient algorithm, *IEEE Trans. on Image Processing*, vol. 8, pp. 202–219, Feb. 1999.

Harikumar, G. and Y. Bresler, Exact image deconvolution from multiple FIR blurs, *IEEE Trans. Image Processing*, vol. 8, no. 6, pp. 846–862, 1999.

Haykin, S., *Neural Networks: A Comprehensive Foundation (2nd edn.)*, Prentice Hall, New York, 1998.

Hecht, E., *Optics (4th edition)*, Addison Wesley, 2002.

Hirakawa, K., T.W. Parks, Adaptive homogeneity-directed demosaicing algorithm, *IEEE Trans. on Image Processing,* vol. 14, iss. 3, 360-369, 2005.

Hirakawa, K., T.W. Parks, Joint Demosacing and Denoising, IEEE ICIP 2005, III, pp. 309-312, 2005.

Hirakawa, K., T.W. Parks, Joint demosaicing and denoising, *IEEE Trans. Image Processing,* vol. 15, iss. 8, 2146-2157, 2006.

Homem, M.R.P., Mascarenhas N.D.A., Costa L da.F., 6th IEEE Southwest Symposium on Image Analysis and Interpretation, pp. 142 - 146, Mar. 2004.

Huber, P.J., *Robust Statistics*, Wiley-Interscience, 1981.

Hurvich, C.M., J.S. Smirnoff, and J.-C. Tsai, Smoothing parameter selection in nonparametric regression using an improved Akaike information criterion, *J. Royal Stat. Soc. B*, vol. 60, pp. 271-293, 1998.

Jalobeanu, A., R. Nowak, J. Zerubia, M. Figueiredo, "Satellite and aerial image deconvolution using an EM method with complex wavelets", 2002 International Conference on Image Processing, Proceedings, vol. 1, pp. 22-25, Sept. 2002.

Jankowski, S., A. Lozowski and J.M. Zurada "Complex-Valued Multistate Neural Associative Memory", *IEEE Trans. on Neural Networks*, vol. 7, pp. 1491-1496, 1996.

Jiang, M., G. Wang, "Convergence studies on iterative algorithms for image reconstruction", *IEEE Trans. on Medical Imaging*, vol. 22, no. 5, pp. 569-579, 2003.

Kalevo, O., H. Rantanen, Noise reduction techniques for bayer-matrix images, Sensors and Camera systems for scientific, industrial, and digital photography applications III, Proceedings of SPIE 4669, 2002.

Katkovnik, V., *Nonparametric Identification and Smoothing of Data (Local Approximation Methods)*, Nauka, Moscow, 1985 (in Russian).

Katkovnik, V., A new method for varying adaptive bandwidth selection, *IEEE Trans. on Signal Proc.,* vol. 47, no. 9, pp. 2567-2571, 1999.

Katkovnik, V., K. Egiazarian, and J. Astola, Adaptive window size image de-noising based on intersection of confidence intervals (ICI) rule, *J. of Math Imaging and Vision* 16, no. 3, pp. 223-235, 2002.

Katkovnik, V., K. Egiazarian, and J. Astola, *Adaptive varying scale methods in image processing,* Tampere International Center for Signal Processing, TICSP Series, no. 19, Tampere, TTY, Monistamo, 2003.

Katkovnik, V., K. Egiazarian and J. Astola, "A spatially adaptive nonparametric image deblurring," *IEEE Trans. on Image Processing*, vol. 14, no. 10, pp. 1469-1478, 2005.

Katkovnik, V., Paliy D., Egiazarian K., Astola J., "Frequency domain blind deconvolution in multiframe imaging using anisotropic spatially-adaptive denoising", EUSIPCO 2006, Sept. 2006.

Katkovnik, V., K. Egiazarian, and J. Astola, *Local Approximation Techniques in Signal and Image Processing*, SPIE Press, 2006.

Katsaggelos, A.K. and J. K. Paik, "Iterative color image restoration algorithms," Proc. 1988 Int. Conf. Acoust., Speech, Signal Processing, pp. 1028-1031, Apr. 1988.

Keren, D., M. Osadchy, Restoring subsampled color Images, *Machine Vision and Applications,* pp. 197-202, 1999.

Khuri, A.I., *Advanced calculus with applications in statistics*, 2nd ed., John Wiley & Sons, 2003.

Kimmel, R., Demosaicing: image reconstruction from color CCD samples, *IEEE Trans. on Image Processing,* Vol. 8, Iss. 9, pp. 1221-1228, 1999.

Klemelä, J., and A. Tsybakov, Sharp adaptive estimation of linear functionals, *Ann. Statistics*, vol. 29, no. 6, pp. 1537-1566, 2001.

Kubota, A., Aizawa K., "Reconstructing arbitrarily focused images from two differently focused images using linear filters", *IEEE Trans. on Image Processing*, vol. 14, iss. 11, pp. 1848 - 1859, Nov. 2005.

Laroche, C.A. and M.A. Prescott, Apparatus and method for adaptively interpolating a full color image utilizing chrominance gradients, U.S. Patent 5 373 322, 1994.

Lagendijk, R.L., J. Biemond and D. E. Boekee, "Identification and Restoration of Noisy Blurred Images Using the Expectation-Maximization Algorithm", *IEEE Trans. on Acoustics, Speech and Signal Processing*, vol. 38, pp. 1180-1191, 1990.

Lee, S., N IK and J. Park, "Directional regularization for constrained iterative image restoration", *Electronic Letters,* vol. 39, Nov. 2003.

Lepski, O., E. Mammen, and V. Spokoiny, Ideal spatial adaptation to inhomogeneous smoothness: an approach based on kernel estimates with variable bandwidth selection, *Ann. Statistics*, vol. 25, no. 3, pp. 929-947, 1997.

Li, X., Demosaicing by successive approximation, *IEEE Trans. on Image Processing,* vol. 14, iss. 3, pp. 370-379, 2005.

Li, J., Agathoklis P., Peet F., Jensen G., Sahota T., Measurement and analysis of defocused point spread functions and optical transfer functions of a microscope, Proceedings of IEEE Pacific Rim Conference on Communications, Computers, and Signal Processing, 1995, pp. 407 - 410, May 1995.

Liang, L., Y, Xu, "Adaptive Landweber method to deblur images", *IEEE Signal Processing Letters,* vol. 10, no 5, pp.129-132,2003.

Likas, A.C., N.P. Galatsanos, "A variational approach for Bayesian blind image deconvolution," *IEEE Trans. Signal Processing*, vol. 52, no. 8, pp. 2222-2233, Aug. 2004.

Lukac, R., K. Martin, K.N. Plataniotis, Demosaicked image postprocessing using local color ratios, *IEEE Trans. on Circuits and Systems for Video Technology*, vol. 14, no. 6, pp. 914-920, 2004.

Lukac, R., K.N. Plataniotis, An efficient CFA interpolation solution, 46th Int Symposium Electronics in Marine, ELMAR, 2004.

Lukac, R., K.N. Plataniotis, Normalized color-ratio modeling for CFA interpolation, *IEEE Trans. on Consumer Electronics,* vol. 50, no. 2, pp. 737-745, 2004.

Lukac, R., K.N. Plataniotis, D. Hatzinakos, M. Aleksic, A novel cost effective demosaicing approach, *IEEE Trans. on Consumer Electronics,* vol. 50, no. 1, pp. 256-261, 2004.

Lukac, R., K.N. Plataniotis, Color filter arrays: design and performance analysis, *IEEE Trans. on Consumer Electronics,* vol. 51, no. 4, pp. 1260-1267, 2005.

Lukac, R., K.N. Plataniotis, Data-adaptive filters for demosaicking: a framework, *IEEE Trans. on Consumer Electronics,* vol. 51, no. 2, pp. 560-570, 2005.

Lukac, R., B. Smolka, K. Martin, K.N. Plataniotis, A.N. Venetsanopulos, Vector filtering for color imaging*, IEEE Signal Processing Magazine,* 74-86, 2005.

Lukac, R., K.N. Plataniotis, Demosaicking using vector spectral model, Proceedings of the 2006 IEEE International Conference on Multimedia and Expo ICME 2006, pp. 1185-1188, 2006.

Lukac, R., K.N. Plataniotis, *Single-sensor camera image processing, In 'Color Image Processing: Methods and Applications', (eds.) R. Lukac and K.N. Plataniotis*, CRC Press/Taylor & Francis, pp. 363-392, 2006.

Luo, G., A Novel Color Filter Array with 75% Transparent Elements, Digital Photography III, Proc. of SPIE-IS&T Electronic Imaging, vol. 6502, 65020T.

Malvar, H.S., L.-W. He, and R. Cutler, High-quality linear interpolation for demosaicing of Bayer-patterned color images, IEEE Int Conf (ICASSP '04), Proceedings on Acoustics, Speech, and Signal Processing 3, pp. 485-488, 2004.

Markham, J., Conchello J., "Fast Maximum-Likelihood Image Restoration Algorithms for Three-Dimensional Fluorescense Microscopy", *J. of Optical Society of America A*, 18, pp. 1062-1071, 2001.

May, K., T. Stathaki and A. Katsaggelos, "Spatially adative intensity bounds for image restoration", *Eurasip J. on Applied Signal Processing,* vol. 12, pp. 1167-1180, Dec. 2003.

McNally, J., Karpova T., Cooper J., and Conchello J., "Three-dimensional imaging by deconvolution microscopy, " *Methods*, vol.19, pp. 373-385, 1999.

Miller, K., Least squares methods for ill-posed problems with a prediscribed bound, *SIAM J. Math.Anal.*, vol. 1, pp. 52-74, 1970.

Molina, R., A.K. Katsaggelos, J. Abad, J. Mateos, "A Bayesian Approach to Blind Deconvolution Based on Dirichlet Distributions", International Conference on Acoustics, Speech, and Signal Processing, 1997, ICASSP-97, vol. 4, pp. 2809-2812, 21-24 Apr 1997.

Molina, R., J. Mateos, A.K. Katsaggelos, and M. Vega, "A general multichannel image restoration method using compound models", IEEE International Conference on Pattern Recognition (ICPR2002), vol. 3, pp. 835-838, 2002.

Menon, D., S. Andriani, G. Calvagno, Demosaicing with directional filtering and a posteriory decision, *IEEE Trans. on Image Processing,* vol. 16, no. 1, pp. 132-141, 2007.

Muezzinoglu, M.K., C. Guzelis and J.M. Zurada, "A New Design Method for the Complex-Valued Multistate Hopfield Associative Memory", *IEEE Trans. on Neural Networks*, vol. 14, no. 4, pp. 891-899, 2003.

Mumford, D. and J. Shah, "Optimal approximation by piecewise smooth functions and associated variational problems," *Commun. Pure Appl.Math.*, vol. 42, pp. 577–685, 1989.

Na, W., J. Paik and C. Lee, "An image restoration system for a single-CCD color camcorder", *IEEE Transactions On Consumer Electronics,* vol. 41, pp. 563-572, Aug. 1995.

Nagy, J.G., and D.P. O'Leary, "Restoring images degraded by spatially variant blur". *SIAM Journal Sci. Comput.*, vol. 19, no. 4, pp. 1063-1082, Jul. 1998.

Neelamani, R., H. Choi, and R. G. Baraniuk, "Forward: Fourier-wavelet regularized deconvolution for ill-conditioned systems". *IEEE Trans. on Signal Processing*, vol. 52, iss. 2, pp. 418-433, Feb 2003.

Nemirovski, A., Topics in non-parametric statistics, Lecture notes in mathematics, 1783, *Springer-Verlag*, New York, pp. 85-277, 2000.

Ng, M. K., "Total Variation Based Image Restoration of Three Dimensional Microscopic Objects", TENCON '96. Proceedings, 1996 IEEE TENCON, Digital Signal Processing Applications, vol. 1, 26-29, pp. 288-293, Nov. 1996.

Oraintara, S., Karl, W.C., Castanon, D.A., Nguyen, T.Q., A method for choosing the regularization parameter in generalized Tikhonov regularized linear inverse problems. International Conference on Image Processing 2000, Proceedings, vol. 1, 10-13, 93-96, 2000.

Paliy, D., V. Katkovnik, and K. Egiazarian, "Scale-Adaptive Inverse in 3D Imaging", Proc. Int. TICSP Workshop Spectral Meth. Multirate Signal Process., SMMSP 2005, Riga, 2005.

Paliy, D., V. Katkovnik, and K. Egiazarian, "Spatially Adaptive 3D Inverse for Optical Sectioning", Proc. of SPIE Electronic Imaging 2006, San Jose, CA, vol. 6065, pp. 61-72, Jan. 2006.

Paliy, D., V. Katkovnik, S. Alenius, and M. Vehviäinen, "Adaptive Neighborhood Interpolation of Noisy Images on Quincunx Grid", International Workshop on Spectral Methods & Multirate Signal Processing, SMMSP 2006, Florence, pp. 155-162, Sep. 2006.

Paliy, D., R. Bilcu, V. Katkovnik, M. Vehvilainen, "Color Filter Array Interpolation Based on Spatial Adaptivity", Proc. SPIE-IS&T Electronic Imaging 2007, Computational Imaging IV, vol. 6497, San Jose, CA, Jan. 2007.

Paliy, D., M. Trimeche, V. Katkovnik, S. Alenius, "Demosaicing of Noisy Data: Spatially Adaptive Approach", Proc. SPIE-IS&T Electronic Imaging 2007, Computational Imaging IV, vol. 6497, San Jose, CA, Jan. 2007.

Paliy, D., V. Katkovnik, R. Bilcu, S. Alenius, K. Egiazarian, "Spatially Adaptive Color Filter Array Interpolation for Noiseless and Noisy Data", *International Journal of Imaging Systems and Technology, Special Issue on Applied Color Image Processing*, vol. 17, iss. 3, pp. 105-122, October 2007.

Paliy, D., V. Katkovnik, S. Alenius, K. Egiazarian, "Selection of Varying Spatially Adaptive Regularization Parameter for Image Deconvolution", International Workshop on Spectral Methods & Multirate Signal Processing, SMMSP 2007, num. 37, pp. 23-28, September 2007.

Panci, G., P. Campisi, S. Colonnese, and G. Scarano, "Multichannel blind image deconvolution using the bussgang algorithm: Spatial and multiresolution approaches," *IEEE Trans. Image Process.*, vol. 12, no. 11, pp. 1324–1337, 2003.

Parulski, K., K.E. Spaulding, *Color image processing for digital cameras, In 'Digital Color Imaging Handbook', (ed.) G. Sharma*, CRC Press, Boca Raton, FL, pp. 728–757, 2002.

Pei, S.-C. and I.-K. Tam, Effective color interpolation in CCD color filter arrays using signal correlation, *IEEE Trans Circuits Systems Video Technol,* vol. 13, no. 6, pp. 503–513, 2003.

Plataniotis, K.N., A. N. Venetsanopulos, Color Image Processing and Applications, Springer-Verlag Berlin Heidelberg 2000.

Polzehl, J., and V. Spokoiny, Adaptive weights smoothing with applications to image restoration, *J. Royal Stat. Soc. B*, vol. 62, pp. 335-354, 2002.

Pratt, W.K., *Digital Image Processing, 2nd Edt*, Wiley, N.Y., 1992.

Preza, C., Conchello J., "Depth-Variant Maximum Likelihood Restoration for Three-Dimensional Fluorescence Microscopy", *Journal of Optical Society of America A*, no. 9, vol. 21, Sept. 2004.

Qiao, J., J. Liu, C. Zhao, "A Novel SVM-Based Blind Super-Resolution Algorithm", IEEE World Congress on Computational Intelligence, IJCNN 2006, Vancouver, pp. 4830-4835, Jul. 2006.

Rajagopalan, A.N., S. Chaudhuri, "An MRF Model-Based Approach to Simultaneous Recovery of Depth and Restoration from Defocused Images", *IEEE Trans. on Pattern Analysis and Amchine Intelligence*, vol. 21, no. 7, pp. 577-589, Jul. 1999.

Ramanath, R., W.E. Snyder, Adaptive demosaicking, *J. Electron Imag* vol. 12, no. 4, pp. 633-642, 2003.

Rekleitis, I., "Optical Flow Recognition from the Power of Spectrum of a Single Blurred Image", Proc. of ICIP 2006, vol. 3, pp. 791-794, Sept. 1996.

Rooms, F., W. Philips, J. Portilla, "Parametric PSF estimation via sparseness maximization in the wavelet domain", Wavelet Applications in Industrial Processing II, Proc. of SPIE 2004, vol. 5607, pp. 26-33, 2004.

Ross, S.M., *Introduction to Probability Models*, 6th ed., Academic Press, 1997.

Rudin, L., S. Osher, and E. Fatemi, "Nonlinear total variation based noise removal algorithms," *Phys. D*, vol. 60, pp. 259–268, 1992.

Rumelhart, D.E. and J. L. McClelland, Parallel Distributed Processing: Explorations in the Microstructure of Cognition, MIT Press, Cambridge, 1986.

Rushforth, C., Image Recovery: Theory and Application, Chap. Signal Restoration, functional analysis, and Fredholm integral equations of the first kind. Academic Press, 1987.

Schaefer, L. H., Schuster D., Herz. H., "Generalized Approach for Accelerating Maximum Likelihood Based Image Restoration Applied to Three-Dimensional Fluorescence Microscopy", *Journal of Microscopy*, vol. 204, pt.2, pp. 99-107, Nov. 2001.

Simonoff, J.S., *Smoothing methods in statistics*, Springer-Verlag, New-York, 1998.

Sroubek, F., and J. Flusser, "Multichannel blind iterative image restoration," *IEEE Trans. Image Process.*, vol. 12, no. 9, pp. 1094–1106, 2003.

Sroubek, F., and J. Flusser, "Multichannel blind deconvolution of spatially misaligned images," *IEEE Trans. Image Process.*, vol. 14, no. 7, pp. 874-883, 2005.

Taubman, D., Generalized Weiner reconstruction of images from colour sensor data using a scale invariant prior, Proc Int Conf Image Proc, 200, 801-804.

Tekalp, M., and G. Pavlovic, "Space-variant and color image restoration using Kalman filtering", *IEEE Symposium on Circuits and Systems,* vol. 1, pp. 8-11, 1989.

Thompson, A.M., Brown, J.C., Kay, J.W., Titterington, D.M., A study of methods of choosing the smoothing parameter in image restoration by regularization, *IEEE Trans. on Pattern Analysis and Machine Intelligence*, vol. 13, iss. 4, pp. 326-339, 1991.

Tico, M., and M. Vehvilainen, "Estimation of Motion Blur Point Spread Function From Differently Exposed Image Frames", Proc. 14th European Signal Processing Conf., EUSIPCO 2006, Florence, Sept. 2006.

Tikhonov, A.N., V.Y. Arsenin, *Solutions of ill-Posed Problems*, Wiley, N.Y., 1977.

Totsky, A., Fevralev D., Lukin V., Katkovnik V., Paliy D., Egiazarian K., Pogrebnyak O., Astola J., "Performance Study of Adaptive Filtering in Bispectrum Signal Reconstruction", *Circuits, Systems, and Signal Processing*, Birkhäuser Boston, vol. 25, no. 3, pp. 315-342, 2006.

Trimeche, M., Paliy D., Vehvilainen M., Katkovnik V, "Multi-Channel Image Deblurring of Raw Color Components", Proceedings of SPIE, vol. 5674, Computational Imaging III, pp. 169-178, Mar. 2005.

Trussel, H.J., E. Saber, M. Vrhel, Color image processing: vector filtering for color imaging*, IEEE Signal Processing Magazine*, pp. 14-22, 2005.

Van Kempen, G.M.P., *Image Restoration in Fluorescence Microscopy*, Doctoral Thesis, Delft University Press, 1999.

Vega, M., R. Molina, and A. K. Katsaggelos, Bayesian reconstruction of color images acquired with a single CCD, *Lecture Notes in Computer Science* 3522, 343-350, 2005.

Vogel, C.R., *Computational Methods for Inverse Problems*, Soc. for Industrial and Applied Mathematics, 2002.

Wu, X., N. Zhang, Primary-consistent soft-decision color demosaicking for digital cameras (patent pending), *IEEE Trans. on Image Processing,* vol. 13, iss. 9, pp. 1263-1274, 2004.

Wu, X., Wang, R., Wang, C., Regularized image restoration based on adaptively selecting parameter and operator. Proceedings of the 17th International Conference on Pattern Recognition, ICPR 2004, vol. 3, pp. 662-665, 2004.

Yuan, L., Sun, J., Quan, L., Shum, H., Image Deblurring with Blurred/Noisy Image Pairs, *ACM Transactions on Graphics*, vol. 26, no. 3, Article 1, July 2007.

Zhang, X., D.A. Silverstein, J.E. Farrel, and B.A. Wandell, Color image quality metric S-CIELAB and its application on halftone texture visibility, in Proc COMPCON Dig. Papers 1997, pp. 44-48, 1997.

Zhang, S. and M.A. Karim, "A New Impulse Detector for Switching Median Filters," *IEEE Signal Processing Letters*, vol. 9, no. 11, pp. 360-363, Nov. 2002.

Zhang, L., X. Wu, Color demosaicking via directional linear minimum mean square-error estimation, *IEEE Trans. on Image Processing,* vol. 14, no. 12, pp. 2167-2178, 2005.

Zhu, D., Razaz M., Lee R., "A Landweber Algorithm for 3D Confocal Microscopy Restoration", Proceedings of the 17th International Conference on Pattern Recognition, ICPR 2004, vol. 1, pp. 552 - 555, Aug. 2004.

Publications

Publication I

Paliy, D., V. Katkovnik, R. Bilcu, S. Alenius, K. Egiazarian, "Spatially Adaptive Color Filter Array Interpolation for Noiseless and Noisy Data", *International Journal of Imaging Systems and Technology, Special Issue on Applied Color Image Processing*, vol. 17, iss. 3, pp. 105-122, October 2007.

Publication II

Paliy D., R. Bilcu, V. Katkovnik, M. Vehvilainen, "Color Filter Array Interpolation Based on Spatial Adaptivity", Proc. SPIE-IS&T Electronic Imaging 2007, Computational Imaging IV, Vol. 6497, San Jose, CA, January 2007.

Publication III

Paliy D., M. Trimeche, V. Katkovnik, S. Alenius, "Demosaicing of Noisy Data: Spatially Adaptive Approach", Proc. SPIE-IS&T Electronic Imaging 2007, Computational Imaging IV, Vol. 6497, San Jose, CA, January 2007.

Publication IV

Paliy D., V. Katkovnik, and K. Egiazarian, "Spatially Adaptive 3D Inverse for Optical Sectioning", Proc. of SPIE-IS&T Electronic Imaging 2006, San Jose, CA, Vol. 6065, pp. 61-72, January 2006.

Publication V

Katkovnik V., Paliy D., Egiazarian K., Astola J., "Frequency domain blind deconvolution in multiframe imaging using anisotropic spatially-adaptive denoising", EUSIPCO 2006, September 2006.

Publication VI

Aizenberg I.N., D.V. Paliy, J.M. Zurada, J.T. Astola, "Blur Identification by Multilayer Neural Network based on Multi-Valued Neurons", *IEEE Trans. on Neural Networks*, (Accepted for publication).

Publication VII

Paliy, D., V. Katkovnik, S. Alenius, K. Egiazarian, "Selection of Varying Spatially Adaptive Regularization Parameter for Image Deconvolution", International Workshop on Spectral Methods & Multirate Signal Processing, SMMSP 2007, num. 37, pp. 23-28, September 2007.

Tampereen teknillinen yliopisto
PL 527
33101 Tampere

Tampere University of Technology
P.O. Box 527
FIN-33101 Tampere, Finland